Studies on Mechanical, Tribological Properties and Metal Flow Behaviour of Developed Al-Cu/Al Two-Layered Composite

A Dissertation

Submitted in partial fulfillment of the requirements for
the award of the degree of

DOCTOR OF PHILOSOPHY

in

MECHANICAL ENGINEERING

by

KOTIKALA RAJASEKHAR

(Roll No.716125)

DEPARTMENT OF MECHANICAL ENGINEERING
NATIONAL INSTITUTE OF TECHNOLOGY,
WARANGAL, TS, INDIA – 506004

November, 2021

Studies on Mechanical, Tribological Properties and Metal Flow Behaviour of Developed Al-Cu/Al Two-Layered Composite

A Dissertation

Submitted in partial fulfillment of the requirements for
the award of the degree of

DOCTOR OF PHILOSOPHY

in

MECHANICAL ENGINEERING

by

KOTIKALA RAJASEKHAR

(Roll No.716125)

Under the guidance of

Dr. V Suresh Babu
Professor, MED
(Supervisor)

Dr. M J Davidson
Associate Professor, MED
(Co-Supervisor)

DEPARTMENT OF MECHANICAL ENGINEERING
NATIONAL INSTITUTE OF TECHNOLOGY,
WARANGAL, TS, INDIA – 506004

November, 2021

THESIS APPROVAL FOR Ph. D.

This thesis entitled **"Studies on Mechanical, Tribological Properties and Metal Flow Behaviour of Developed Al-Cu/Al Two-Layered Composite"** by **Mr. Kotikala Rajasekhar** is approved for the degree of Doctor of Philosophy.

Examiners

Supervisors

Dr. V Suresh Babu
Professor, MED
(Supervisor)
Mechanical Engineering Department,
NIT Warangal

Dr. M J Davidson
Associate Professor, MED
(Co-Supervisor)
Mechanical Engineering Department,
NIT Warangal

Chairman

Prof. Adepu Kumar
Head, Mechanical Engineering Department, NIT Warangal

DEPARTMENT OF MECHANICAL ENGINEERING
NATIONAL INSTITUTE OF TECHNOLOGY,
WARANGAL, TS, INDIA – 506004

CERTIFICATE

This is to certify that the dissertation work entitled **"Studies on Mechanical, Tribological Properties and Metal Flow Behaviour of Developed Al-Cu/Al Two-Layered Composite"** which is being submitted by **Mr. Kotikala Rajasekhar" (Roll No. 716125)**, is a bonafide work submitted to the Department of Mechanical Engineering, National Institute of Technology, Warangal in partial fulfillment of the requirement for the award of the degree of **Doctor of Philosophy** in **Mechanical Engineering.**

To the best of our knowledge, the work incorporated in this thesis has not been submitted elsewhere for the award of any degree.

Dr. V Suresh Babu
Professor, MED
(Supervisor)
Mechanical Engineering Department,
NIT Warangal

Dr. M J Davidson
Associate Professor, MED
(Co-Supervisor)
Mechanical Engineering Department,
NIT Warangal

Prof. Adepu Kumar
Head, Mechanical Engineering Department, NIT Warangal

DEPARTMENT OF MECHANICAL ENGINEERING
NATIONAL INSTITUTE OF TECHNOLOGY,
WARANGAL, TS, INDIA – 506004

DECLARATION

This is to certify that the work presented in the thesis entitled **"Studies on Mechanical, Tribological Properties and Metal Flow Behaviour of Developed Al-Cu/Al Two-Layered Composite"** is a bonafide work done by me under the supervision of **Dr. V. Suresh Babu** and **Dr. M. J. Davidson,** and was not submitted elsewhere for the award of any degree. I declare that this written submission represents my ideas in my own words, and where other ideas or words have been included, I have adequately cited and referenced the original sources. I also declare that I have adhered to all principles of academic honesty and integrity and have not misrepresented or fabricated or falsified any idea/data/fact/source in my submission. I understand that any violation of the above will be a cause for disciplinary action by the Institute and can also evoke penal action from the sources which have thus not been properly cited or from whom proper permission has not been taken when needed.

Date: 30-11-2021 (**Kotikala Rajasekhar**)

(Roll No.: 716125)

Dedicated to

My Parents

and

My Wife

ACKNOWLEDGEMENT

I would like to express my sincere thanks and gratitude for my supervisors, P**rof. V. Suresh Babu** and **Dr. M. J. Davidson**, Associate Professor, Mechanical Engineering Department, National Institute of Technology, Warangal, for their continuous guidance, support, enthusiasm, and motivation in my Ph.D. research work.

I extend my sincere gratitude to **Prof. N. V. Ramana Rao**, Director, National Institute of Technology Warangal, India, for providing the necessary facilities and encouragement throughout my work. I am thankful to **Prof. A. Kumar**, Head, Department of Mechanical Engineering, NIT Warangal, and other faculty members for their encouragement and support extended during this period.

It's my great opportunity to express my deepest gratitude to the Departmental Scrutiny Committee members, **Prof. P. Bangaru Babu,** and **Dr. B. Satish Ben**, Associate Professor, Department of Mechanical Engineering, and **Dr. R. Arockia Kumar**, Asst. Professor, Department of Metallurgical and Materials Engineering for their adeptness and many discussions during the research period. I extend my thanks to **Dr. G. Raghavendra**, Department of Mechanical Engineering for the fruitful discussion.

I sincerely express my deepest gratitude to my senior researchers Dr. R. Seetharam, Dr. Mahammad Ali Shaik, G. Arun Manohar, and Dr. G. Uma Maheswararao for their help and extreme support. I express my special thanks to my co-scholars Mr. Abeyram Nithin, Mr. K. Kranthi and Mr. Bhargav Middemedi for their support, help, and advice during my entire project.

Finally, I would also like to acknowledge the help given by all the persons who have directly or indirectly supported the work.

Kotikala Rajasekhar
(Roll No: 716125)
Research Scholar
Department of Mechanical Engineering
National Institute of Technology,
Warangal- 506004.

Abstract

A study was carried out on the hot formability and densification characteristics, microstructure modelling, corrosion and wear resistance of Al-Cu/Al two-layered composite structure. The two-layered samples were fabricated by powder metallurgical method with various Cu percentages in the Al-Cu layer (Cu: 5wt. %, 10wt. %, and 15wt. %). The composites were fabricated layer by layer hot-pressing in a steel cylindrical die at 500 ^{0}C, 550 ^{0}C and 600 ^{0}C sintering temperature for 3 h. with a constant pressure of 400 MPa. In the interface region of 15wt. % copper, the highest value of micro-hardness (100.6 HV) was attained at a temperature of 550 ^{0}C. In the interface region of 15wt. % copper, the greatest level of micro-hardness (100.6 HV) was attained at a temperature of 550 degrees Celsius. The susceptibility of corrosion increases at the interface region of the sample with addition of copper content in Al-Cu layer and 15wt. %Cu sample observed higher susceptibility to corrosion.

The wear behaviour of Al layer, interface region and Al-10wt. %Cu layer of Al-10%Cu/Al sample was studied. The wear rate and coefficient of friction were determined using a pin-on-disc test. Tribological working of the two-layered composite structure was found to be affected by wear parameters such as applied load, sliding velocity, and sliding distance. Al-10wt. %Cu layer shows better tribological properties than pure Al and interface region. The worn surface investigation shows that abrasion was the predominant wear mechanism occurs at Al-10wt. %Cu layer than interface region, pure aluminium exhibit adhesion wear mechanism.

The hot formability and densification characteristics of Al-Cu/Al two-layered structured composite with the addition of various Cu composition were studied. The samples were hot-pressed at 550 ^{0}C temperature for 45 minutes with 0.9 initial relative density (IRD) and 0.1 s^{-1} strain rate. The preforms were hot deformed at a temperature range of 150 ^{0}C – 450 ^{0}C under triaxial stress state condition. The results revealed that (10wt. %Cu) preform achieved good cooperative deformation behaviour between Al-Cu and Al layers at the interface region. The relationship between the process parameters was discussed.

The hot upsetting test was used to investigate the dynamic recrystallization (DRX) behaviour of an Al–10 weight percent Cu/Al two-layered composite structure at the interface area. In this study, the activation energy (Q) and Zener–Hollomon parameter of Al–10wt. % Cu/Al sintered samples were computed under a variety of deformation circumstances and IRDs, and the results were presented. Increasing the Zener–Hollomon parameter results in a reduction in DRXd grain size, it was observed. A series of tests were carried out between measured and anticipated DRXd grain size for a variety of IRDs. The results revealed that the absolute and mean absolute error were 8.91 and 3.75 percent respectively.

CONTENTS

LIST OF FIGURES

LIST OF TABLES

ABBREVIATIONS

Abbreviation	Description
ASTM	American Society for Testing and Materials
BSE	Backscattered electrons
COF	Coefficient of friction
Rcorr	Corrosion resistance
DRX	Dynamic recrystallization
DRV	Dynamic recovery
Ecorr	Corrosion potential
EDAX	Energy-dispersive X-ray analysis
EIS	Electrochemical impedance spectroscopy
FCC	Face-centered cubic
HRC	Rockwell C hardness number
HV	Vickers number
Icorr	Corrosion current density
IRD	Initial relative density
PDP	Potentiodynamic polarization
PFS	Peak flow stress
SEM	Scanning electron microscope
UTM	Universal testing machine
WH	Work hardening

Chapter 1

Introduction

1. 1. Background

The high growth in requirement of these lightweight metals alloys in nuclear power plants, automotive, building, aerospace, marine and architecture industries, transportation and other sectors is the main reason to conducting exhaustive investigations on these materials by researchers. Now a days Powder Metallurgy method is preferred to conventional manufacturing techniques like machining, forging, stamping and casting to develop engineering products to fulfil the necessity of the above said industries. Generally, powder metallurgical method is a high volume, inexpensive and rapid manufacturing method to develop samples and it generates samples with accuracy, strength, high wear resistance. When the obligation for intricate and near net parts, higher material consumption and lower energy requirement method are in demand, it is better to choose powder metallurgical method than conventional manufacturing technique [1].

Over last decades due to non-stop growth in high-performance samples, there has been high growth in powder metallurgical industries. Due to the existence of inherent porosity in samples after sintering, the powder metallurgical parts are deprived of the desired mechanical properties. Therefore, industries primarily choose high volume forming techniques such as rolling, forging and hot deformation to lower or remove porosity. Thus, study of high volume forming of powder metallurgical component has become a stimulating new field in metal alloy forming industries due to its uniqueness in providing better mechanical and superior metallurgical properties and process flexibility over other conventional manufacturing processes. Powder metallurgical manufacturing materials are widely used as refractory metals (heating elements and lamp filaments), cemented carbides (deep drawing dies, wire drawings, cutting tools), friction materials (brake band and clutch liners), porous materials (filters and self-lubricating bearing), structural materials and bio-materials in defence industries, automotive and aerospace.

1.2. Hot Upsetting and constraint of powder metallurgy preforms

Several secondary processes are needed for manufacturing powder metallurgical samples like conventional techniques to enhance the mechanical properties while reducing or removing porosity. Among such techniques, upset hot compaction is recognized by means of an economic and highly influential way of refining the density and also mechanical properties [2]. The manufacturing process is carried out by upsetting cylindrical billets between two parallel flat dies. Hot compaction offers benefits like low material waste, better isotropic properties, fewer die requirement and lower tooling costs over the secondary processes [3].

Hot compaction upsetting test involves exposing the material to compression either at cold or hot working conditions. Through the hot compaction process, the material flows into the pores, and material density increases, which improves in mechanical properties and reduce non-uniformity of metallurgical properties. Therefore, the final product attained after hot compaction of sintered samples is better than cast materials with equivalent chemical composition. Several studies have been carried out by [4-6] on upset hot compaction of powder metallurgical samples and its comparative merits. An experimental investigation was carried out by various researchers [7-9] on hot compaction and they observed that upset hot compaction of porous materials is a reasonable and economical method for manufacturing aircraft, automotive and machine tool components.

Induced strain leads to consequent cross flow of metals that upset hot compaction of sintered samples leading to fracture of metals. Therefore, the effective change in powder metallurgical materials depends not only on material properties but also on related forming parameters like initial relative density, aspect ratio, temperature, and friction and strain rate [10, 11]. An examination was done by Narayanasamy et.al. [12] on deformation behaviour of sintered sample effects of parameters like initial relative density, percent content, aspect ratio and size of particulate.

1.3. Densification behavior of powder metallurgical samples

The metal flow into pores through hot compaction of porous material increases density and decreases the volume of material. Through hot compaction the densification of powder metallurgical samples was explained by Narayan et.al [14] and Kim et.al. [13]. After deformation the performance and service life of the components is determined by density. Therefore, the

secondary processes worked out in this present study involves hot upsetting procedure, the intention being to minimize the issues arising from poor mechanical properties and non-uniformities in the metallurgical properties through reducing or removing pores and brand powder metallurgical samples for advanced applications.

1.4. Hot deformation constitutive modelling

In industries, to know the hot deformation behaviour of porous materials is essential for manufacturers of metal forming processes because the metal deformation mechanism can be notably influenced by hot compaction process parameters such as strain, strain rate, temperature and porosity. As a result, the final product's microstructure and mechanical qualities vary. The flow behavior of Al and its alloys plays a dominant role in designing developing mechanical working processes. The material flow stress is affected by hot upsetting conditions like reinforced material, microstructure, strain, strain rate and temperature.

A number of authors [15-17] determined constitutive equations to define the plastic flow of metals through deformation at high temperature. The constitutive equation planned for porous materials which take into account the effect of porosity had very limited applicability. Thus, it is also interesting to investigate hot deformation behaviour and develop a constitutive equation to forecast the flow stress by considering the influence of porosity and other process parameters like strain rate, temperature etc. on deformation and densification behaviour.

1.5. Corrosion behaviour of powder metallurgical samples

Aluminium composites were taken as material for substituting conventional alloys in several industries like automotive, sport, and aerospace because of their desirable properties. Two main approaches normally work for large-scale manufacturing of metal matrix composites: powder metallurgy technique and molten metal process method with the latter considered most economical. The advantage of powder metallurgical technique is to reduce hot compaction temperature, which gives potentially good control of the reinforcement interface. In powder metallurgy method, powders of the metal and reinforcement phases are carefully mixed at solid state, compacting to coarsely 80% density, degassing, joined by vacuum hot pressing and finally by hot pressing. Potential limitations of applications of the materials relate to higher manufacturing cost and increased corrosion susceptibility. Normally, composites need combining of materials with notably different corrosion behaviours to offset the adverse effects on corrosion resistance

compared to monolithic alloys. A number of researchers [18-22] carried out investigations on the corrosion behaviour of powder metallurgical parts. The corrosion behaviour mostly depends on the electrolyte, sintering temperature and reinforcement. The analysis was done by EIS and potentiodynamic polarization tests in NaCl solution. The results showed key factor effects the general corrosion in Al-4.5Cu alloy 1. Corrosion potential differences and 2. The different corrosion rates between intermetallic particles and the Al-rich phase [23].

1.6. Wear behaviour

Despite enhanced mechanical properties of Aluminium alloys, most of these alloys suffer from low wear resistance and hardness at high temperature. To apply appropriate lubricants between contact surfaces is one solution to deal with the phenomenon of wear, but reduction in volume loss and coefficient of friction may not be reached under challenging conditions, such as high pressure and high temperature. There have been a number of initiatives to enhance the wear resistance of aluminium alloys and this phenomenon includes introduction of perfect reinforcing materials into alloys and surface coating applications to achieve the required engineering application.

Table 1.1 Wear resistance enhancement of aluminium alloys

Composition	Wear test Conditions (Load in N, Distance in m, Velocity in m/s/Speed in rpm)	Motion Contact Type	Counter part	Specific Wear Rate (10^{-6} mm^3/Nm)	Ref
Al-5wt. %Cu	(29.43, 3000, 0.83/NA)	Sliding pin-on-disc	EN31	94.3	[86]
Al-5wt. %Cu-5 ZrB_2	"	"	"	27.1	"
Al-5wt. %Cu-10 ZrB_2	"	"	"	27.6	"
Al-5wt. %Cu-20 ZrB_2	"	"	"	29.3	"
Al-4.3wt. %Cu	(6-40, 10000, 1/NA)	Sliding pin-on-disc	Cl	50	[87]
Al-4.3wt. %Cu- 20 Al_2O_3	"	"	"	20	"

Several researchers [24-27] carried out investigation on wear behaviour of powder metallurgical alloys. The friction coefficient and wear behaviour were influenced by various parameters like sliding velocity, lubrication, surface roughness, relative humidity and normal load. The parameters

which elaborate the alloys and metals tribological functioning mainly are sliding velocity and normal load.

1.7. Modelling aspect of microstructure evolution and modelling

Sintered powder metallurgical samples have poor mechanical properties due to the existence of porosity and therefore, to enhance the mechanical properties, powder metallurgical parts usually experience through forming processes like extrusion, rolling, forging and hot deformation to deduct or remove porosity [28]. As a result, the grain size or microstructures of the samples differ continually because of the effect of deformation conditions like temperature, initial relative density and strain rate. The final quality product can be attained by evolution of grain size and microstructure of the product structure. The grain size and microstructure evolution happen through hot forming process, it has high effect on hardness and strength of the desired product. Consideration of final grain size and microstructure of the powder metallurgical samples after high volume forming process is necessary because it regulates the service performance of components. Nowadays, powder metallurgical components manufacturers are many in number and are interested in optimizing the process parameters and forecasting the microstructure of the components. A number of researchers [29-33] have investigated the microstructure and grain size of powder metallurgical compacts. The powder metallurgical components' microstructure information is notably different from the corresponding cast metals the similar composition due to porosity [34, 35]. Thus, the information about fully dense material may not be set for powder metallurgical materials with similar composition. Dynamic recrystallization is the key mechanisms to the microstructure and grain size to reduce material resistance force through the hot forming process [36, 37]. The average DRX grain size of the materials measured by mathematical equation as a function of Zener-Hollomon parameters at various deformation conditions like temperature, strain, initial relative density and strain rate. It is necessary for designers to understand the correlation between microstructure and deformation process parameters of all engineering materials through the hot forming process, to obtain good quality product. Various researchers [38, 39] established mathematical model to show the average DRX grain size of the material in terms of Zener-Hollomon parameters through deformation at high temperature. But, microstructure evolution and mathematical models proposed for porous material which take into account the effect of porosity are limited. Thus, it is interesting to investigate the mathematical model and

microstructure evolution to forecast the grain size by taking the effect of porosity and other deformation conditions into consideration.

1.8. Applications of aluminium powder metallurgical alloys

Nowadays, aluminium metal matrix and its alloys are widely used in a wide range of engineering applications, including aerospace and defence [45]. Powder metallurgy and related alloys are chosen in a majority of technical applications due to their strength, better wear resistance, good corrosion resistance, and best stiffness, among other characteristics [40]. Aluminium-copper two-layered composites are one of the most interesting materials because they can be used in a variety of applications without compromising electrical, thermal, or corrosion resistance. Examples of such applications include induction cooking pans, conductive bus bars, heat exchangers for AC liners, and more.

1. 9. Organization of the thesis

The entire thesis is presented in eight chapters including the present part which is chapter 1 and presents the introduction part of sintering, wear, and densification behaviour, and discusses the microstructure of dynamic recrystallized grain size of aluminium powder metallurgical composites.

Chapter 2. This chapter provides a detailed survey of literature relevant to the current investigation. The gaps existing in the current knowledge of sintering, wear, and densification behaviour and model in microstructure evolution of powder metallurgy preforms have been identified.

Chapter 3. In this chapter the experimental details, which includes selection of materials, specimen preparation, hot compression test, microstructure analysis by optical microscope and characterization of investigated material have been discussed.

Chapter 4. This chapter provides a detailed discussion of the effect of sintering temperature and the properties of hot-pressed Al-Cu/Al two-layered composite structure generated through powder metallurgy.

Chapter 5. In this chapter, the wear behaviour of hot-pressed Al–10wt % Cu/Al two layered composite structure by powder metallurgy is discussed.

Chapter 6. This chapter gives Hot-upsetting of two-layered structure powder metallurgical Al-Cu/Al composites with a powder metallurgical structure that was used to investigate the formability and densification behaviour.

Chapter 7. This chapter provides data pertaining to hot upsetting, microstructure modelling of dynamically recrystallized grain size of Al–10 wt. % Cu/Al two-layered structure sintered composite

Chapter 8. This chapter contains conclusion drawn from the current research and presents the scope of future work.

Chapter 2

Literature Review

2. 1. Introduction

Powder metallurgy is a forming process of metal through which semi-finished or finished outcomes are produced from missed metallic powders. The art of producing samples by pressing powdered metal is not a new method. The older civilization experienced this technology in prehistoric times. As a significant witness the iron pillar at Delhi, some Egyptian tools and the articles of expensive metals produced by Incas. Modern powder metallurgy technology was originated in the 1920s, more growth took place through the period of the 2nd world war, and a steady development period took place through the years of post war of the early 1960s. Since then, the development of powder upsetting has expanded very rapidly, specifically for three reasons – captive, economical processing and its unique properties. In the last few decades, the technology of powder metallurgy has been established for making powders into specific engineering parts in defence, aerospace, automobile, nuclear and electronic industries which have comparable properties with conventional upsetting. Powder metallurgy is the best choice for material utilization, fast, large volume production, best strength products, and wear resistance. The powder metallurgy method gives more competitive than other fabrication techniques such as stamping machining and casting.

The main steps in the powder metallurgy method are mixing powder, hot upsetting and sintering. Sintering plays a very important role in the powder metallurgy process. The sintering process includes merging of loosely attached powders under melting temperature. To merge the loosely powder, die compaction method is mostly used because it is rapid and is appropriate for large mass production. Many techniques of powder metallurgy are available: pressure assisted sintering is most common technique which is used mostly now a days, where sintering and powder compacting happen at once [40]. Apart from this technique many other compaction methods are

available such as frictionless isostatic pressing [41], high speed compaction [42] rotary die pressing [43].

The preforms require sintering which is cold compacted by powder metallurgy method. In that way some properties increase such as densification and strength while other properties change such as corrosion and wear behaviour. An effective method of sintering needs a good control on time and temperature parameters, otherwise it tends to a disappointing result in densification [44]. A successful sintering method involves strong bonding of loosely attached particles along with low oxides and a perfect control on properties such as densification and dimensions so that the finished product is effective and valid for all practical environments.

2.2. Corrosion behaviour

Al alloys have been frequently used in many fields of space technology, automobile and so on, because of their good mechanical properties and high strength to weight ratio [45]. Furthermore, to evaluate the application of structure material, corrosion behavior is treated as an important characteristic. Hence, a special focus has been placed on corrosion behavior of Al alloys. Generally copper decreases resistance in general corrosion and the stress corrosion susceptibility occurs due to particular material conditions and compositions [46]. The corrosion behaviour mostly depends on the electrolyte, sintering temperature and reinforcement.

The electrochemical characteristics of Al-Cu (Cu: 5, 10 and 15%) alloys were observed after immersion in NaCl and H_2SO_4 solution. The effect of Al_2Cu related to the dendritic arm spacing on Al-Cu alloy's general corrosion resistance was analyzed. With the percentage addition of Cu content to Al-x% Cu alloy, greater susceptibility to corrosion behaviour was detected in NaCl solution. Similar actions were carried out with H_2SO_4 solution [47]. The electrochemical behaviour of Al–4.5Cu alloy was investigated, which was fabricated using casting. The analysis was carried out by EIS and potentiodynamic polarization tests in NaCl solution. The results showed key factor which impact general corrosion in Al-4.5Cu alloy are [1]. Corrosion potential differences [2]. The different corrosion rates between intermetallic particles and the Al-rich phase [46]. Infiltration (liquid phase sintering) was also used to produce Al-Cu alloy [48, 49]. A. E. Ares et al. developed a correlation between corrosion behavior, dendritic spacing, thermal parameters, and structures of Zn-Al alloys. It is observed that dendritic spacing increases when Al content increases[50]The carrion resistance can be analyzed by electrochemical impedance spectroscopy

(EIS) as a principal technique [51]. The corrosion wear is directly related to the thermal properties of the materials since as temperature increases, the corrosion resistance decreases [52].

Mustafa Acarer [53] explained that Al-Cu bi-metal (original materials formed the joint) produced average electrical conductivity compared to Al and Cu. From the electrochemical test result, the Al portion in Al-Cu bimetal acts as high anodic material because of its high electronegativity; thus, the Al portion was exposed to more corrosion when compared to copper side, where the corrosion resistance of Al, Cu and Al-Cu bimetal was 28.2, 16.8 and 24.1Ωcm respectively and conductivity was 0.350, 0.596 and 0.416 mS/cm respectively. Electrochemical tests were carried out on three Al–Si–Cu– Mg alloy with 15% and 19% reinforced B4C before, during and after the sliding tests by [54]. It was reported that with the addition of B_4C during the sliding in 0.05M NaCl solution, the corrosion tendency and the corrosion rate decreased. [55] investigated the exfoliation and intergranular corrosion of Al-3.5%Cu-1.5%Li-0.22% (Sc + Zr) alloys. The exfoliation and intergranular corrosion are caused during aging because of anodic dissolution of a precipitate-free zone (PFZ) and age hardening phase. As aging time increases, the susceptibility to exfoliation and intergranular corrosion increases because if aging time increases, PFZ widens and coarsens the age-hardening phase. [46] Reported that the solidified Al_2Cu under fast cooling conditions attained a corrosion rate, which was 10-times higher than pure-Al conducted through polarization test through 0.5 M NaCl solution at 25^0C. A higher corrosion potential was exhibited by Al_2Cu particles than Al-rich phase. This implied that when compared to pure Al, Al_2Cu particles are highly susceptible to corrosion. Also, it was evident from corrosion test results that there are 2-key factors that affect general corrosion of Al–4.5 wt.% Cu sample, these being differences in corrosion potential and on corrosion rate between Al-rich phase and the Al_2Cu (intermetallic). The increase in %Sc and %Zr to 2xxx Al-Cu alloy causes a decrease in corrosion current density by approximately 2-fold and reduction in pitting by 50 mV. Such improvements in the electrochemical behavior were associated with microstructural differences caused by the addition of Sc and Zr to the alloy. Nevertheless, no significant differences in open circuit potentials and corrosion were observed by addition of Sc and Zr to the alloy. The addition of Sc and Zr to Al-Cu alloy decreased damages caused by pitting. Pits were formed as trenches on Al-Cu and Al-Cu-Sc-Zr alloys, dissolving the Al- matrix at the periphery of Al2Cu, AlxFe3-4Cu and W-phase (AlxCu5-8ScZry) particles as summarized by [56].

2.3. Wear Behaviour

The mechanical action between sliding faces creates deformation and material removal on the surfaces as a result of wear, which is a process of surface interaction. Plastic deformation wear is often referred to as dimension loss. Wear and degradation of metal surfaces are caused by plastic deformation. The friction coefficient and wear behaviour are influenced by various parameters like sliding velocity, lubrication, surface roughness, relative humidity and normal load. Several investigations have been performed to find the effect of contact geometry, temperature, material, vibration and stick-slip on coefficient of friction and wear rate [57-67]. The parameters which determine the alloys and metals tribological functioning mainly is sliding velocity and normal load. Pure aluminium and aluminium alloys are typically employed in applications where corrosion is a concern. In applications where minimal friction is required, aluminium alloys are treated as bearing material [68]. Cu alloys are used as bearing material in applications where high wear resistance is required [69]. Al, Cu. Pb, Sn alloys are treated as steel bearing coating materials because of their higher wear properties [70-72]. At higher load environment in several metallic alloys with load, coefficient of friction decreases because of increased surface roughness and high volume of wear debris [73, 74]. Because of the differences in alloys, the coefficient of friction can either decrease or rise with increasing sliding velocity. Through the process of friction, with increase in sliding velocity, friction also increases due to increase of adhesion pin on disc [75]. The wear test is normally carried out through sliding wear environments with pin-on-disk tests. However a large amount of hard reinforcements normalize wear resistance, and the wear rate is highly improved due to abrasive wear behaviour of reinforcement [76]. It is observed that the addition of alloys such as Cu, Si, Mg and Ni can enhance the tribological and mechanical properties of Al-Zn alloys [77-80]. Cu is a useful reinforcement addition in the direction of enhancing tribological and mechanical properties of Al alloys [81-83].

Dewan and Mohammad observed the coefficient of friction and wear behaviour of aluminium and copper disc using steel pin slides. Then found from the investigation that wear rate and coefficient of friction of copper at normal load and sliding velocity are considerably lower than aluminium [84]. An experimental investigation was carried out by Adel et.al on wear behaviour and friction of Al-Mg-Cu alloys and Al-Mg-Cu composites with SiC particles. The study aimed to find out the effects of copper addition as an alloy and SiC as reinforcement to Al-4Mg metal matrix. It was

observed that the amount of loss in wear test of Al-Mg-Cu alloy decreased unceasingly up to 5%. Also it was observed that SiC particles play an important role in enhancing wear resistance of Al-Mg-Cu alloys [85]. An experimental investigation was carried out by Rama and Brahma Raju on improving mechanical properties of Al-5%Cu alloy with various ZrB2 content. It was discovered that the wear mechanisms of Al-5%Cu converted to abrasion wear and then to adhesion wear predominantly with the addition of ZrB2. At the end of the day, it was determined that this class of materials shown good compression strength, high hardness and reduce the wear rate. [86]. Miyajima et.al [87] investigated the influence of various reinforcements on the wear behaviour of Al-Cu alloys produced through infiltration method and stated that the composite samples wear behaviour depends on the type and amount of reinforcement. Wang et al. [88] concluded that at lower loads, the composite sample wear resistance was higher and at higher loads it was lower.

2.4. Formability and Densification behaviour

The existence of porosity in powder metallurgy samples after sintering reduces the mechanical properties. Because of reduction in mechanical properties to enhance density, the samples were exposed to other processes, namely extrusion, forging and hot deformation; therefore, density increase in component because of plastic deformation is represented as densification. The final value of density fixes the ability and life of powder metallurgy samples because cracks occur and lead to failure of the component. To produce the desired powder metallurgy samples with superior properties without cracks, it is very important to know the forming limit of material. Formability mostly affected by parameters such as ductility and process parameters. Therefore, the formability behaviour of preforms was analysed until the cracks begin on the cylindrical preform at the outer surface. The densification behaviour was affected by some parameters such as, initial relative density, temperature, friction, deformation load, aspect ratio so on. Narayan and Rajeshkannan [89, 90] focused on the influence of different carbide compositions with aluminium on the stress ratio parameters, relative density and workability at various aspect ratios such as 0.4 and 0.6. It was observed that titanium carbide preforms showed good workability characteristics and densification rate. It was found that highest densification and better workability was achieved by aluminium-4% titanium carbide composite. A study on the workability behavior of Al-Cu sintered preforms was carried out [91, 92]. The parameters impacting, the workability behavior of Al, Al-3%Cu, and Al-6%Cu sintered performs in the course of cold deformation were investigated.

Cold deformation of sintered preforms was carried out with various frictional conditions such as no lubricant, zinc-stearate and graphite lubricant. They found that the lower (0.45) aspect ratio composites with no lubricant achieved higher densification, better workability characteristics and axial stresses. They also found that while the addition of copper as reinforcement to the aluminium was possible, the copper reinforcements (3% and 6%) should not be used. [91] And [92] developed the forming limit plots for Al-Cu preforms under various copper content and preform densities. It was observed that at similar working conditions, with an increase of Cu content in composite, the densification increased. Liu and Wang, [93] investigated the influence of bonding interface on strain rate as well as deformation temperature through hot deformation of Cu/Al laminated composites. They found that to attain interface coordination during deformation, hard copper layer should produce higher tension on the adjacent soft aluminium layer to maximize the dislocation slip resistance significantly. Deformation at highest temperatures tends to dynamic softening of Al matrix, which leads to dynamic recrystallization. Ahasan et al. [94] Showed that, with the addition of titanium bi-carbide (TiB_2: 5%, 10%) to Al, changed densification significantly. The, report also established the association between relative density and stress ratio parameters such as (σ_θ/σ_z), (σ_z/σ_m) and (σ_{eff}/σ_z) under triaxial stress state condition. Canakci et al. [95] focused on 2-layered structure of Al-10wt. %B_4C / Al fabricated through powder metallurgy and observed the microstructural, physical (density), and mechanical properties.

2.5. Microstructure evolution and constitutive Modelling

In the forming process, the important technological aspects are the metal and alloy both of which are controlled by grain size, because grain size plays an important role and is closely related to the mechanical performance and properties of the desired product. Through hot deformation Dynamic Recrystallization (DRX) plays a key role in the microstructure and grain size control that decreases the resistance of material [96, 97].

Hot upsetting process is an essential test in the making of engineering tools which demand dimensional accuracy along with appropriate mechanical and microstructural properties. Thus, it is required to study and predict materials behavior while hot upsetting [99]. Therefore, while compression, various experiments has been carried out by [99-101] to know deformation behavior at high temperatures. To show metals working as good and effective it is necessary to examine the constitutive equations at different strain, strain rate and temperatures. An experimental

investigation was done on Al 3003 alloys hot deformation behavior by Guo et al. [102] at different strain rates and temperatures. They concluded that with temperature increase there is a decrease in flow stress.

The flow behavior of Al and its alloys plays a dominant role in designing developing mechanical working processes. The material flow stress was affected by hot upsetting conditions like reinforced material, microstructure, strain, strain rate and temperature. During hot upsetting, the forming energy and microstructure were influenced by dynamic recrystallization (DRX), work hardening (WH) and dynamic recovery (DRV). Therefore, to show better results in metals, it is necessary to explore flow stress, hot upsetting process and expansion of the constitutive model.

Dynamic recovery happens more than dynamic recrystallization in aluminium alloys because of the high stacking fault energy [103]. Several constitutive type of investigations of Al alloys were done by whole hot compression method by [104-107], and flow stress acts as a function of strain, strain rate and temperature.

An experimental investigation was carried out by Liu et.al. [122] on hot upsetting behavior of aluminium alloy and then stated that dynamic recrystallization (DRX) was highly sensitive to hot upsetting temperature than to strain rate. An investigation was carried out by Wolla et.al. [108] on the hot upsetting constitutive base of Al-4%Cu powder metallurgical preforms. The results revealed that the flow stress is especially affected by strain rate, relative density and temperature and the flow stress shows peak value at a particular strain value.

Basically, constitutive equations define materials behavior and are interrelated with deformation temperature, strain rate and flow stress. To foresee the constitutive behavior in alloys and metals several phenomenological, empirical, artificial neural network, physical and analytical patterns have been designed [109]. High-temperature flow behaviour of aluminium alloy AA2030 was investigated experimentally by H.R. Rezaei and colleagues using strain-dependent constitutive models to predict the behaviour of the alloy at high temperatures. From the result it was observed that there was a better bond between calculated and predicted results [98]. An experimental investigation was done on Fe-36wt%Ni Invar alloy by [110] to forecast flow behavior using Arrhenius- type equation. The results revealed that the generated constitutive equation have consistent and unchanging capability at various temperatures to forecast material hot flow

behavior. In the meantime, as per generated constitutive equation, Zener-Holloman parameter map was formed and it was used to predict the amount of dynamic recrystallization.

From the past few years, many experiments has been conducted by researchers on evaluating of grain size in alloys and metals because of the grain size effect on manufactured products mechanical properties. Normally, the material grain size is influenced by deformation conditions like initial microstructure, strain rate, material composition, temperature, initial relative density and strain. During the forming process, DRX grains of materials here influenced by deformation conditions, a phenomenon studied by some researchers [111-114]. It is important to observe the bonding between DRcrx grains and deformation conditions, to achieve high hardness, wear resistance and strength while hot upsetting alloys and models. An experimental investigation was carried out by Shban and Eghbali [112] on Nb -Ti steel alloy through hot torsion method. The results revealed that the DRcrx grains are highly impacted by hot upsetting conditions and establishing bonding with steady strain, critical strain, Zener-Hollomon parameter and DRcrx grain size. An investigation was carried out by Guo et al. [115] and Li.et al. [111] on the development of microstructure and DRcrx grain size of 625 Inconel super alloy. According to the findings, the influence of deformation temperatures on the mechanisms of nucleation of DRX is significant, and the volume fraction and size of the DRcrx grains rise as the temperature of the deformation increases. Some of the researchers studied the influence of deformation situations on the DRcrx grains and microstructures of the cast material and developed an association between Zener-Hollomon parameter and DRX grain size [112, 113, 116, 117]. The behavior of DRX grains and microstructure of powder metallurgical sample after deformation is different from before deformation of the sample (fully dense) [118]. Powder metallurgical sample generated through the process of plastic deformation experienced densification hardening and geometric hardening because of increase of flow stress and work hardening of the material [119]. Due to considerable quantity of pores existing the powder metallurgical preforms, it was observed that the density was distributed unevenly in powder metallurgical samples at low initial relative densities, because of high friction between the work and the tool [120]. Thus, DRX grains, microstructure and deformation behavior of cast material are not appropriate for porous materials developed by powder metallurgical method with a similar chemical composition [121].

2. 6. Gaps in the literature survey

Following a thorough review of literature, the following are some of the major limitations in the existing literature on processing powder metallurgy parts:

I. There is limited literature available on the study of properties on hot-pressed Al-Cu two-layered composite such as hardness and corrosion.

II. There is no literature available on the study of formability of sintered Al-Cu two-layered composite related to its process parameters of strain rate, temperature and porosity.

III. The deformation behavior of sintered Al-Cu two-layered composite with various initial relative densities at different temperature and strain rate conditions has not adequately been explained.

IV. Mathematical relations to predict the DRX grain size of sintered Al-Cu two-layered composite after plastic deformation considering the effect of temperature, strain rate and initial relative density are limited.

V. There is no literature available on the study of wear properties on hot-pressed Al-Cu two-layered composite such as COF, Wear rate.

2. 7. Objectives and Scope

Based on the gaps identified from literature on the deformation of P/M components during hot working, the following objectives were formulated. The main objectives of the thesis are:

I. To study the effect of sintering temperature and properties of hot-pressed Al-Cu/Al two-layered composite structure by powder metallurgy.

II. To investigate Wear behaviour of hot-pressed Al-Cu/Al two-layered composite structure by powder metallurgy.

III. To study the formability and densification behavior of two-layered structure powder metallurgical hot-pressed Al-Cu/Al composites during hot-upsetting.

IV. To model the microstructure of dynamic recrystallized grain size of two-layered structure Al-Cu/Al composites during hot-upsetting.

Chapter 3

Experimental Details

This chapter describes the details of experiments conducted for a) material selection, b) sample preparation, c) corrosion test, d) wear test, e) hot upsetting test and f) metallurgical analysis by an optical microscope.

3.1. Selection of materials

The materials chosen for the present investigations were pure aluminium (Al) powder and copper (Cu) powder. Atomized aluminium powder (Al) of particle size 44µm and purity of 99.47% were chosen while the rest were insoluble impurities. Copper powder (Cu) of particle size 44µm as used as reinforcement while Al had a purity of 99.99% and both were procured from SR. Laboratories, Mumbai, India. Al alloys are commonly employed as matrix materials because of their light weight, high elastic modulus and strength, as well as their good wear resistance [16] and copper is one of the good reinforcements. Aluminium alloy can be enhanced by reinforcement with other materials and heat treatment to make composite due to its lightweight which can be loaded and heat-treated to comparatively higher level stresses at low cost [17]. By the copper addition to aluminium, increases creep resistance and fatigue, hardness, tensile strength and machinability [9].

Moreover, literature studies related to the deformation, densification and microstructure evolution studies of the candidate materials are scarce. P/M processed components have superior practical and industrial importance than corresponding wrought material of the same composition. The aluminium and copper material properties are tabulated in Table 3.1.

Table 3.1 Properties of aluminium and copper

Parameters	**Al**	**Cu**
Molecular Weight (g/mol.)	26.98	63.54
Theoretical Density (g/cm^3)	2.7	8.96

Color	Dark gray	Red-orange metallic luster
Crystal Structure	FCC	FCC
Tensile Strength (MPa)	90	210
Yield Strength (MPa)	50	137
Young's Modulus (GPa)	70	120
Shear Modulus (GPa)	26	48

3.1.1. SEM, EDAX and XRD

Aluminium and Copper particles of morphologies were examined using a scanning electron microscope to determine their particle size and form. Aluminium and Copper powders, illustrated in Figs. 3.1 and 3.2, respectively, aluminium particles in the combined form of semi-spherical and elongated rod shape and copper particles as flaky shape, which are consistent with their compositions. The morphology and Energy-Dispersive X-ray Analysis plot of as-received copper (Cu) particles is shown in Fig. 3.3. EDAX peaks corresponding to the Cu were found in good agreement. The microstructure of powders and hot-pressed samples were carried out using an optical microscope and the scanning electron microscope (SEM: Tescan Vega 3 LMU). The compositional analysis of Al-Cu two layered structure was carried out by energy dispersive spectroscopy (EDS: Oxford Instruments). Metallographic sample preparation was done to reveal the microstructure of hot-pressed samples. The polishing of samples was carried out using grinding, disc polishing with silicon carbide papers up to 2000 grade and they were further polished to mirror finish by using alumina liquid suspension. The surface of these samples was etched with ammonia (50%) and distilled water (50%) solution for a few seconds. The microstructural characterization of etched and fracture surface of samples were inspected with SEM-EDS (Fig. 3.4 (a)). The elemental quantification of the Cu-Al alloys was measured using the electron probe micro-analysis (EPMA: Camebax Micro, Cameca). The phase analysis of starting, milled powders and the sintered compacts were carried out by X-ray diffraction (XPERT-Pro, Pan Analytical), using CuKα radiation (λ=1.5405Å), which was operated at 45 kV and 30 mA (Fig. 3.4 (b)). The volume fraction of individual phases in the hot-pressed samples was estimated by the Rietveld

analysis of XRD patterns. The XRD data were collected at a scanning rate of 0.0166 o/sec and the patterns analyzed by X'Pert High Score software with Inorganic Crystal Structure Database (ICSD). For dislocation density measurements, the curve was fitted after stripping the Kα2 component from the raw data using X'Pert High score software. The full width half maximum (FWHM) values and diffraction angles of major peaks from the X-ray diffraction patterns were considered for Williamson–Hall analysis.

3.2. Specimen preparation

3.2.1. Mixing of powders

The required mass of aluminium and copper powders (5%, 10% and 15%) was accurately weighed using electronic mass balance (± 0.01 mg repeatability) and mixed in a pot mill for 2 hrs. to get a homogeneous mixture. The homogeneous powder mix has the advantage of improving sinter-ability of the powder and making ejection of compaction easy. Fig. 3.5 shows that SEM analysis revealed the blended Al-Cu morphology was homogenous.

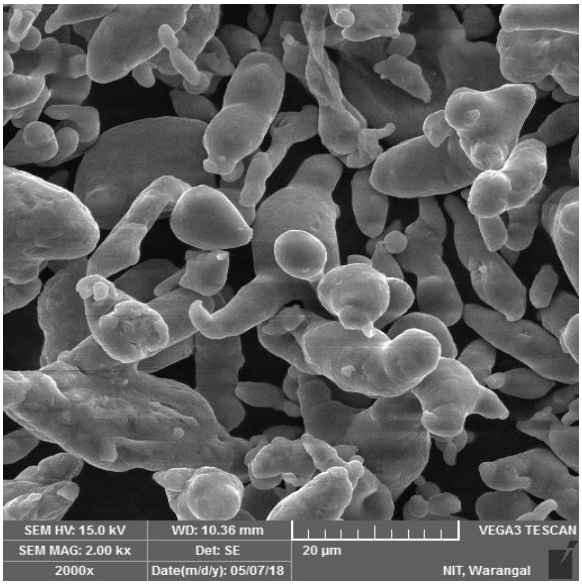

Fig. 3.1 SEM image of Aluminium particles

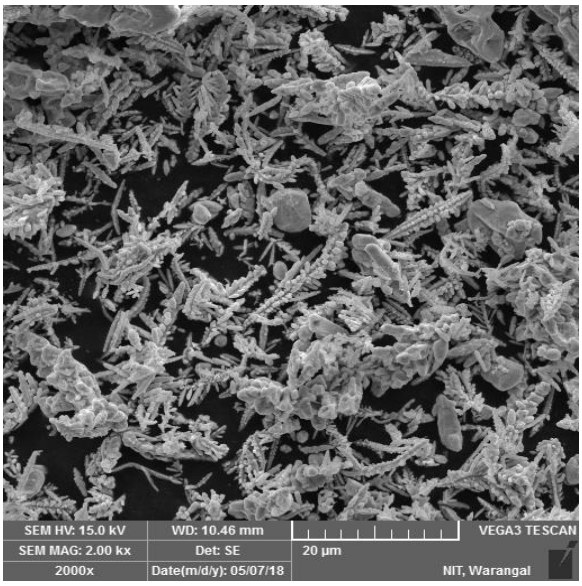

Fig. 3.2 SEM image of Copper particles

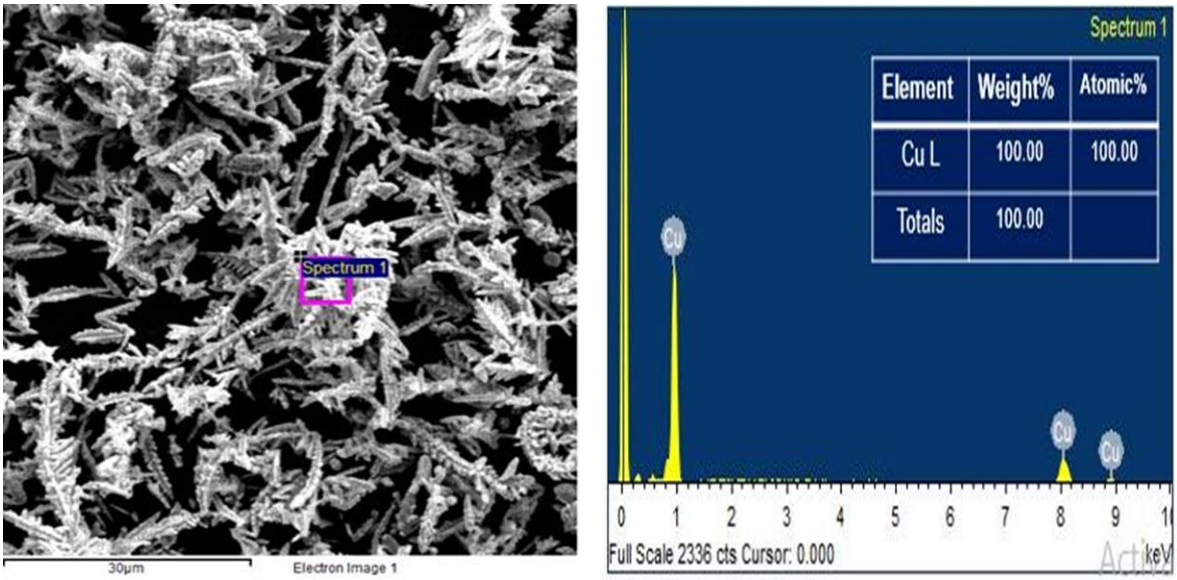

Fig. 3.3 EDAX analysis of Cu

Fig. 3.4 (a) Scanning electron microscope and (b) X-ray diffraction equipment

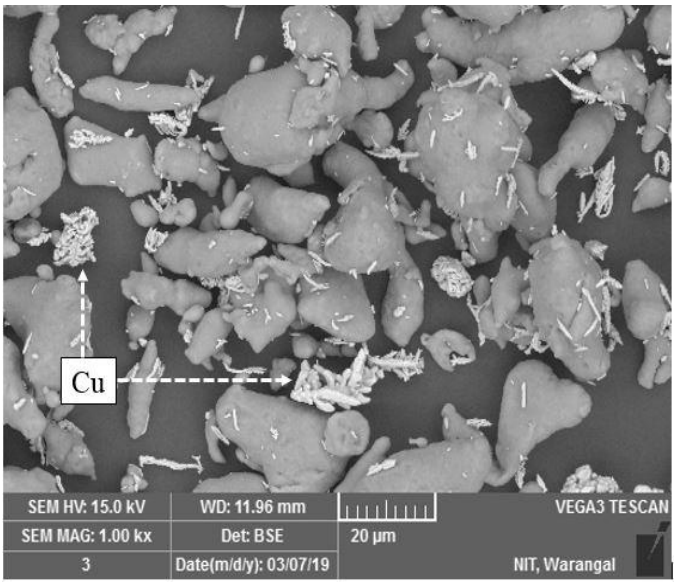

Fig. 3.5 Scanning electron microscope image of Al-Cu composition

3.2.2. Dealing out with the two-layered Al-Cu/Al samples

Sintering temperatures were maintained at 550°C for 45 minutes under 400MPa hydraulic ram pressure in an atmosphere of (1.3×10^{-2} mbar), as depicted in Fig. 3.6 of the hot press (Model:

CMM, VB Ceramic Consultants, India) which was used to consolidate Al-Cu and Al powders. At a rate of 10 ^{o}C/min throughout the heating cycle of hot pressing, sintered samples were expelled from H13 steel die at room temperature after the furnace had cooled.

Fig. 3.6 Hot press equipment with vacuum pump arrangement

The samples had a diameter of 15 mm and a height of 15 mm when they were made. Weighing balances with precision weighing capabilities were used to calculate the density of hot-pressed samples, which were connected to the density were calculated system (Model: BSA224S-CW, Sartorius). The samples with bulk density determined using Archimedes approach, which was performed in accordance with ASTM B962-08. The bulk densities of several compositions were standardised with respect to theoretical density in order to examine the densification responses of different compositions.

3.2.3. Measuring the mechanical characteristics

Polished samples were tested for 15 seconds at 300 g force in a Vickers Micro-Hardness Tester (Shimadzu, HMV, Japan) in accordance with ASTM E384-11e1 specifications. The image of the Vickers microhardness tester is shown in Fig. 3.7. To determine the hardness of the material, a minimum of three indentations were produced.

Fig. 3.7 Photograph of Vickers microhardness tester

Fig. 3.8 a picture of a Universal testing machine is shown. An (Instron, Model No: 5982, USA) Universal Testing Machine (UTM) was used to conduct the compression test for both pure aluminium and Al-10wt. %Cu composites at a strain rate of 0.02 mm/min. During the compression test, grease was applied to the top and bottom specimen-platen surfaces on both sides of the specimen in order to prevent friction and wear during the test. For the compression test, a set of cylindrical samples of diameter (d) of 10 mm and length (l) of 15 mm, and a length-to-diameter ratio of 1.5, were manufactured, and the diameter and length measurements were used to determine the compression strength. A minimum of two measurements were taken for the purpose of reporting the findings of the compression test, which was performed.

Fig. 3.8 Universal testing machine

3.2.4. Wear behavior test

In order to determine the wear resistance of Al-Cu/Al two-layered composites, a pin-on-disc wear test equipment was used (Ducom Bangalore, Model: TR-20). As seen in Figure 3.9, a configuration for pin-on-disc wear testing was used (a). The specimens were ground up to 1500 grit SiC abrasive paper in order to achieve total contact with the counter body during the testing process. Polished specimens were properly cleaned with ethanol prior to the testing procedure. The cylindrical samples (10 mm x 15 mm) used in the wear testing were produced in advance. For each sample, the samples with a contact area of 78.5 mm^2 were kept in original condition. It was necessary to measure the initial and end weights of samples using an accurate analytical weighing balance with a resolution of less than 0.0001 g.

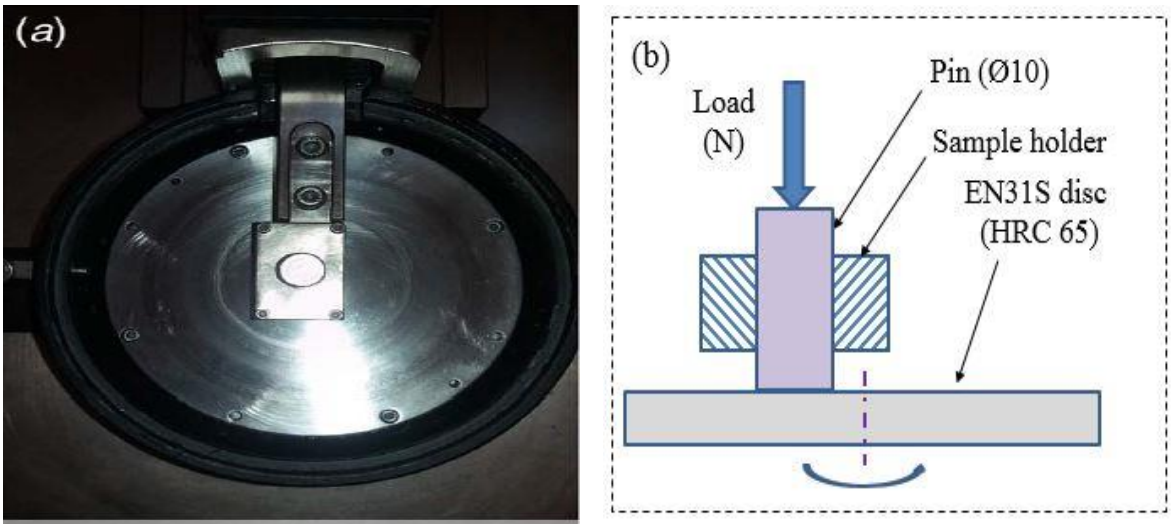

Fig. 3.9 (a) Surface of the pin on disc and (b) Pin on disc schematic representation

The wear behavior of two-layered Al-10 %wt. Cu/Al composite was tested by using pin-on-disc testing machine (Model: TR-20, Ducom Bangalore), parameters influencing the wear behaviour can be adjusted such as sliding speed, distance and applied stresses. Under a sliding velocity of 5 m/s and a maximum load of 39.2 N in conditions of dry sliding, the pin-on-disk wear test followed ASTM G99 standards. The pin-on-disc test configuration is depicted in Fig. 3.9. The wear test samples had a size of Ø10×15 mm and were manufactured in this manner. Primarily the wear test was conducted at the end phase of Al layer and then conducted at the other end phase of Al-Cu layer and lastly at the interface region by cutting the interface region with a wire cut machine. For the wear test, Al-10wt %Cu/Al composite samples were polished with silicon carbide sheets with a grit size of 1500. For the tests to be done in a temperature-controlled environment, the experimental preforms were kept in same circumstances and were tested in same place (room) to ensure that the environment had the least impact on wear. The composites were polished with 400, 600, and 800 grit sandpapers in order to maintain a consistent surface roughness throughout the samples. In order to remove any undesired particles that could interfere with wear testing, the preforms were properly cleaned by acetone while going to test. By polishing the disc after each trial, the average Ra (surface roughness) of the disc was maintained at 1.86 microns for the duration of all experiments. The counter body for the wear test was an EN 31 Grade steel disc (C: 0.90-1.20%, Si: 0.10-0.35%, Mn: 0.30-0.75%, Cr: 1.00-1.60%, S: 0.05%, and P: 0.05%) with a hardness of 65 HRC. The trials were performed at 3(three) applied loads of 19.6 N, 29.4 N and

39.2 N. When the weights were applied, the applied pressure was 0.5 MPa. When the weights were greater than 39.2 N and the speeds higher, the samples were more likely to break. When the loads were lower than 19.6 N, there was no repeatability in the testing, and the wear rates recorded at 39.2 N load deviation were approximately 50 percent higher. As a result, the minimum and maximum loads in the investigation were established at 19.6 N and 39.2 N, respectively, and intermediate load of 29.4 N was taken to examine the behaviour. Various sliding speeds were taken throughout the experiment in order to investigate the wear attributes of different sliding speeds. The tests were carried out at five different speeds: one metre per second, two metres per second, three metres per second, four metres per second, and five metres per second. Through sliding the preforms for 500 m, 1000 m, 1500 m, and 2000 m, the researchers were able to observe the influence of the sliding distance on the wear rate and coefficient of friction, as well. Multiple runs of the test were carried out, and the findings were averaged together to get the final report.

3.2.5. Corrosion measurement

Working electrodes (Al-5Cu, Al-10Cu, and Al-15Cu) were polished with emery papers up to 2000 grit size and then completely cleaned with distilled water after which they were dried. Corrosion experiments were carried out using a three-electrode cell glass association with Al-Cu/Al interface as a working electrode with an exposed area of 0.7854 cm^2, Ag/AgCL/1M KCl electrode taken as a reference electrode, and a platinum spiral electrode as a counter electrode after polishing. A neutral 3.5 mass per volume (m/v) percent NaCl solution (pH: 8.2) was used for all electrochemical tests, which were carried out at room temperature in a stagnant and naturally aerated solution. The electrochemical impedance spectroscopy (EIS) research and polarisation experiments were carried out with the help of a PARSTAT 4000 Potentiostat/Galvanostat system shown in Fig. 3.10.

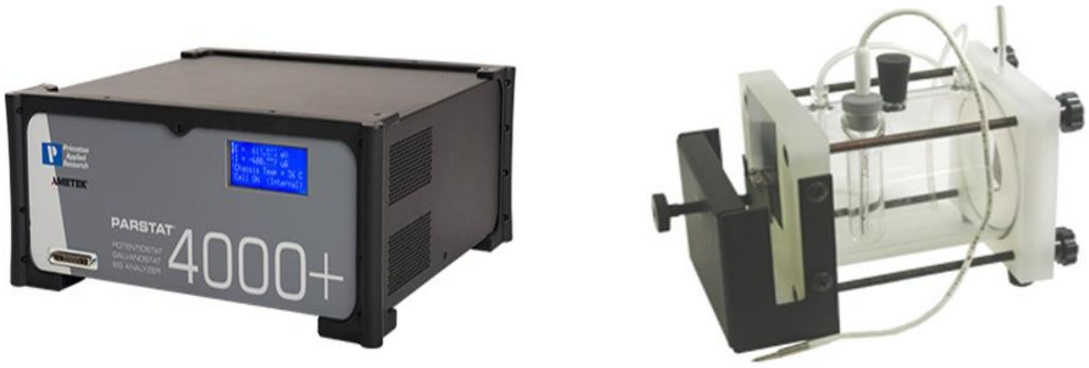

Fig. 3.10 Photograph of the corrosion test setup. (a) Corrosion work station and (b) corrosion test cell

Saturated calomel and hydrogen electrodes were used as reference electrodes to measure the electro-potentials. Measurements of impedance (Z) in the frequency range 0.1 Hz to 60 kHz were made during the polarisation studies, with a scan rate of 1 mVs^{1}. The AC signal's amplitude was set to 20 mV with a peak to the peak measurement system's output. For the sake of reproducibility, all electrochemical tests were repeated at least twice. Morphology of the Al-Cu alloys outer surface was studied using SEM-EDS after conducting electrochemical tests.

3.3 Hot deformation test

3.3.1 Formability and densification behaviuor

The initial dimensions of hot-pressed preforms such as height (H), diameter (D) were measured and taken for initial preform density calculations. The hot-upsetting was carried out at various deformation temperatures such as 150 ^{0}C, 250 ^{0}C, 350 ^{0}C, and 450 ^{0}C for different Cu composition of preforms. After attaining the required temperature, the preform was soaked for 30 min before deformation. The hot upsetting process was performed between two flat dies inside a muffle furnace (an electrical resistance type) placed on a robust bed of hydraulic machine until a visible crack appeared at the outer surface. Seven preform samples were taken for each test and hot deformed with an incremental compressive load. After the deformation, dimensional changes such as final height (H_f), top contact diameter (D_{tc}), bottom contact diameter (D_{bc}), bulged diameter (D_b) of the preforms were measured using a vernier caliper.

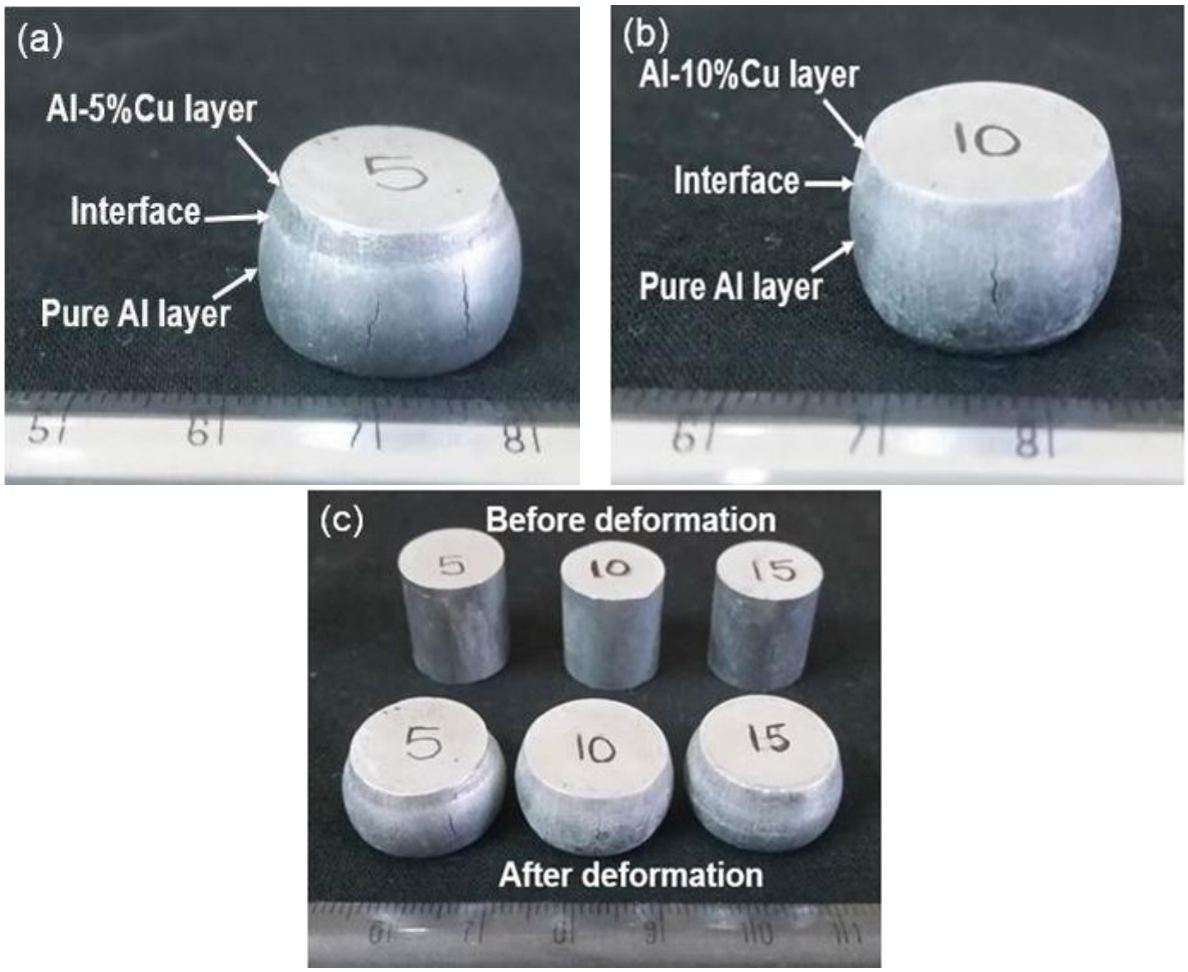

Fig. 3.11 Photographs of performs at various Cu compositions (a) 5wt. % after deformation, (b) 10wt. % after deformation and (c) 5wt. %, 10wt. % and 15wt. % before and after defamation

Before and after the hot-deformation of Al-Cu/Al preforms with various compositions of Cu (5wt. %, 10wt. %, and 15wt. %) in the Al-Cu layer are shown in Fig. 3.11(c). It is observed from Fig. 3.11(b) that the deformation behavior in Al-Cu layer was almost equal to that of soft pure Al layer in 10wt. % content preform than 5wt. % Cu and 15wt. % Cu content preforms. The copper particles were fewer at the grain boundaries in Al-5wt. % Cu layer of preform, which causes precipitation of intermetallic phases in grain boundaries. $CuAl_2$ intermetallic phase's precipitation at grain boundaries stopped grain movement during deformation at the interface region. Therefore, the deformation behavior in both Al and Al-Cu layers were non-homogeneous in 5wt. % Cu content preform, as shown in Fig. 3.11(a). The addition of 10wt. % Cu into the Al-Cu layer, lead to intermetallic precipitations dispersed the grains into grain boundaries, which would result in an

increase of dislocation slip with expansion continuing in Al-Cu layer with Al layer. The deformation behavior in both Al and Al-Cu layers was homogeneous for 10wt. % Cu content preform, as shown in Fig. 3.11(b).

3.4 Pin sample preparation

The pin samples were fabricated through powder metallurgy (P/M) technique under hot-press condition. The purchased Cu powder was blended with the Al powder with various percentages of copper (Cu) content (5wt. %, 10wt. % and 15wt. %) by mortar mixer to make a homogeneous mixture. The blended powders were poured into the steel die and the compacts were prepared under the pressure of (400 MPa) using 0.5 MN hydraulic press under various hot-pressed conditions such as 500 ^{0}C, 550 ^{0}Cand 600 ^{0}C for 3h. Zinc stearate was used for lubrication purpose and it is applied on the contact surfaces of dies, top and bottom punches before the compaction. The geometry of prepared composites was (Al layer thickness: 10 mm, Al-Cu layer thickness: 5 mm and diameter: 15 mm). The schematic representation of three different types of Al-Cu/Al composites were hot-compacted as layer after layer each in a stepwise manner with various Cu percentages (5wt. %, 10wt. % and 15wt. %) as shown in Fig.3.12 (a). The photographs of before and after wire cut composites across the section as shown in Fig.3.12 (b).

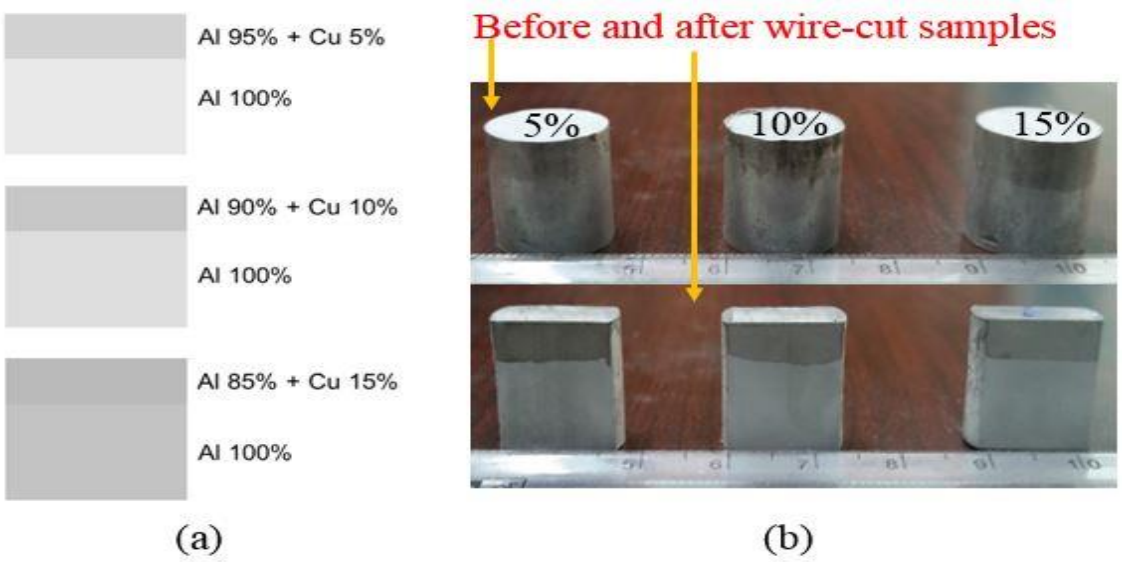

Fig 3.12 (a) schematic representation of hot pressed two-layered composites, (b) photograph of before and after wire-cut composite samples.

Chapter 4

Effect of sintering temperature and properties of hot-pressed Al-Cu/Al two-layered composite by powder metallurgy

4.1. Introduction

The present work is focusses on the study of properties like microhardness, density and corrosion behaviour of hot pressed Al-Cu/Al two-layered composite. The properties were mostly depend on the sintering temperature and the percentage of reinforcement added to Al-Cu layer of the composite. Aluminium alloy can be enhanced by reinforcement with other materials and heat treatment to make the composite lightweight and this can be loaded and heat-treated comparatively higher level stresses at low cost. The addition of copper to aluminium, increases creep resistance and fatigue, hardness, tensile strength and machinability. Generally copper decreases resistance and corrosion while stress corrosion susceptibility occurs due to particular material conditions and compositions. The Al-Cu alloys microstructure plays a dominant role in alloys corrosion and mechanical behaviour.

Aluminium matrix was hot-pressed at 500 ^{0}C, 550 ^{0}C, and 600 ^{0}C for three hours at a constant pressure of 400 MPa with varying percentages of Cu content (x: 5wt. percent, 10wt. percent, and 15wt. percent) in aluminium matrix. Optical and scanning electron microscopes were used to examine the microstructure of two-layered samples. It was found that the maximum micro-hardness (100.6 HV) was found at 15wt. percent Cu sample interface at 550 ^{0}C. With increasing copper content, potentiodynamic polarisation tests revealed an increase in corrosion susceptibility of Al-Cu/Al two-layered samples at the interface. For EIS test, it was determined that the best-fit circuit model is the one that delivers the lowest chi-square value, and that circuit model was used as the best-fit model. The EIS results showed that a 10wt. percent Cu sample circuit had the lowest chi-square value.

4.2. Results and Discussion

4.2.1. Analysis of microstructure

The hot-pressed two-layered composite samples were cut vertically into two pieces using wire-cut machine for investigating the microstructure at the interface. Initially, the surface of the sectioned composite specimens was polished using different types of silicon carbide (SiC) emery papers and this was followed by disk polishing to achieve mirror finish polish. The detailed microstructures at the interface of the composite samples were analysed using the optical microscope. It is observed from Fig. 4.1 (a-i) microstructures that bright phase was Cu content in the dark phase of Al matrix. Also, a macroscopic interface was observed in which the compositions of the materials were integrated into one another (marked as '▼') as shown in Fig. 4.1. It was found from Fig. 4.1 that the interface of the image was not at macro level in the developed composites shown in Figs. 4.1(a), (d) and (g) and a sharp interface region was present between Al and Al-Cu layer in the composites of 5wt. %, 10wt. % and 15wt. % of Cu as shown in Figs. 4.1(b), (c), (e), (f), (h) and (i). However, a smooth interface region was observed in Fig. 4.1(d) between two layers of Al-10wt. %Cu/Al composite at 550 ^{0}C compared to Figs. 4.1(a) and (g). Therefore, the Al-10wt. %Cu/Al composite showed smooth transition interface at 550 ^{0}C.

Scale bar 200 microns

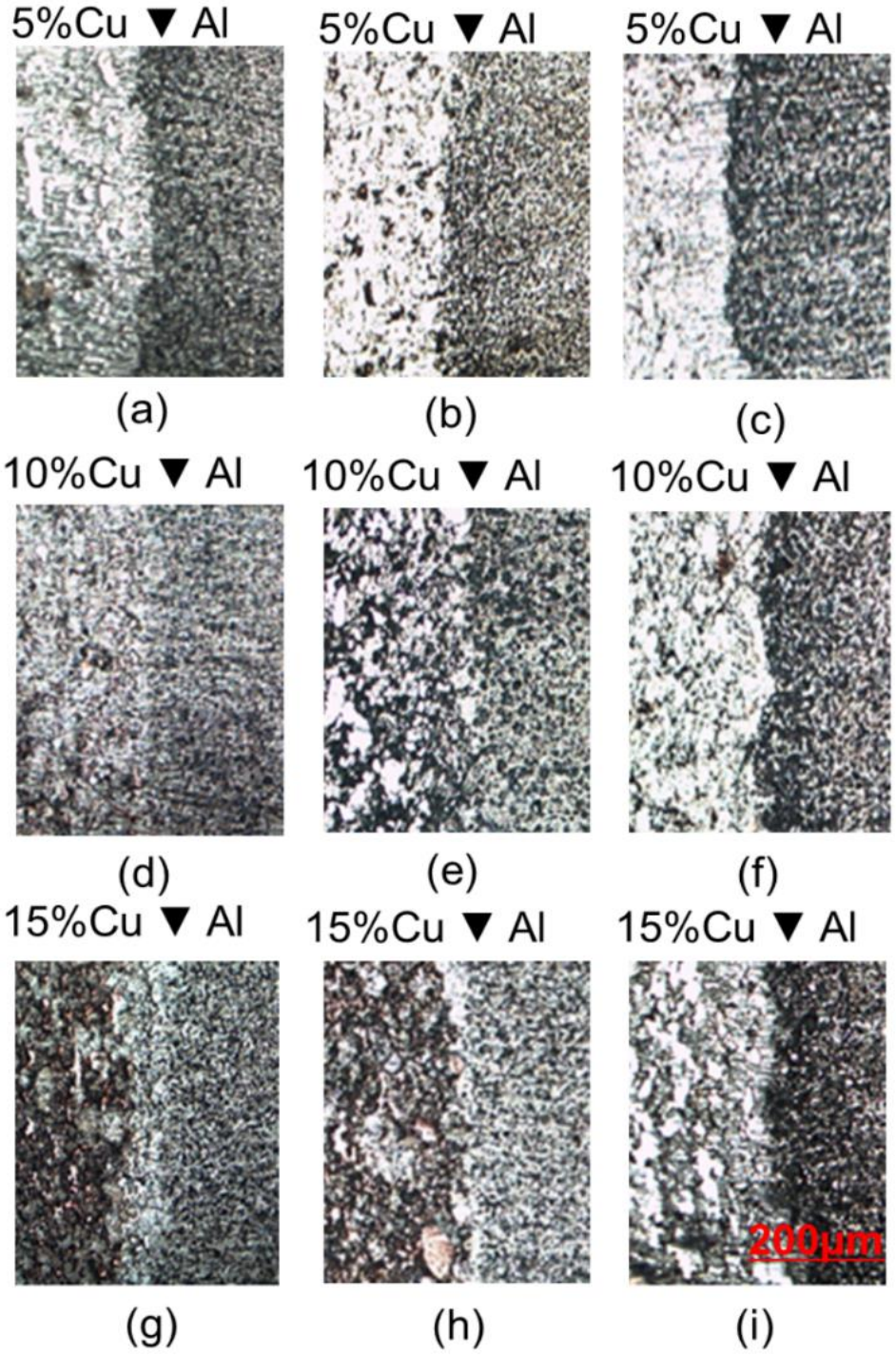

Fig. 4.1 Optical microstructures of Al - Cu / Al two-layered composite samples at interface region under different hot-pressed temperatures, (a) 500 ^{0}C, (b) 550 ^{0}C, (c) 600 ^{0}C, (d) 500 ^{0}C, (e) 550 ^{0}C, (f) 600 ^{0}C, (g) 500 ^{0}C, (h) 550 ^{0}C and (i) 600 ^{0}C

Fig. 4.2 (a-c) shows a clear microstructure with various interfaces. There were no cracks on interface on individual layers, indicating that the composite had good strength and produced good results for hardness and densification. Addition of Cu percentage to Al-Cu layer increases the number of copper particles. The change in microstructure as shown in Figs.4.5 – 4.7 can vary the hardness of the composite samples. The SEM and EDAX analysis of hot pressed Al-10wt. % Cu / Al composites are shown in Fig. 4.2 (d), which confirm the existence of Al-rich and Al_2Cu phases. From the Fig. 4.2 (d), it is seen that pure Al layer surface exposes a dark phase and Al-Cu layer exposes two phases α- grey which is Al-rich phase and θ - bright which is Al_2Cu phase.

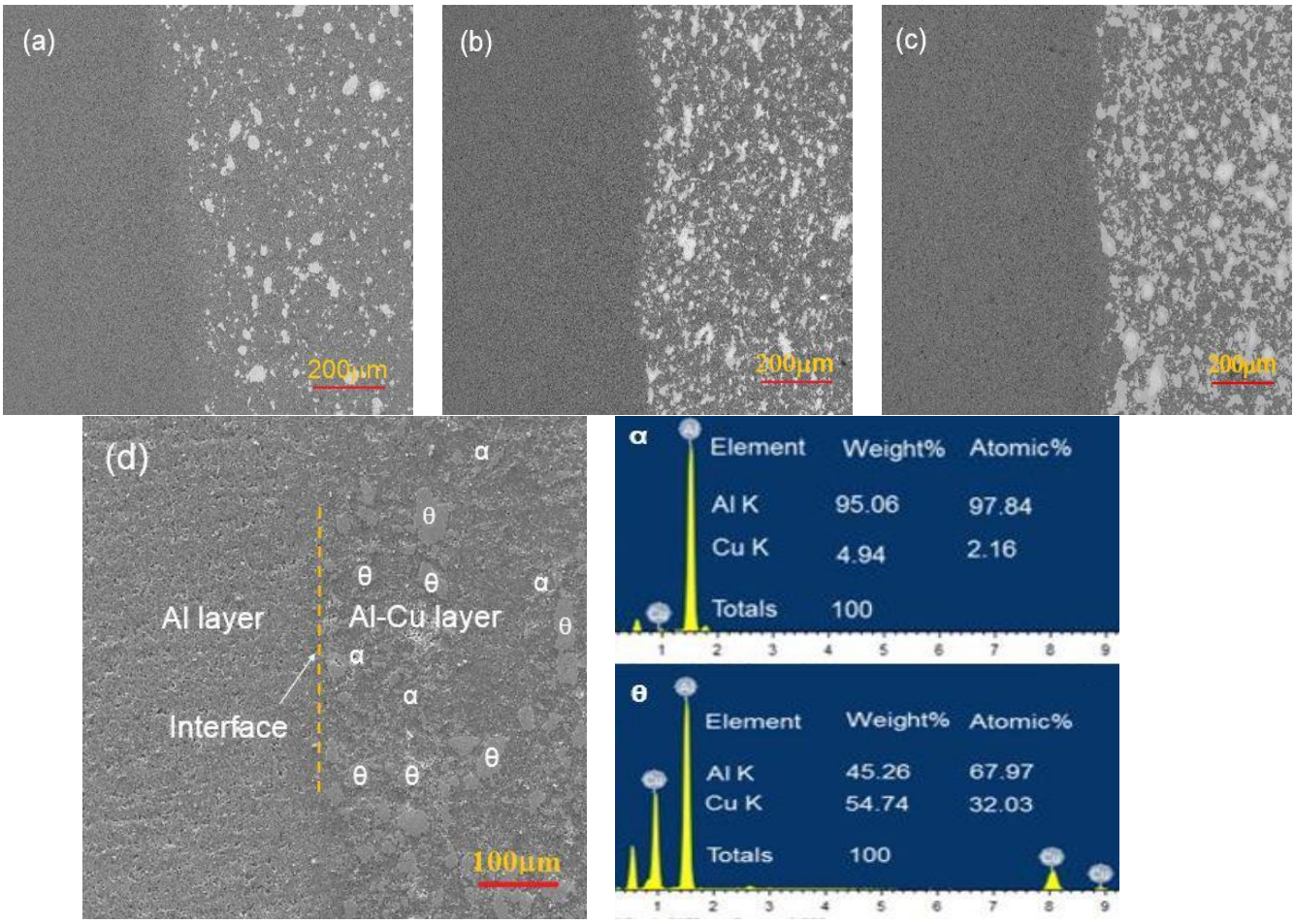

Fig. 4.2 SEM-BSE microstructure images of developed composite samples for different percentages of Cu contents in the Al matrix, (a) 5 %, (b) 10 %, (c) 15 % and (d) SEM micrographs of hot-pressed Al-5Cu/Al composite sample with different phases marked as α-(Al rich) and θ-(Al_2Cu) at interface region and Al-Cu layer with corresponding EDAX

4.2.2. X-ray diffraction (XRD) pattern of composites

Fig. 4.3 shows the XRD patterns of hot-pressed composite samples for different percentages of Cu content (5wt. %, 10wt. % and 15wt. %) in the Al matrix at 600 ^{0}C. The phases which were Al rich and Al_2Cu were formed in the composite samples and the other phases are not present in the material. Also, it is noticed that the peaks of Al contain higher diffraction intensity and the peaks of Al_2Cu contain lower diffraction intensity. The XRD pattern of hot-pressed Al-5wt. %Cu, Al-10wt. %Cu and Al-15wt. %Cu composite samples peaks were matched from JCPDS reference code numbers (Al:98-009-8667 and Al_2Cu:98-012-1659), (Al:98-009-8667 and Al_2Cu:98-008-1747) and (Al:98-009-8667 and Al_2Cu:98-01-3614) respectively.

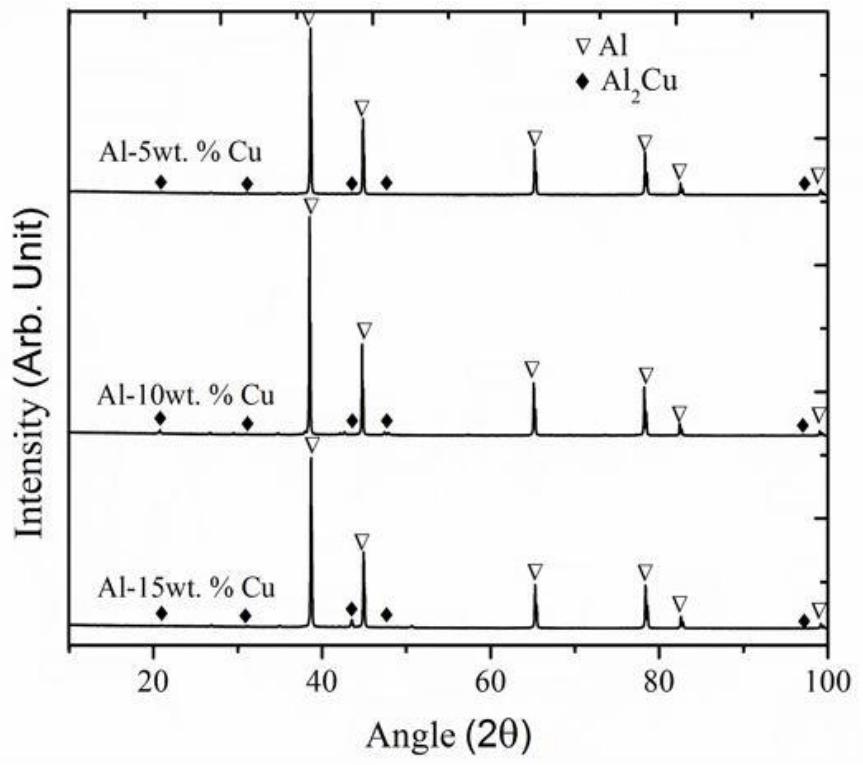

Fig. 4.3 XRD results of hot-pressed samples for different percentages of Cu particles in the Al matrix at 600 ^{0}C with a pressure of 400 MPa for 3 h

4.2.3. Effect of Cu addition and sintering temperature on the density of the composites

The sintered densities of two-layered composites samples were analysed under different working conditions. Fig. 4.4 shows the effect of Cu content on the density of the developed composites for different compositions of Cu (5wt. %, 10wt. % and 15wt. %) in the Al matrix under

various hot compaction conditions (500 ^{0}C, 550 ^{0}Cand 600 ^{0}C). The dwelling time and the pressures were kept constant (3 h and 400 MPa) during the compaction.

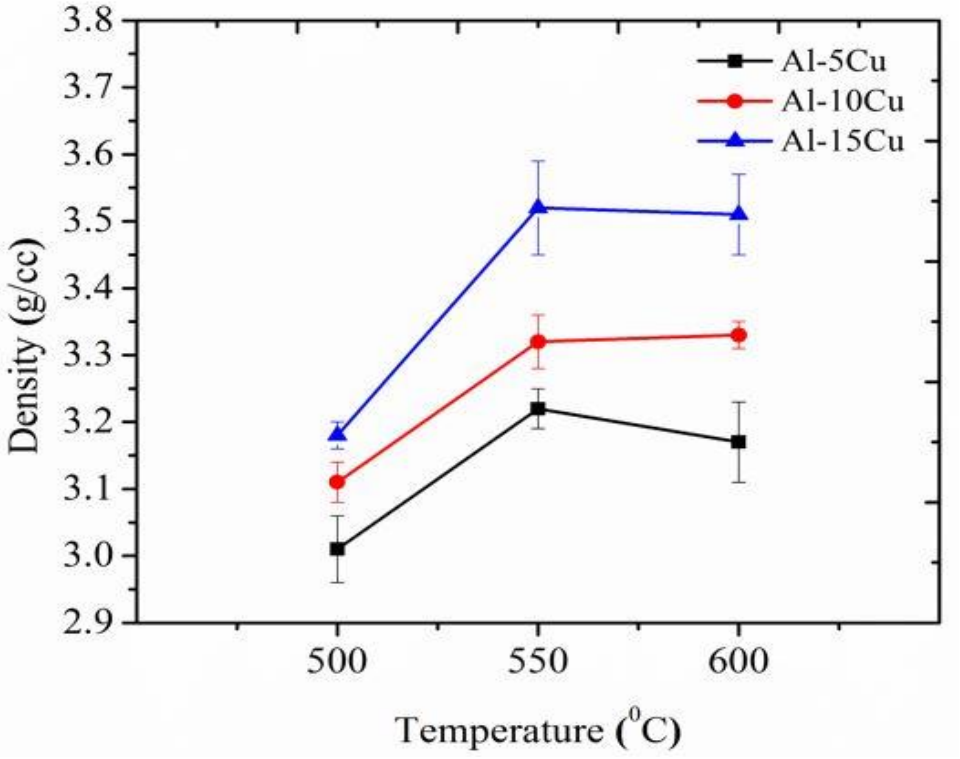

Fig. 4.4 Effect of hot press sintering temperature and different percentages of Cu particles in the Al matrix on density of Al-Cu / Al two-layered composites

It is observed from Fig. 4.4 that the sintered density increases from 500 ^{0}C to 550 ^{0}C rapidly irrespective of Cu composition. It shows a weak decreasing trend with increase in compaction temperatures (550 ^{0}C- 600 ^{0}C). The liquid-phase formation is important in the sintering of Al powder metallurgy samples, the samples sintered at temperatures with no liquid phase (515 ^{0}C – 545 ^{0}C) experienced minimal densification. Further increase of sintering temperature, the quantity of liquid phase would also have increased, leading to more density in sintered samples [123]. Therefore, the highest density was achieved at 550 ^{0}C irrespective of Cu content. Also, it was noticed that the sintered density of the developed samples varied with increase in the Cu percentage in the composite. It is observed from Fig. 4.4 that the sintered density of composite samples increased from 5wt. % to 10wt. % Cu and for further addition of Cu (15 wt. %) it is observed that there was a slight increase in density because of agglomeration formation [124].

4.2.4. Vickers Microhardness

Figs. 4.5 – 4.7 shows the effect of copper addition and sintering temperature on Vickers microhardness of P/M composites. The hardness value in Al-Cu layer and at interface increases from increasing Cu content irrespective of sintering temperatures. Hardness increases with increasing the sintering temperature from 500 ^{0}C to 550 ^{0}C and it was also noticed that there was a slight decrease in hardness with increasing temperature from 550 ^{0}C to 600 ^{0}C. The layered composites show increment in hardness from 500 ^{0}C to 550 ^{0}C indicating the finer dispersion of reinforcement in Al-Cu layer strengthening compositing. At higher temperatures between 550 ^{0}C to 600 ^{0}C there was a drop in hardness value which cloud be attributed to the grain growth in matrix [124]. The Vickers micro-hardness shown in Figs. 4.5 – 4.7 at interfacial zone was measured to specify the consequences of intermetallic compound and chemical composition. The micro-hardness was high at the interface region. It is evident that micro-hardness was higher at interface region than for metal components, which was caused by changes in composition at interfacial zone [125]. As with Al-Cu layer, the hardness value at interface increases from increasing sintering temperature from 500 ^{0}C to 550 ^{0}C and hardness from 550 ^{0}C to 600 ^{0}C decreases. It is also observed that the hardness value increases in Al layer with increasing sintering temperature.

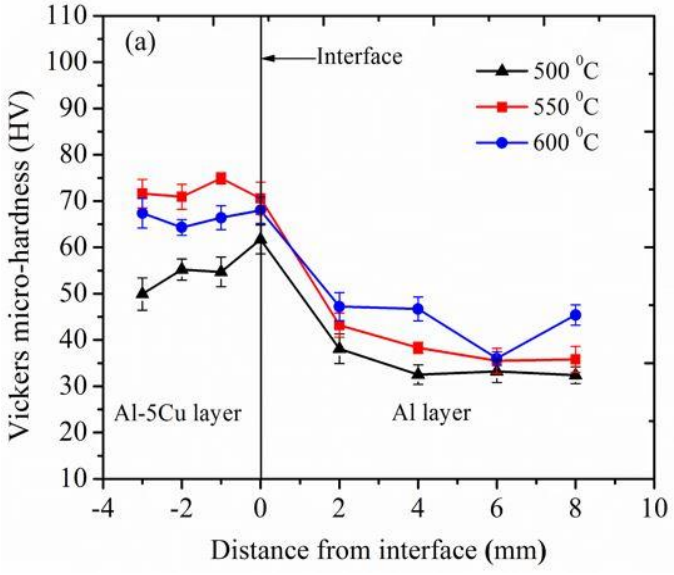

Fig. 4.5 Vickers micro-hardness profiles across interfacial region of (a) Al-5%Cu/Al composite samples

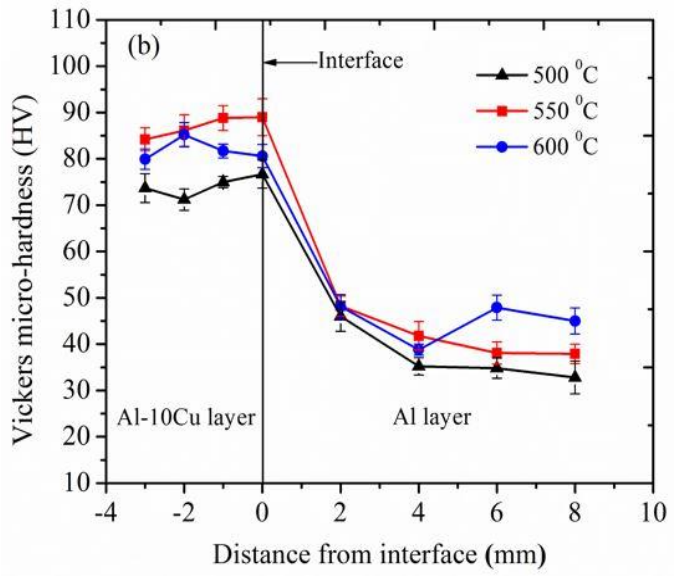

Fig. 4.6 Vickers micro-hardness profiles across interfacial region of (b) Al-10%Cu/Al composite samples

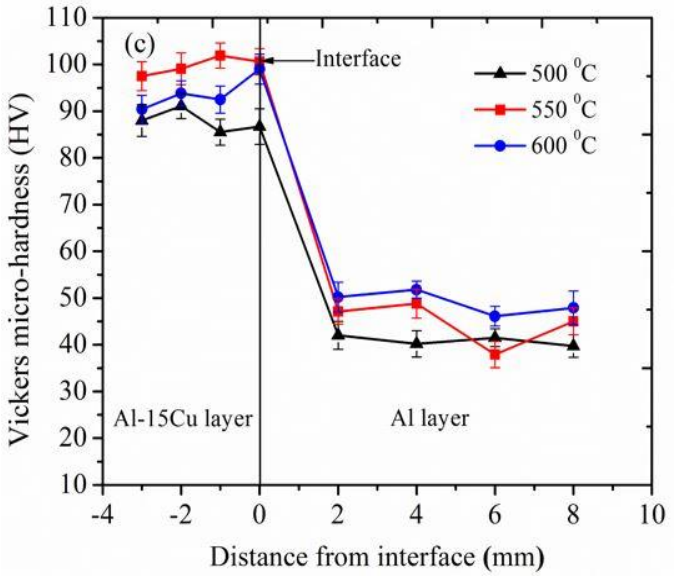

Fig. 4.7 Vickers micro-hardness profiles across interfacial region of (c) Al-15%Cu/Al composite samples

4.2.5. Corrosion Behaviour

The corrosion resistance (Rcorr) was determined at the interface of a three two-layered samples, fabricated by powder metallurgy and hot-pressed at temperature of 550 ^{0}C with 3 h

dwelling time with different percentages of Cu content (5wt. %, 10wt. % and 15wt. %). The prepared samples were cut into dimensions of 1 cm x 1 cm to conduct electrochemical tests for analysing the corrosion behaviour in the interface region on an exposed area of 0.42 cm^2. The potentiodynamic polarization (PDP) experiment was conducted on the above two layered Samples in 3.5% NaCl electrolyte with a minimum of three samples per test to ensure exactness of the tests [126]. The typical polarization curves shown in Fig. 4.8 for the three measured composite samples with the curve shapes almost same. The gradual increase of current density was observed at the corrosion potential, resulting in pitting corrosion occurring on three composites at the interface region. The anodic current density for 15wt. % Cu composite was higher than that of 5wt. %Cu and 10wt. % Cu composites. The negative potential of 10wt. % Cu sample (990mV) was lower than 5wt. % Cu sample (1002mV) and 15wt. % Cu sample (1084mV). The experiments suggested that the corrosion susceptibility of 15wt. % Cu sample was higher.

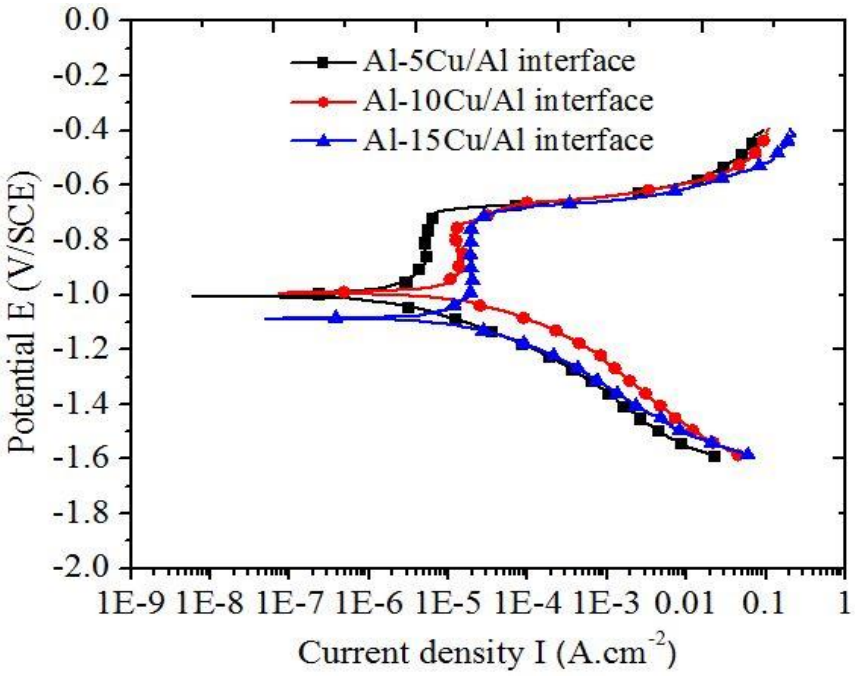

Fig. 4.8 Potentiodynamic polarization curves for Al-5wt. % Cu, Al-10wt. % Cu and Al-15wt. % Cu two-layered composite samples measured in 3.5% NaCl

The change in (-ve) negative potential can be associated with the difference in passive (oxide) layer formation at the interface. From the potentiodynamic polarisation test, the measured values are listed in Table 4.1.

Table 4.1 Parameters polarisation of two-layered composite samples measured in 3.5% NaCl after1hr.

Sample reference	I_{corr} ($\mu m.cm^{-2}$)	E_{corr} (mV)	R_p (W - cm^{-2})	Corrosion rate (mpy)
Al – 5Cu / Al interface	1.41	-1002	18478	0.6074
Al – 10Cu / Al interface	8.61	-990	3029.2	3.7090
Al – 15Cu / Al interface	10.10	-1084	2582.2	4.3548

The corrosion rates of Al-Cu/Al (Cu: 5%, 10%, 15%) samples at interface were measured under same conditions. The corrosion potential (Ecorr) and corrosion current density (Icorr) were evaluated from the tafel plot for arriving at the best fitting curve. The corrosion rate was calculated by Eq^{n} (4.1) [127].

$$Corrosion\ rate\ (mmpy) = 0.0116 \times I_{corr} \quad (4.1)$$

It is observed from Fig. 4.2, that increasing Cu content of Al_2Cu particle also increased and they were perfectly distributed in the matrix. The Al-rich phase enveloped the Al_2Cu particles acting as a protective layer at the interface. However, as the Cu% increases (Al_2Cu fraction increases), a higher susceptibility to corrosion was detected in NaCl solution [128]. Higher corrosion rate was observed in Al-15wt. % Cu/Al two layered sample interface (4.35 mpy) than at 5wt. % Cu (0.60 mpy) and 10wt. % Cu (3.70 mpy) samples. The Al-5wt. % Cu/Al composite Corrosion rate at interface was 6.69 times lower than 15wt. % Cu composite. Therefore, the Al-5wt. % Cu/Al sample exhibit good corrosion resistance at interface.

4.2.6. Electrochemical impedance spectroscopy (EIS) and corrosion mechanisms

An electro chemical test was conducted to know whether a passive layer existed on the surface of the composite. The EIS tests data were produced by Versa Studio software. The data which measured the tests was imported to a software called ZSimpWin and the imported data was executed with various circuit models. Then, it was required to find out which equivalent circuit model provides minimum chi-square value and that circuit model was taken as best-fit circuit

model. The Nyquist impedance plots with the equivalent circuit model used for impedance (Z) data fitting of Al-xCu/Al (x: 5wt. %, 10wt. %, and 15wt. %) composites at interface region are shown in Figs. 4.9 (a-d).

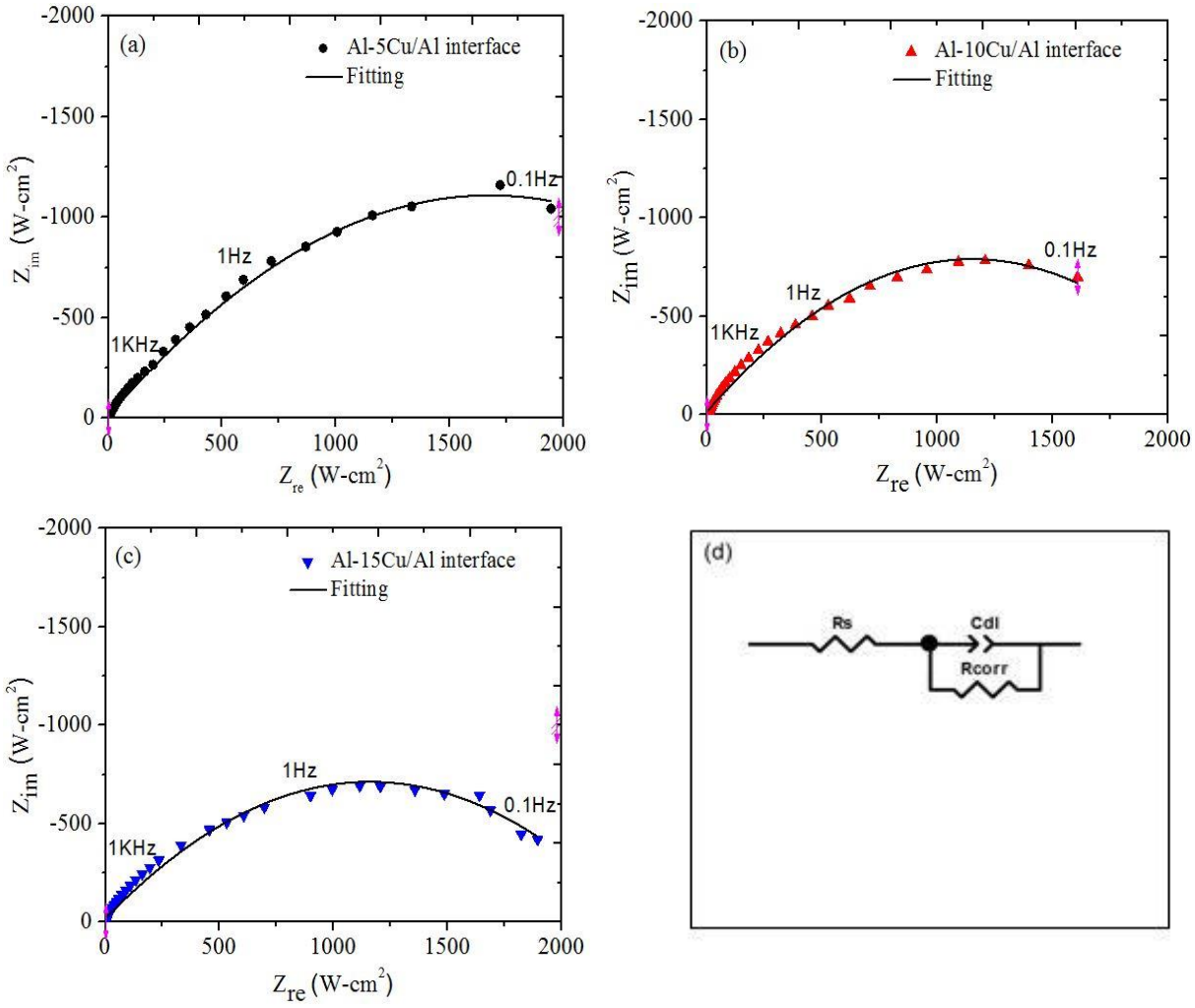

Fig. 4.9 Nyquist impedance plots of interfacial region of the composite samples at various hot-pressed temperatures with different percentage of Cu content, (a) 5 %, (b) 10 %, and (c) 15 % after 1hr. immersion in stagnant 3.5% NaCl solution at room temperature. (d) Equivalent circuit models used for impedance data fitting of 5%, 10% and 15% Cu at interface region

From Figs. 4.9 (a-c) the Nyquist impedance curves of Al-xCu/Al (x: 5wt. %, 10wt. % and 15wt. %) two layered samples are fitted with R (CR) as shown in Fig. 4.9 (d), different researchers [129, 127, 130] suggested the same type of best-fit equivalent circuit model. It denotes randles circuit model with a chi-square value at interfaces of Al-5%Cu/Al is 8×10^{-3}, Al-10%Cu/Al is 5

X $10^{-3}$and for Al-15%Cu/Al is 10 X 10^{-3}, which consists of two resistance one due to an electrolyte or solution resistance (Rs), and the other corrosion resistance (Rcorr) and double layer capacitance (Cdl). The Nyquist plots from Figs. 4.9 (a-c) layer show only 1-capacitive semicircle, and it denotes samples dissolution by a single path. Al-Cu/Al sample dissolution in NaCl solution leads to fast charge, which indicate a capacitive semicircle found in higher frequency region. NaCl acts as an electrolyte or semi-infinite medium. At the interface of Al-Cu/Al (Cu: 5%, 10%, 15%), the electro-active species are Al, Cu and Cl. The Nyquist plots for Al-5%Cu/Al at interface denote only one capacitive loop and the diameter (D) of the loop is higher when compared with 10% and 15% samples. The low current density is specified by higher capacitive loop which means high corrosion resistance. An examination of impedance (*Rcorr* : 2790Ω-cm^2) of the Nyquist curve denotes the thick oxide layer on formation on the surface of the sample which denotes extreme decrease the corrosion rate for 5% sample than for 10% and 15% samples. The EIS results for three samples at the interface is shown in Table 4.2 after 60 min. of immersion in 3.5% NaCl solution.

Table 4.2 Electrochemical-impedance-spectroscopy (EIS) parameters for Al – Cu / Al composites after one hour of immersion in 3.5% NaCl solution.

Parameters	Al – 5Cu / Al interface	Al – 10Cu / Al interface	Al – 15Cu / Al interface
$R_s\,(\Omega.cm^2)$	2.082	1.726	0.895
$C_{dl}\,(\mu F.cm^{-2})$	1.96	4.21	2.32
n	0.771	0.769	0.753
$R_{corr}\,(\Omega.cm^2)$	2790	2163	1925
χ^2	8 X 10^{-3}	5 X 10^{-3}	10 X 10^{-3}

It is observed from EIS results that film resistance (*Rcorr*) of Al-15%Cu/Al sample decreased from 2790 - 1925 Ω-cm^2, when compared to Al-5%Cu/Al sample. The average corrosion resistance observed at Al-10%Cu/Al compared to Al-5%Cu/Al sample and Al-15%Cu/Al sample was 2163 Ω-cm^2. At the same time, the double layer capacitance of Al-5%Cu/Al sample increased from 1.96 - 4.21×10^{-6} S-sec^n cm^{-2}. Also, the average double layer capacitance observed in Al-15%Cu/Al sample was 2.32 ×10^{-6} S-sec^n cm^{-2}. High (*Rcorr)* value indicates the formation of thick oxide layer on Al-5%Cu/Al sample. This protective layer lowered further reaction of cl^- (chloride ions) on the surface of the sample. The formation of Al_2O_3

protective layer and incorporation of Al ions into Cu_2O layer enhanced the corrosion resistance of Al-5%Cu/Al at the interface.

Fig. 4.10 and Fig. 4.11 represents SEM-EDAX of the surface morphology of the Al-5wt. %Cu/Al and Al-15wt. %Cu/Al samples which were immersed in 3.5% NaCl solution for 1h. From EDAX, it is apparent that there was chlorine (Cl) and oxygen (O) presence at Al-Cu sample surface after immersion in NaCl (sodium chloride) solution. The microstructure of corrosion tested Al-5%Cu/Al and Al-15%Cu/Al two layered samples can be observed in Fig. 4.10 and Fig. 4.11. The corrosion at spectrum 1 in Fig. 4.10 (a) and Fig. 4.11 (a) indicates that light corrosion region is 'α' at solid solution phase and at spectrum 2 the high corrosion area is 'θ' (intermetallic phase). Because of the local cell formation in between those 2-phases. In α solid solution phase, there was no preferential dissolution observed because it was treated as a cathode (electron source), where the anodic oxidation of 'θ' results in high dissolution of sample in chloride. Fig. 4.10 (b) and Fig. 4.11 (b) shows highly magnified images of SEM which revealed intergranular and pitting corrosion at various areas of the θ phase. However, the corrosion rate of Al-5wt. %Cu/Al was lower than for Al-15wt. %Cu/Al. The SEM-EDAX of 5%Cu sample at various regions reveals the existence of base Al and Cu along with higher amount of O_2 (oxygen) (30.06-34.33 wt.%) and low amount of Cl (chlorine) (0.23 –0.31 wt.%).

The oxygen percentage was high and chlorine considerably less for Al-5%Cu/Al sample when compared to Al-15%Cu/Al two layered sample (Fig. 4.10 and Fig. 4.11). The presence of Cl (0.41 wt. %) denotes that the corrosion rate of Al-15%Cu/Al sample was less than that of 5% sample. And Al-15%Cu/Al sample diffusion parameter (*n*) from the equivalent circuit was 0.753, which is lower than remaining two samples denotes that the reaction is inhomogeneous.

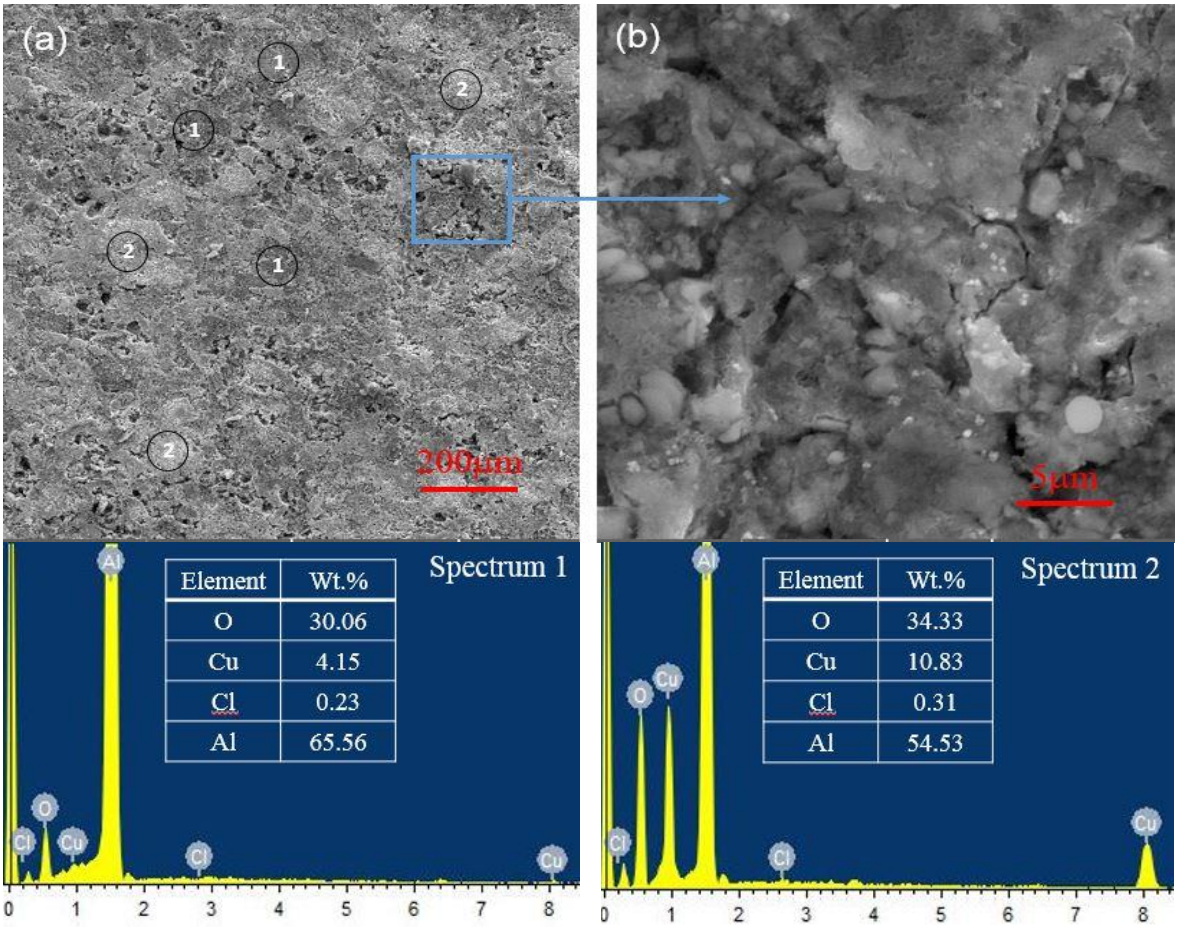

Fig. 4.10 The SEM micrographs of (a) Al-5Cu after 1hr. immersion in 3.5% (m/v) NaCl solution, (b) the corresponding high magnified SEM micrographs and elemental distribution measured from various regions by EDAX

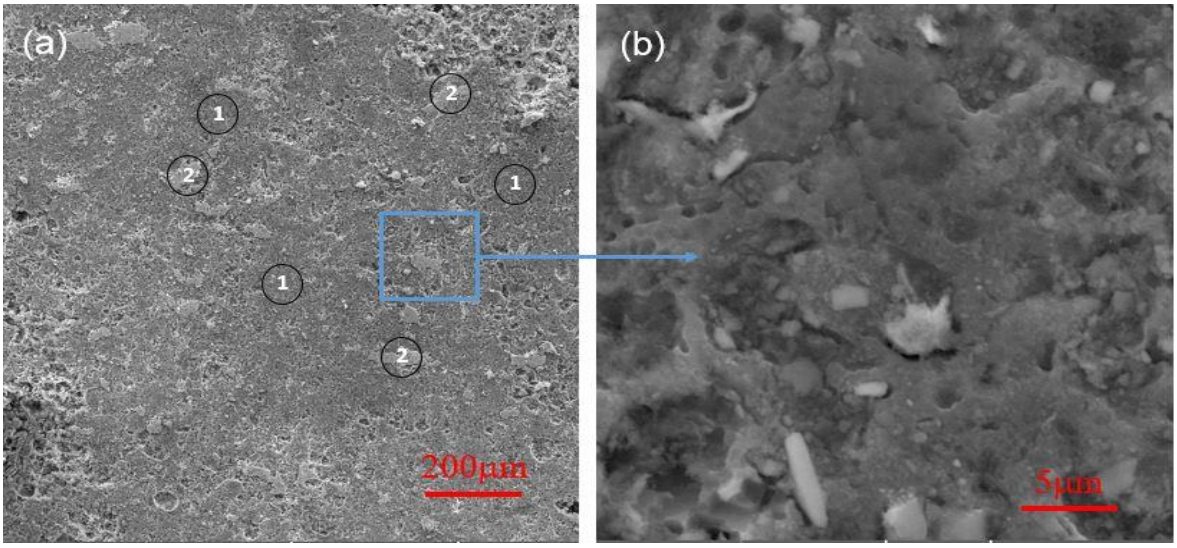

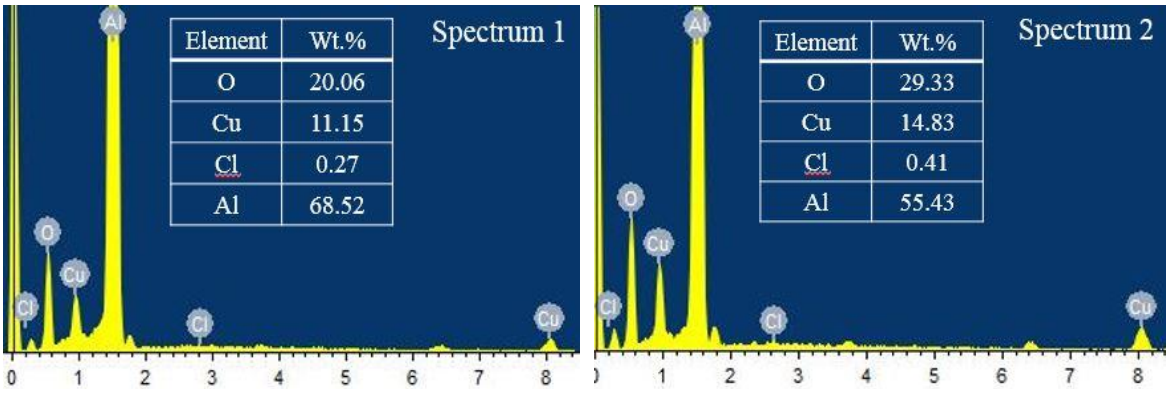

Fig. 4.11 The SEM micrographs of (a) Al-15Cu after 1hr. immersion in 3.5% NaCl solution, (b) the corresponding high magnified SEM micrographs and elemental distribution measured from various regions by EDAX

In Aluminium (Al) containing composites the surface dissolution of Al leads to an additional passivation process and Al_2O_3 formation according to [131, 132]:

$$Al + 4Cl^- \rightarrow AlCl_4^- + 3e^- \quad (4.2)$$

$$2AlCl_4^- + 3H_2O \rightarrow Al_2O_3 + 6H^+ + 8Cl^- \quad (4.3)$$

It was suggested that the existence of $CuCl_2^-$ on the sample surface leads to hydrolysis reaction and the formation of Cu_2O [133] as given below:

$$2CuCl_2^- + H_2O \rightarrow Cu_2O + 4Cl^- + 2H^+ \quad (4.4)$$

Therefore, corrosion resistance in Al - wt. %Cu /Al at interface rapidly decreases in 15%Cu sample when compared to 5%. The presence of Cu with Al leads to oxygen reduction in Al-Cu alloys. The expected layer formation on the surface is Cu_2O. A fresh open surface reveals the corroding environment after the Cu_2O film breaks and dissolves into NaCl. Therefore, Al-5%Cu/Al sample exhibits lower current density (1.41 $\mu m.cm^{-2}$) than 10%Cu and 15%Cu samples.

4.3. Chapter Summary

In this work, the relative density, microstructure and hardness of Al-xCu / Al two-layered samples were investigated with various percentages of Copper (Cu) in Al matrix under different hot-pressed temperatures. The main findings are reported below.

- A two-layered Al - Cu / Al was developed successfully for different percentages (5wt. %, 10wt. % and 15wt. %) of Cu content in Al matrix at different hot-pressed temperatures (550 ^{0}C, 575 ^{0}C and 600 ^{0}C) through P/M route.
- The sintered density increases from 500 ^{0}C to 550 ^{0}C rapidly with irrespective of Cu composition. It shows a weak decreasing trend with increase in compaction temperatures (550 ^{0}C- 600 ^{0}C).
- Therefore, the highest density was achieved at 550 ^{0}C irrespective of Cu content. The sintered density of composite samples increases from 5wt. % to 10wt. % Cu and for further addition of Cu (15 wt. %) it was observed to increase more in density because of agglomeration formation.
- The XRD and EDAX tests were analyzed and the results confirmed that the Al_2Cu (intermetallic compound) was present in Al-rich phase and this particle increased proportionally with an increase in Cu content.
- Hardness increases with increase in sintering temperature from 500 ^{0}C to 550 ^{0}C and it was noticed that there was a slight decreases in hardness with increasing temperature from 550 ^{0}C to 600 ^{0}C. Composition change at interfacial zone results in micro hardness which is the higher at interface regions thanks to component metals.
- The corrosion behaviour of the two layered Al-Cu/Al sample was determined using potentiodynamic polarization test at interface region. The negative potential of 10wt. % Cu sample (990mV) was lower than 5wt. % Cu sample (1002mV) and 15wt. % Cu sample (1084mV). The experiments suggested that the corrosion susceptibility of 15wt. % Cu sample was higher.
- With the addition of copper content, susceptibility to corrosion increases. It was found that 10wt. % Cu sample circuit provides minimum chi-square value. From the SEM-EDAX analysis of the samples, it was clear that there was intergranular and pitting corrosion at various areas of θ phase.

Chapter 5

Wear behaviour of hot-pressed Al-10%Cu/Al two-layered composite by powder metallurgy

5.1. Introduction

The present work focused on the wear behavior of Al layer, Al-10wt. %Cu layer and the interface region (along the cross section) of Al-10%Cu/Al two layered composite which is fabricated by powder metallurgical method. Several efforts have been made out to enhance the wear resistance of Al alloys, and this includes introduction of perfect reinforcing materials into alloys and surface coating applications to achieve the required specific engineering application. The friction coefficient and wear behavior are impacted by various parameters such as sliding velocity, lubrication, surface roughness, relative humidity and normal load. Pure Al and Al alloys are mostly used in applications where corrosion is a problem. Al alloys are treated as bearing material in applications where lower friction is needed. The wear test is normally done on sliding wear environments with pin-on-disk tests. However, large number of hard reinforcements normalize wear resistance, and the wear rate is highly improved due to abrasive wear behavior of reinforcement [134]. Cu is a useful reinforcement addition in the direction of enhancing tribological and mechanical properties of Al alloys [135].

The wear behavior of Al layer, interface region and Al-10wt. %Cu layer of Al-10%Cu/Al sample was studied. In terms of wear rate and the coefficient of friction of regions, the studies were carried out using a pin-on-disc test. The effect of the wear parameters such as applied load (19.6N, 29.4N and 39.2N), sliding velocity (1m/s,1.5m/s and 2m/s) and sliding distance (500m, 1000m, 1500m and 2000m) on the tribological performance of the two layered composite structure was reported. Al-10wt. %Cu layer shows better tribological properties than pure Al and interface region. The worn surface examination shows that adhesive dominant wear mechanism occurs at Al-10wt. %Cu layer than at the interface region. Abrasive wear mechanism was observed in pure Al layer.

5.2. Results and Discussion

5.2.1. Vickers Microhardness

Fig. 5.1 shows the Vickers micro-hardness profiles across interfacial region of Al-10 wt. % Cu composite. The hardness value in Al-Cu layer and at interface increases with increasing Cu content irrespective of sintering temperatures. Hardness increases with increase in sintering temperature from 500 ^{0}C to 550 ^{0}C and it was also noticed that there was a decrease in hardness with increase in temperature from 550 ^{0}C to 600 ^{0}C. The layered composites show increment in hardness from 500 ^{0}C to 550 ^{0}C, indicating the finer dispersion of reinforcement in Al-Cu layer strengthening the compositing. At higher temperature (550 ^{0}C to 600 ^{0}C) there was a drop in hardness attributed to grain growth in matrix. The Vickers micro-hardness shown in Fig. 5.1 at interfacial zone was measured to specify the consequences of intermetallic compound and chemical composition. The micro-hardness is higher at the interface region. It is evident that micro-hardness high at interface region than at the zone of metal components, caused by the changes in composition at the interfacial zone.

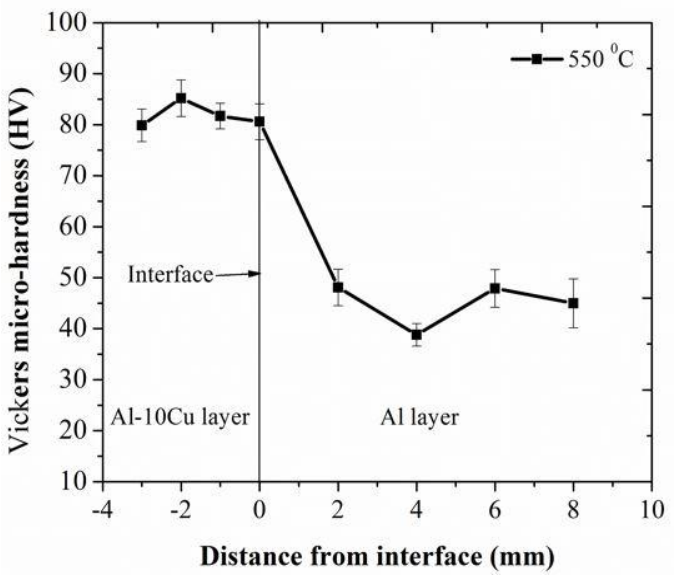

Fig. 5.1 Vickers micro-hardness profiles across interfacial region of Al-10 wt. % Cu composite sample

Table 5.1 Density properties of pure Al and Al-10wt. %Cu layers

Sample name	Bulk density (g/cc)	Theoretical density (g/cc)	Relative density (%)
Pure Al	2.60	2.70	96.29
Al-10%Cu	2.75	2.90	95

The densities of pure Al layer and Al-10wt. %Cu layer are shown in Table 5.1. The bulk density and theoretical densities of pure Al were enhanced after the addition of 10wt. %Cu. The relative density of pure Al layer and Al-10wt. %Cu is almost similar but slight decrease was observed in Al-10wt. %Cu as some of the researchers investigated and showed the relative density of pure Al to be 97%.

5.2.2. Compression properties

Fig. 5.2 (a) illustrates compression stress-strain plots of hot pressed pure Al and Al-10wt. % Cu composites. The complete details of compression properties of all the composites are summarized in Table 5.2. The compression yield strength of pure Al increased nearly by 91% with the addition of Al-10wt. %Cu. The ultimate compression strength also increased from 552 to 761 MPa and the compressive strain reduced from 33.9 to 25.76%. It can be understood that Al-10wt. % Cu composite exhibits maximum strength and with low amount of strain before fracture. On the other hand, the pure Al was characterized by low strength and very high strain than Al-10wt. % Cu. The fractured surfaces of Al-10wt. % Cu composite after compression test are presented in Fig. 5.2 (b). Exhibit show both intergranular and transgranular fracture. It shows having more roughness indicating large energy spent during fracture.

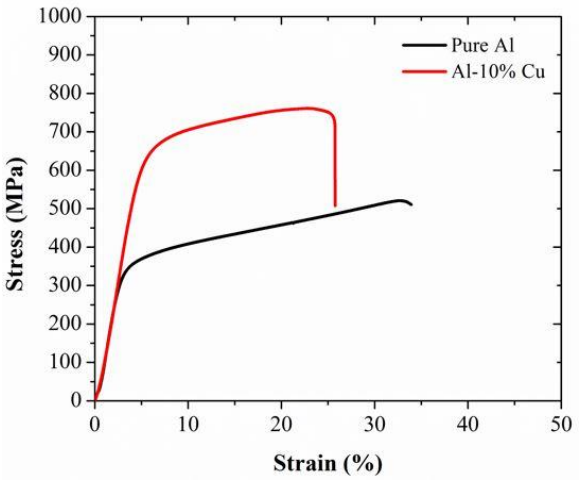

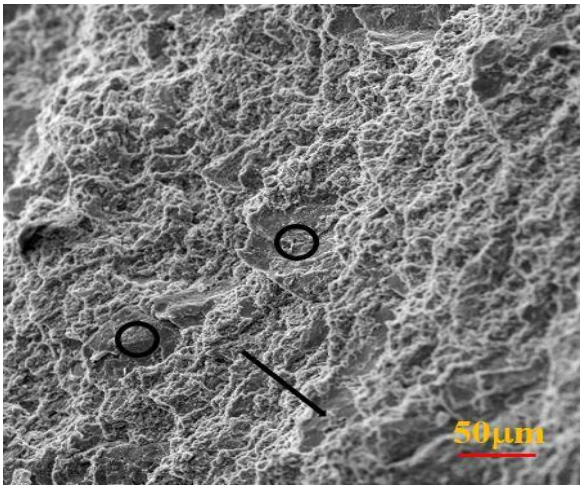

Fig. 5.2 **(**a) Engineering stress–engineering strain curves of the samples and (b) Al–10wt. %Cu sample fractured surface after compression test

Table 5.2 Compression properties of pure Al and Al-10wt. %Cu composites

Sample No	YS(MPa)	UTS(MPa)	E(MPa)	El (%)
Pure Al	282	520.88	128.52	33.90
Al-10%Cu	541	761.03	142.53	25.76

5.2.3. Coefficient of friction of two-layered Al-10wt. %Cu/Al composite

Fig. 5.3 shows the sliding distance as a function of the coefficient of friction (COF) between the composite and the counter surface. Very little variation in the coefficient of friction was observed. There weren't any aberrant inclusions or imperfections in the composite near the surface that may alter the coefficient of friction, as seen by this small fluctuation. The friction coefficient of Al-10wt. % Cu layer was much lower than that of other two layers. There was a modest increase in coefficient of friction with the sliding distance at first, before it dropped off and remained constant throughout the entire test. The interface zone had an approximately average coefficient of friction.

It is demonstrated in Fig. 5.4 that when the composite's sliding velocity increased, so did the friction coefficient. The results show a comparison of friction coefficient between a pure Al layer and one with 10wt. % Cu. The friction coefficient of Al-10wt. % Cu layer increases from 0.25 to 0.36 as the sliding velocity increases from 1 to 2 m/s in trials. In contrast, when the sliding speed increases, the friction coefficient of Pure Al layer increases from 0.46 to 0.60. The frictional heat generated by the asperities of two contact surfaces results in a rise in temperature at the contact points. Increased friction is caused by increased adhesion of pin material to the disc as sliding velocity increases [136].

As demonstrated in Fig. 5.5, the normal load has a significant effect on the friction coefficient, and the findings provide a comparison between the friction coefficients of pure aluminium layer and Al-10wt. %Cu layer. The results reveal that as the normal load increases from 19.6N to 39.2N, the coefficient of friction reduces from 0.71 to 0.55 and 0.64 to 0.43 for pure Al layer and Al-10wt. %Cu layer, respectively, for pure Al layer and Al-10wt. %Cu layer, respectively. When the contact region is subjected to normal load, the average coefficient of

friction is the norm. The load at the composite and disc interface is lower for lower loads and higher for higher loads so that the effect of pure Al layer and Al-10wt. %Cu layer on the friction coefficient is smaller at lower loads than it is at higher loads.

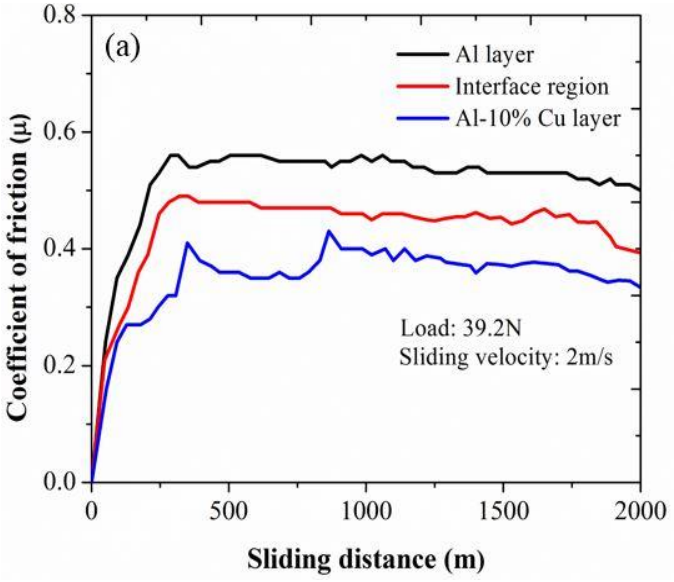

Fig. 5.3 The influence of sliding distance on COF of (a) pure Al layer, Interface region and Al-10wt. %Cu layer

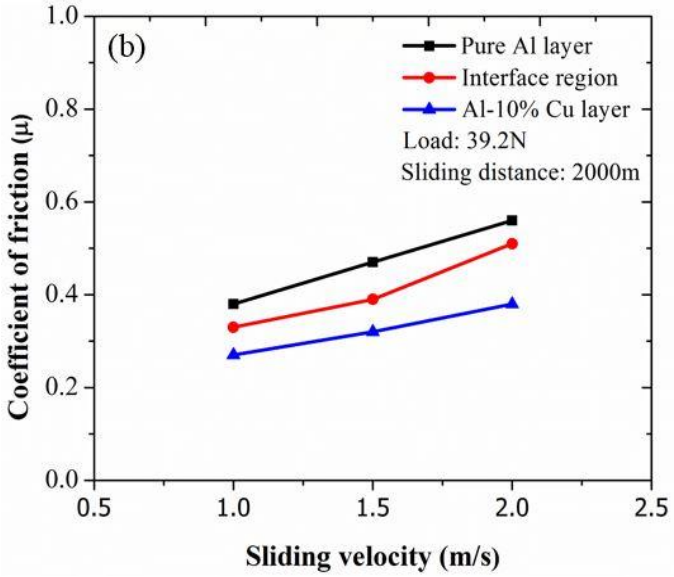

Fig. 5.4 The influence of sliding velocity on COF of (b) pure Al layer, Interface region and Al-10wt. %Cu layer

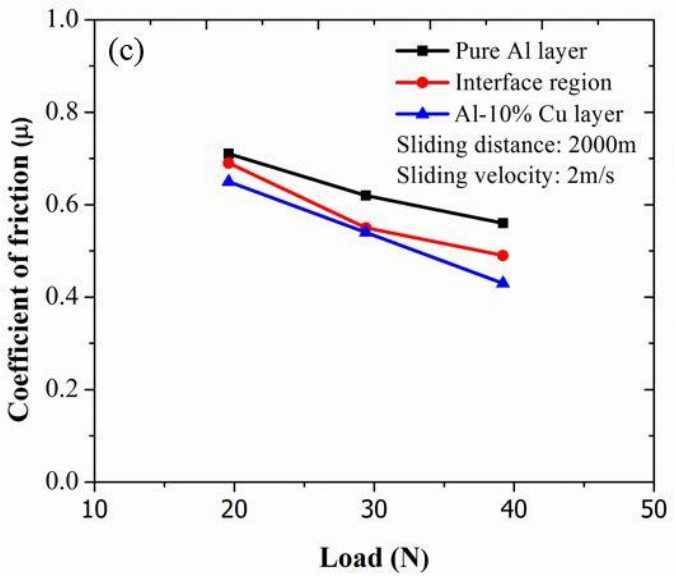

Fig. 5.5 The influence of normal load on COF of (c) pure Al layer, Interface region and Al-10wt. %Cu layer

5.2.4. Wear Rate

Fig. 5.6 show the weight loss plots for pure Al, interface region and Al-10wt. % Cu layer under 39.2N applied load. It is generally believed that the contribution of hard particles to Al results in an improvement of the base alloy to a great extent based on the result under the load the amount of weight loss of all particles.

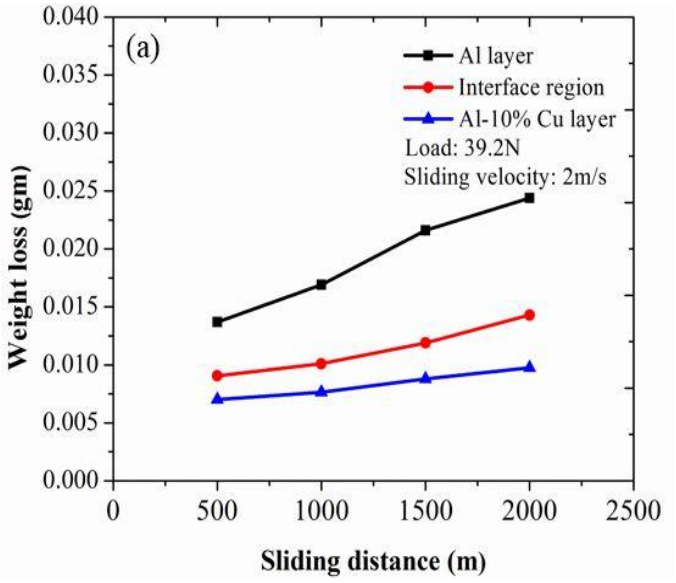

Fig. 5.6 The influence of sliding distance on weight loss of (a) pure Al layer, Interface region and Al-10wt. %Cu layer

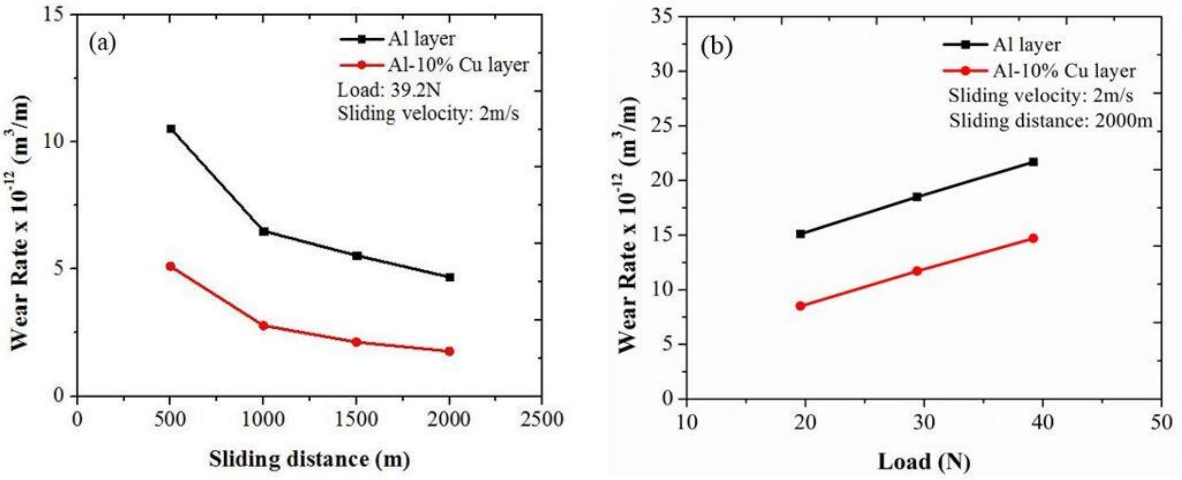

Fig. 5.7 The influence of sliding distance on wear rate of (a) pure Al layer and Al-10wt. %Cu layer. The influence of normal load on wear rate of (b) pure Al layer and Al-10wt. %Cu layer

The influence of sliding distance on the wear rate of pure Al and Al-10wt. %Cu is shown in Fig. 5.7 (a). It is observed that an increase in sliding distance from 500 to 2000 m, decreased wear rate of pure Al layer from (10.54 - 4.69) $X10^{-12}$ (m^3/m). On the other hand, Al-10wt. %Cu layer showed decreased wear rate from (5.11 - 1.77) $X10^{-12}$ (m^3/m). During the initial stages of the wear test, the harder surface asperities on the sample and counter surface interacts and after a certain distance, the harder asperities wear off, and the material flows smoothly over the counter surface. Tt is observed from Fig. 5.7 (b) that for an increase the normal load increases from 19.6N to 39.2N, the wear rate of Pure Al layer increases from (15.1 - 21.17) $X10^{-12}$ (m^3/m). On the other hand, Al-10wt. %Cu layer shows increased wear rate from (8.52 - 14.75) $X10^{-12}$ (m^3/m). Because of the increase in normal load, frictional thrust is increased and real surface area is also increased, hence causes higher wear.

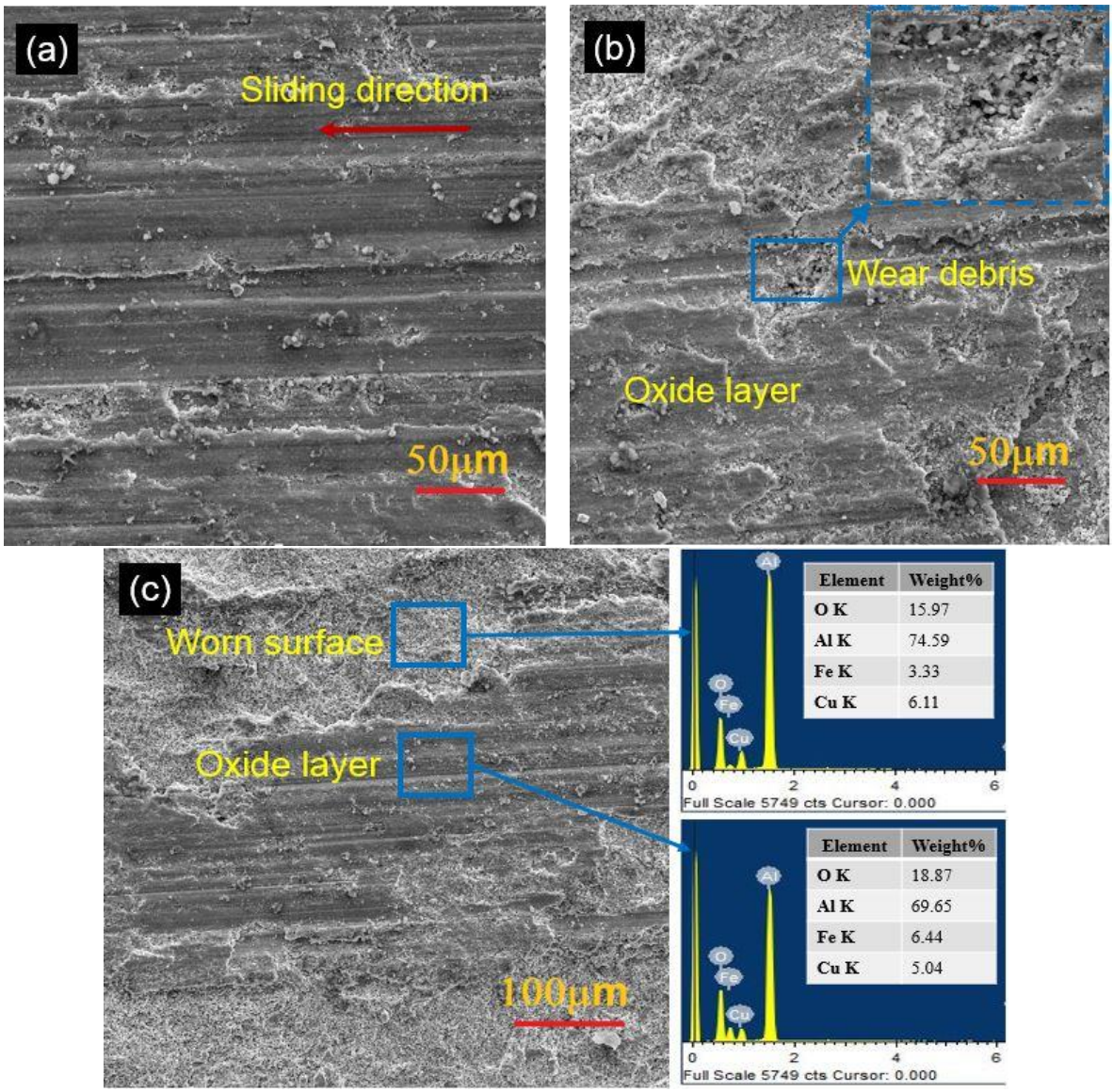

Fig. 5.8 (a) SEM image of worn surface sliding direction, (b) SEM images of worn surface in high magnification (c) Low magnification worn surface. The corresponding EDS of worn surface and oxide layer is also presented

In case of Al-10wt. %Cu layer and interface, the worn surfaces are characterized with an oxide layer and moderately small amount of wear debris can be seen (Fig. 5.8 and 5.9). Small amount of wear debris was observed on the worn surface of Al-10wt. %Cu layer as compared to interface, which may be the variations in COF being lower than interface as shown in Fig. 5.3 – 5.5. A careful observation at the worn surface also exposes the existence of abrasion grooves on the oxide layer and its delamination Fig. 5.8 (b), (c) and Fig. 5.9 (b), (c). The oxide layer contains low quantity of oxygen than the interface and a minute fraction of Fe along with base Al and Cu elements. The

adhesion may be negligible in the wear of Al-10wt. %Cu layer due to the presence of low quantity of Fe. A scanning electron microscopic study was carried out on the two-layered Al-10wt %Cu/Al composite. Some samples randomly chosen and cut at different locations were used for this purpose. The worn surfaces on completion of the wear test were also studied to determine the mechanism of wear that had occurred. Energy dispersive X-ray spectroscopy (EDAX) analysis was done to find the composition of the samples at different locations on the surface to check the distribution of the components in the composite.

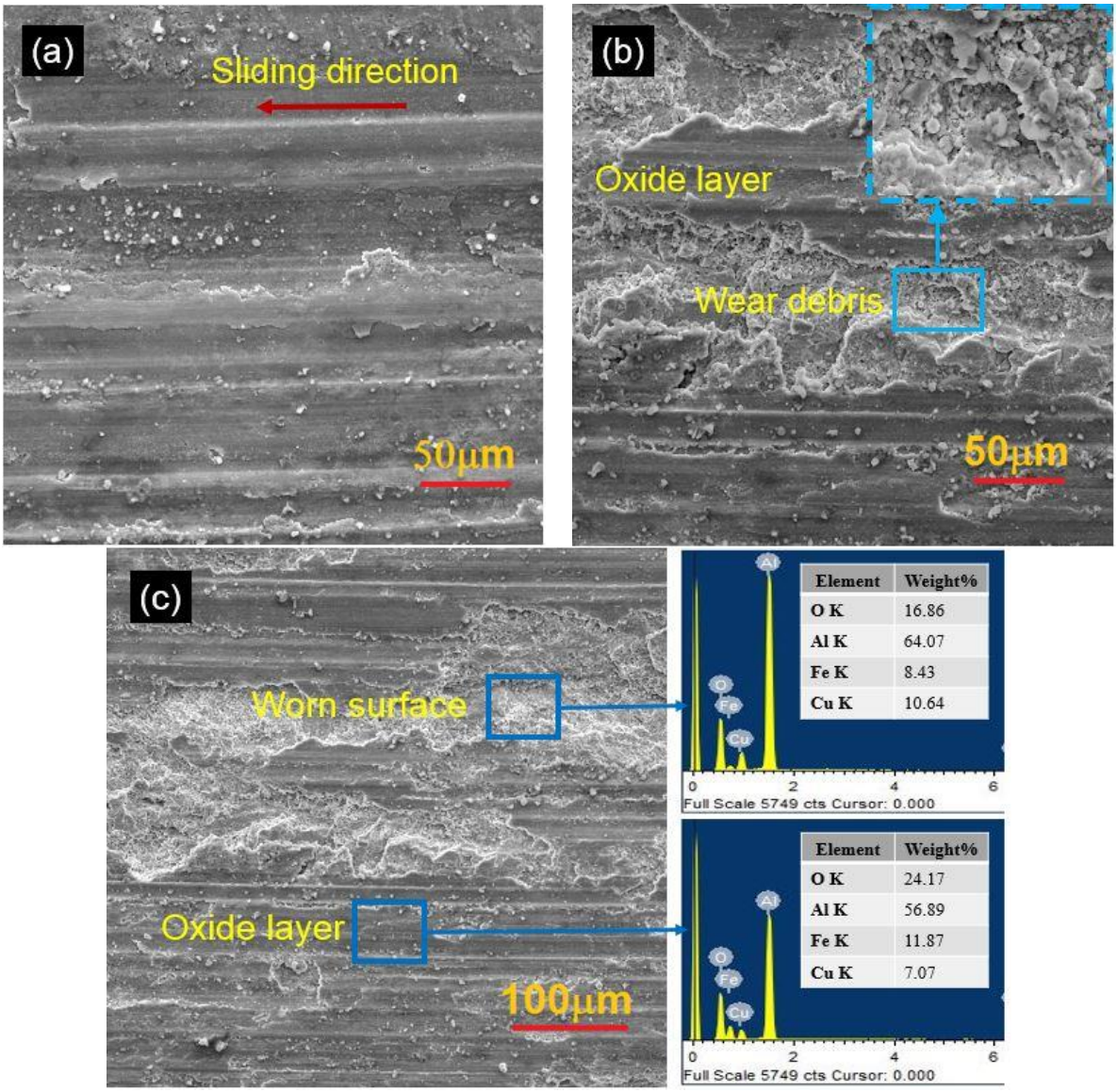

Fig. 5.9 (a) SEM images of worn surface sliding direction (b) corresponding high magnification (c) corresponding low magnification. The corresponding EDS of worn surface and oxide layer is also presented

5.2.5. Analysis of wear debris

To comprehend the wear mechanisms, additionally an analysis of the micro structure was carried out on wear debris. The SEM micrographs of pure Al, interface region and Al-10wt. %Cu layer wear debris after wear test were stored on the steel disk as shown Fig. 5.10 (a-c). It can be seen from the Fig. 5.10 (a) that there was fine agglomerated wear debris for pure Al. On the other hand, as shown in Fig. 5.10 (c) the size of the wear debris was notably flaky and coarse.

During the wear of Al-10wt. %Cu layer, due to the micro-cutting action of harder particles flaky wear debris were developed. The big flaky debris roll or slides between the hard contacting pairs during sliding. During wear at the interface, the debris seems to be in between agglomerated and flaky as shown in Fig. 5.10 (b).

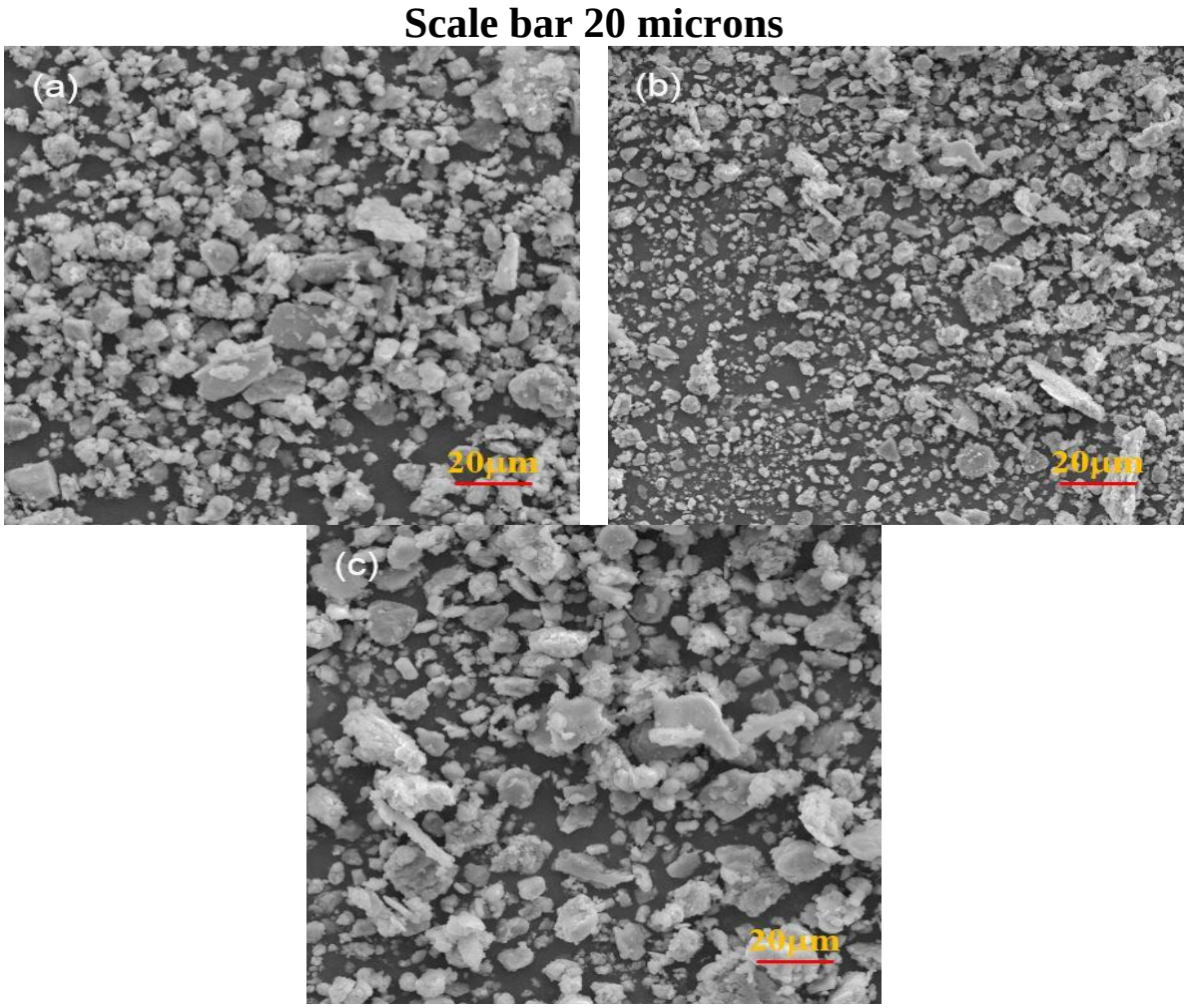

Fig. 5.10 (a) SEM images of pure Al layer, (b) Interface region and (c) Al-10wt. %Cu layer wear debris

5.3. Chapter Summary

- Within the observed range, coefficient of friction increases with increase in sliding distance and sliding velocity after which it becomes steady for all pure Al layer, interface region and Al-10wt. %Cu layer. Moreover, it is apparent that for identical conditions, with increasing sliding distance and sliding velocity, Al-10wt. %Cu layer shows lower coefficient of friction than Al and interface region.
- Friction coefficient decreases with increase in normal load for all pure Al layer, interface region and Al-10wt. %Cu layer. With increasing normal load, Al-10wt. %Cu layer shows lower friction than Al layer and interface region.
- The wear rate decreases with increase in sliding distance for pure Al layer and Al-10wt. %Cu layer. Wear rate increases with increase in normal load for pure Al layer and Al-10wt. %Cu layer.
- A low amount of wear debris was noticed on the worn surface of Al-10wt. %Cu layer compared to interface region, hence the fluctuations in COF were lower than at interface region and Al layer.

Chapter 6

Formability and densification behaviour of two-layered structure powder metallurgical hot-pressed Al-Cu/Al composites during hot-upsetting

6. 1. Introduction

The main aim of the present work was to study the formability and densification characteristics of the two-layered Al-Cu/Al composites with various Cu content in Al-Cu layer prepared by powder metallurgy method. These characteristics depends on sintering temperature, initial relative density, stress state condition, aspect ratio, and hot-compaction temperature. And the effect of various percentages of Cu addition and different deformation temperatures on the formability characteristics and deformation mechanism of Al-Cu/Al preforms were studied by hot upsetting tests and microstructural observations. Aluminium is a relatively low cost, light weight metal that can be heat treated and loaded to relatively high level of stresses, and it is one of the most easily produced of the high performance materials, which results in low manufacturing and maintenance costs. Automotive sector, missile technologies and aerospace industries focus on advanced engineering materials, which led to rapid development of metal matrix composite.

An experimental investigation was performed on hot formability and densification characteristics of Al-Cu/Al two-layered structure composites. The two-layered composites with different Cu compositions in Al-Cu layer such as (Cu: 5wt. %, 10wt. %, and 15wt. %) were prepared using powder metallurgy (P/M) route. The composites were hot-pressed layer by layer in a steel cylindrical die at 550 ^{0}C temperature with 0.9 initial relative density (IRD) and 0.1 s^{-1} strain rate. The preforms were hot deformed between two flat dies with a capacity of 50-ton hydraulic press machine at a temperature range of 150 ^{0}C – 450 ^{0}C under triaxial stress state condition. The hot-upsetting behaviour of preforms was observed until the cracks begin on the cylindrical preform at the outer surface. The effect of different Cu composition and various deformation temperatures on two-layered preforms were discussed. Results revealed that (10wt. %Cu) preform achieved good cooperative deformation behaviour between Al-Cu and Al layers at the interface region. The

relationship between process parameters was discussed such as the effect of axial stress (σ_z) and relative density (R) on axial strain (ε_z) and the impact of formability stress index (β) and different stress ratio parameters (σ_e/σ_{eff},σ_m/σ_{eff}) on relative density (R).

6. 2. Theoretical analysis

The hot-upsetting parameters, which are used to observe the workability and deformation behavior through the triaxial stress state conditions, were calculated using mathematical equations. The mathematical calculations for the aforesaid parameters stated in this paper - axial stress(σ_z), axial strain (ε_z), formability stress index (β), hoop strain (ε_θ), hoop stress(σ_θ), hydrostatic stress (σ_m) and effective stress (σ_{eff}) are given below.

According to Abdel-Rahman and El-Sheikh, [137] axial strain(ε_z) and axial stress (σ_z) parameters of powder metallurgy compacts can be calculated from the following equations.

$$\varepsilon_z = \ln\left(\frac{H_f}{H}\right) \tag{6.1}$$

$$\sigma_z = \frac{load}{contact\ surface\ area} \tag{6.2}$$

And the hoop strain ε_θ is

$$\varepsilon_\theta = \varepsilon_r = \ln\left(\frac{D_f}{D}\right) \tag{6.3}$$

Hoop strain ε_θ established, [138] is given below and it contains the deformed bulged diameter ($D_{b)}$ and deformed contact diameter ($D_{c)}$ of the preform.

$$\varepsilon_\theta = ln\left[\frac{2D_b^2 + D_C^2}{3D^2}\right] \tag{6.4}$$

Here, D_C represents the normal surface diameter of the deformed preform.

The stress state is given in as : [139]

$$\alpha = \frac{d\varepsilon_\theta}{d\varepsilon_z} = \frac{(2+R^2)\sigma_\theta - R^2(\sigma_z+2\sigma_\theta)}{(2+R^2)\sigma_z - R^2(\sigma_z+2\sigma_\theta)} \tag{6.5}$$

Here α denotes Poisson's ratio, where the axial strain (ε_z) and relative density (R) are known before, the hoop stress (σ_θ) was calculated using Eq^n. (6.5) as

$$\sigma_\theta/\sigma_z = \ln\left[\frac{(2\alpha+R^2)}{2-R^2+2R^2\alpha}\right] \quad \text{where } \alpha = \frac{d\varepsilon_\theta}{d\varepsilon_z} \tag{6.6}$$

The cylindrical coordinates ($\sigma_\theta = \sigma_r$) were used to calculate hydrostatic stress as

$$\sigma_m = \frac{\sigma_r+\sigma_\theta+\sigma_z}{3} = \frac{2\sigma_\theta+\sigma_z}{3} \tag{6.7}$$

$$\frac{\sigma_m}{\sigma_z} = \frac{1}{3}\left(1 + \frac{2\sigma_\theta}{\sigma_z}\right) \tag{6.8}$$

The effective stress given below, [140]

$$\sigma_{eff}^2 = \frac{(\sigma_z{}^2+\sigma_\theta{}^2+\sigma_r{}^2) - R^2(\sigma_z\sigma_\theta+\sigma_\theta\sigma_r+\sigma_r\sigma_z)}{2R^2-1} \tag{6.9}$$

Since ($\sigma_\theta = \sigma_r$) at cylindrical axisymmetric deforming operation, the Equation (6.9) becomes

$$\sigma_{eff}^2 = \frac{(\sigma_z{}^2+2\sigma_\theta{}^2) - R^2(\sigma_z\sigma_\theta+\sigma_\theta{}^2+\sigma_r\sigma_z)}{2R^2-1}$$

$$\sigma_{eff} = \left[\frac{(\sigma_z{}^2+2\sigma_\theta{}^2) - R^2(\sigma_\theta{}^2+2\sigma_r\sigma_z)}{2R^2-1}\right]^{\frac{1}{2}} \tag{6.10}$$

Vujovic and Shabaik, [141] proved the formability stress index experimentally from the stress state of the spherical component (hydrostatic).

$$\beta = \frac{3\sigma_m}{\sigma_{eff}} \tag{6.11}$$

As reported in Vujovic and Shabaik, [141] the formability stress index, β determines the limit of fracture.

6. 3. Results and discussion

Figs. 6.1 – 6.3 shows the axial stress - axial strain curves of Al-Cu/Al preforms at various deformation temperatures such as 150 ^{0}C, 250 ^{0}C, 350 ^{0}C, and 450 ^{0}C and different Cu contents in Al-Cu layer such as 5wt. %, 10wt. % and 15wt. % at 0.1s^{-1} strain rate. The Cu composition and deformation temperature have a significant influence on the flow stress of preforms. The flow stress increases with decreasing deformation temperature and irrespective Cu content. The flow stress of preforms increased rapidly and obtained peak stress at lower axial strain (approximately 0.02) during the starting stage of deformation due to higher closure of pores. At low deformation temperature (150 ^{0}C) after peak stress, the flow stress continues to increase due to work hardening. However, with further increase in strain, it produces a large quantity of deformation heating. So

that the mechanism of dynamic softening starts at a certain strain, then flow stress exhibits a dropping tendency and reaches stable conditions with an increase of strain as reported by Liu and Wang [142]. At higher deformation temperature of 450 ^{0}C, the isothermally activated process strongly controls the hot deformation process and atomic movement so that dislocation slip become easy. Thus, at peak flow stress, the softening mechanism is initiated. Therefore, at high deformation temperatures, the interface constraint effect on the flow of softening aluminium layer deteriorates a little. The hot deformation which is mainly focused on the softer Al layer, combined with interface constraint effect, leads to low flow stress at high deformation temperature. The effects of Cu composition are negligible in the early stage of deformation where the axial strain is up to 0.02 (peak stress), but significant in the strain hardening phases. Therefore, the axial strain decreases with increasing Cu content.

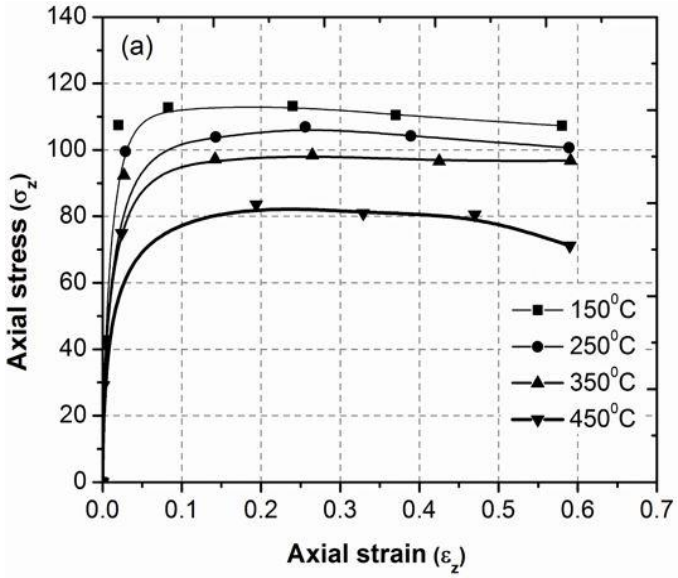

Fig. 6.1 Axial stress-Axial strain curves of (a) Al-5%Cu/Al composite during hot deformation with IRD of 90% at strain rate of 0.1 s^{-1}

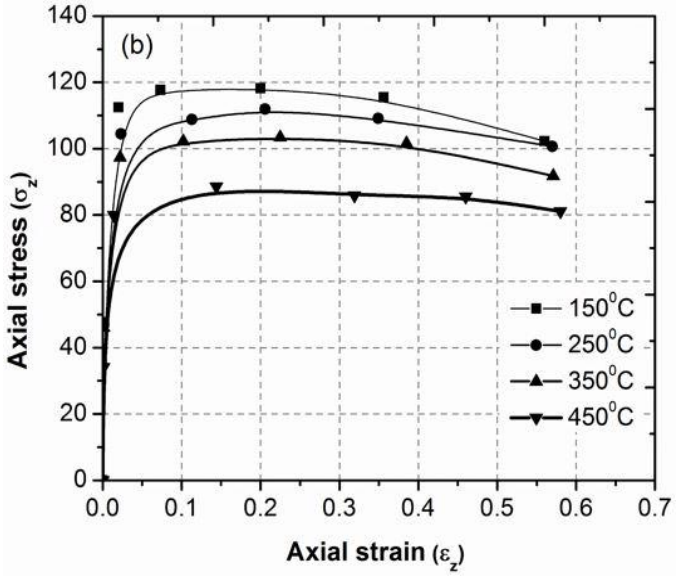

Fig. 6.2 Axial stress-Axial strain curves of (b) Al-10%Cu/Al composite during hot deformation with IRD of 90% at strain rate of 0.1 s^{-1}

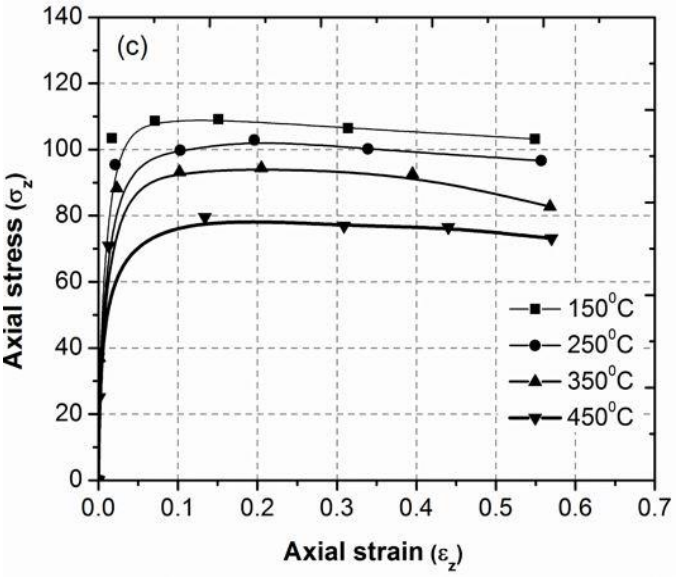

Fig. 6.3 Axial stress-Axial strain curves of (c) Al-15%Cu/Al composite during hot deformation with IRD of 90% at strain rate of 0.1 s^{-1}

The relative density (*R*) - axial strain (ε_z) curves of preforms at various deformation temperatures and different percentages of Cu content with a 0.9 relative density under triaxial stress state condition, are shown in Figs. 6.4 - 6.6. The densification increases with an increase of deformation temperature in preforms. Better densification is attained due to lower porosity during deformation [143]. Therefore, the amount of densification increases with the addition of Cu

content (up to 10wt. %) to preforms. The material flow is similar in both Al and Al-Cu layers of preform. In the beginning, the densification rate increases steeply with increasing axial strain and proportional to the closure of pores significantly improves the densification. The densification is gradually decreased with increasing axial strain during the stage of 0.02 to fracture. With further increase of axial strain, the pore size decreases and leads to fracture. It is observed from Figs 6.4 - 6.6, that densification characteristics are dissimilar for various amounts of Cu present in the perform at different deformation temperatures. The maximum densification was attained for 10wt. % Cu content preforms compared to 5 wt. % Cu and 15 wt. % Cu for any given axial strain. The material flow behavior of preforms increases by the addition of Cu content (up to 10wt. %) to Al-Cu layer by means of Cu particles which enhance the free movement in material flow from center to periphery. Consequently, hoop stress is high 10wt. % Cu preforms. Moreover, it is found from Fig 6.5 that highest relative density of 0.95 was attained by 10wt. % Cu preforms at 450 ^{0}C deformation temperature.

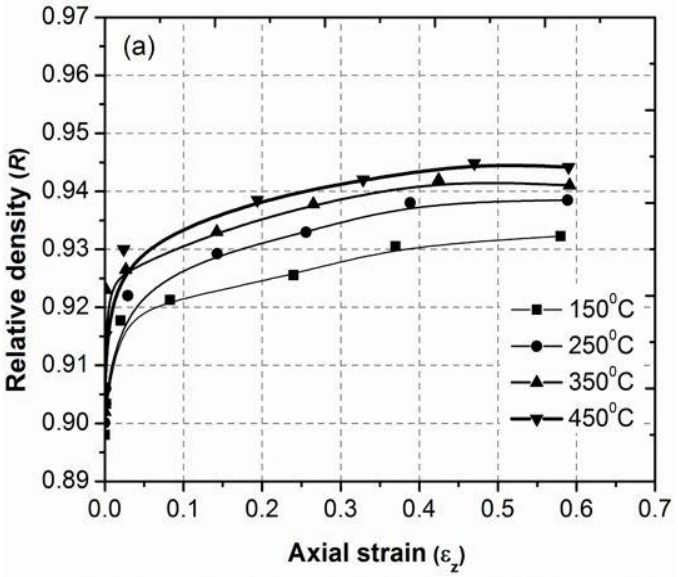

Fig. 6.4 Effect of axial strain (ε_z) on relative density (R) of (a) Al-5%Cu/Al composite for various temperatures under the tri-axial stress state condition.

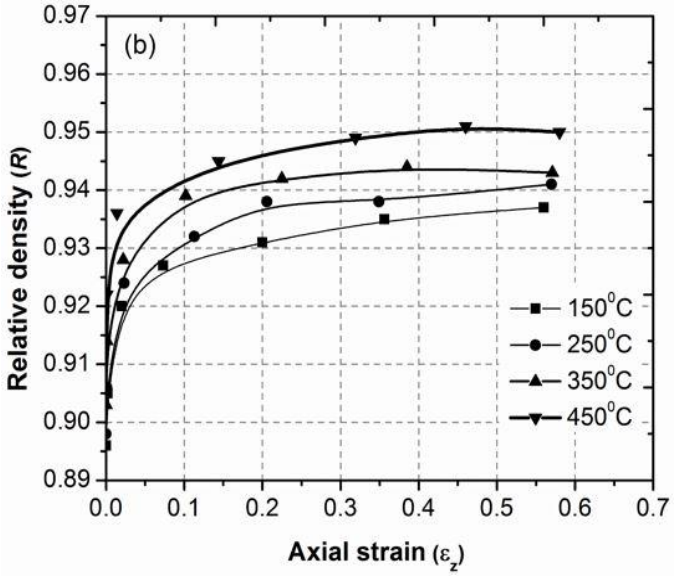

Fig. 6.5 Effect of axial strain (ε_z) on relative density (R) of (b) Al-10%Cu/Al composite for various temperatures under the tri-axial stress state condition.

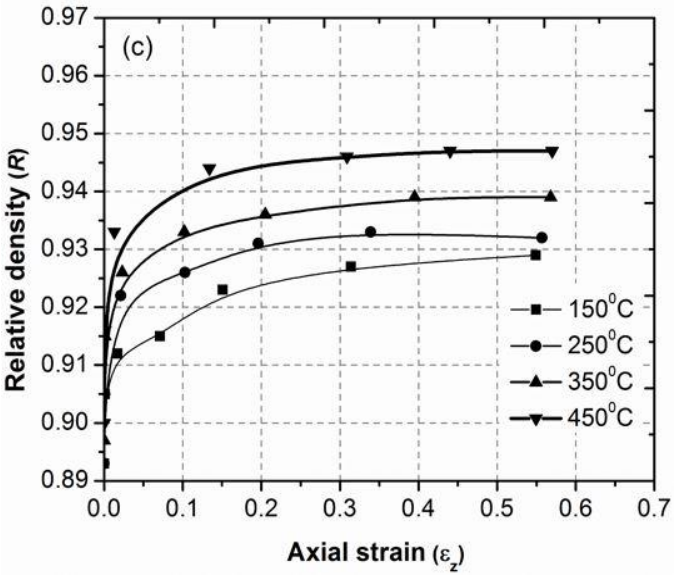

Fig. 6.6 Effect of axial strain (ε_z) on relative density (R) of (c) Al-15%Cu/Al composite for various temperatures under the tri-axial stress state condition.

The design of forming operations of Powder metallurgy components has the most significance, and the formability stress index (β) is an important parameter, which establishes a safe working zone for manufacturing defect-free part. Figs. 6.7 – 6.9 show the effect of different deformation temperatures and Cu content at 5wt. %, 10wt. %, and 15wt. % on axial strain (ε_Z) against the formability stress index (β) under triaxial stress state condition. The formability stress

index (β) increases with increasing deformation until work hardening. With little increase of axial strain (ε_z), the formability stress index (β) increased at any deformation temperature irrespective of Cu percentage in Al-Cu layer. The formability stress index (β) increases along with increasing deformation temperatures irrespective of Cu content in the Al-Cu layer. From Figs 6.7 – 6.9, it can be seen that the fracture limit curve increases with increasing deformation temperature and is irrespective of Cu content.

The decrease in pore size and also increase in fluidity at high deformation temperatures causes more density in preform than at low deformation temperatures. Therefore, more formability stress index (β) is attained at a high deformation temperature for any Cu content percentage in the Al-Cu layer. With the addition of Cu content in Al-Cu layer, the fracture limit curve is moves towards the left side. However, the early fracture occurred in Al-layer of high Cu content (15wt. %) preform. Cluster formation occurs with increasing cu content in t Al-Cu layer, which leads to an early fracture in Al layer of 15wt. % Cu content preform.

It was found that low formability stress index (β) was observed in 15wt. % Cu content preform with reference to axial strain, at any deformation temperature. The higher formability stress index (β) was attained in 10wt. % Cu preform at 450 ^{0}C deformation temperature and its fracture at higher axial strain.

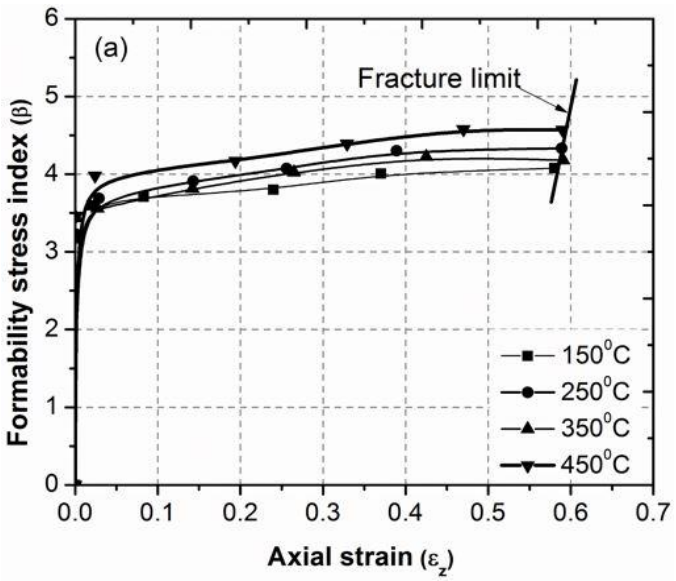

Fig. 6.7 Effect of axial strain (ε_z) on formability stress index (β) of (a) Al-5%Cu/Al composite for various temperatures under the tri-axial stress state condition.

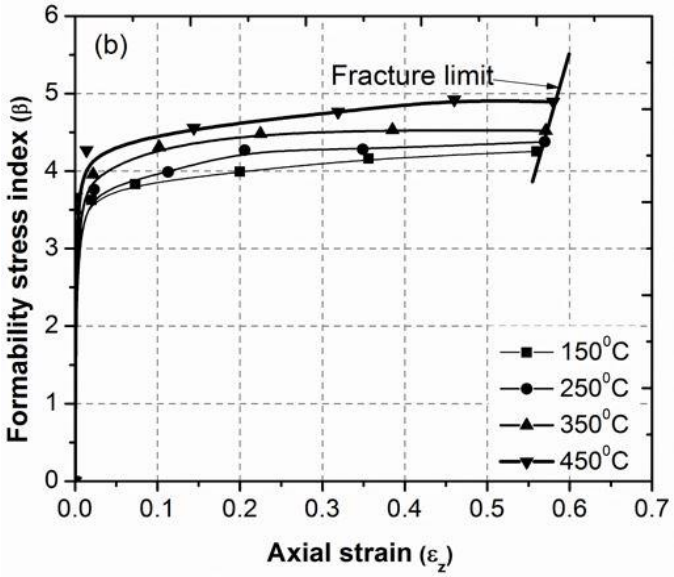

Fig. 6.8 Effect of axial strain (εz) on formability stress index (β) of (b) Al-10%Cu/Al composite for various temperatures under the tri-axial stress state condition.

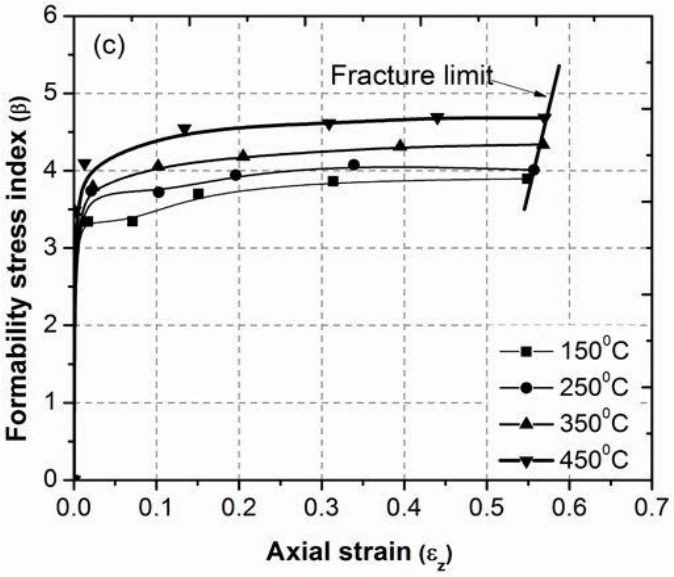

Fig. 6.9 Effect of axial strain (εz) on formability stress index (β) of (c) Al-15%Cu/Al composite for various temperatures under the tri-axial stress state condition.

Figs. 6.10 – 6.12 show the effect of different deformation temperatures and addition of Cu content 5wt. %, 10wt. %, and 15wt. % on relative density (*R*) against stress ratio parameter

($\sigma_\theta/\sigma_{eff}$) under triaxial stress state conditions. With an increase in relative density (*R*), the stress ratio parameter ($\sigma_\theta/\sigma_{eff}$) increases irrespective of deformation temperature and Cu percentage in the Al-Cu layer. While increasing deformation temperature, the material flow increases from center to outer edge. Thus high densification is achieved due to closes of pores. Therefore, with increasing deformation temperature and relative density (*R*), the stress ratio parameter increases at any Cu percentage in the Al-Cu layer. The material flow behavior of preforms increases by the addition of Cu content (up to 10wt. %) to the Al-Cu layer, which causes Cu particles to enhance free movement in material flow from center to outer edge, increasing the closure of pores. Consequently, hoop stress is high in 10wt. % Cu preforms. The stress ratio parameter ($\sigma_\theta/\sigma_{eff}$) increases along with hoop stress. The high-stress ratio parameter ($\sigma_\theta/\sigma_{eff}$) and relative density *(R)* observed in 10wt. % Cu preform at 450 ^{0}C deformation temperature.

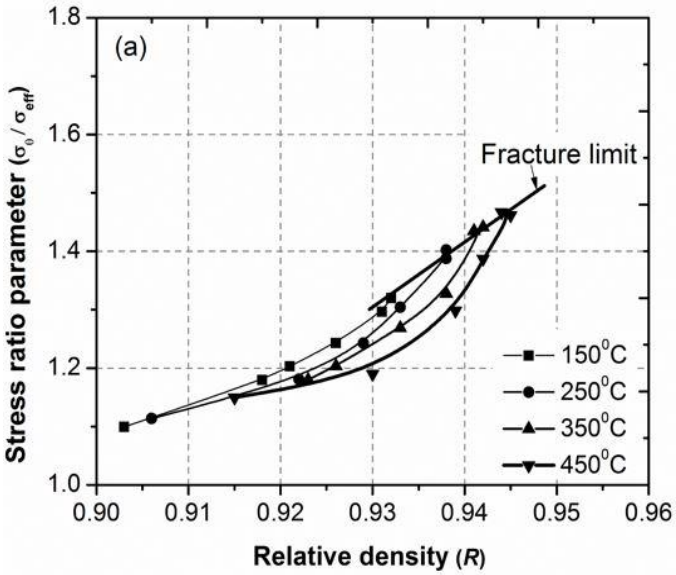

Fig. 6.10 Effect of relative density *(R)* on stress ratio parameter ($\sigma_\theta/\sigma_{eff}$) of (a) Al-5%Cu/Al composite for various temperatures under the tri-axial stress state condition.

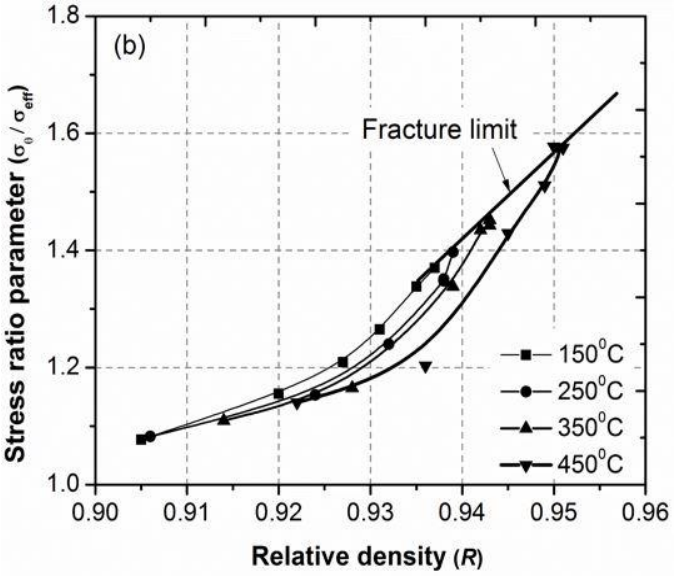

Fig. 6.11 Effect of relative density *(R)* on stress ratio parameter ($\sigma_\theta/\sigma_{eff}$) of (b) Al-10%Cu/Al composite for various temperatures under the tri-axial stress state condition.

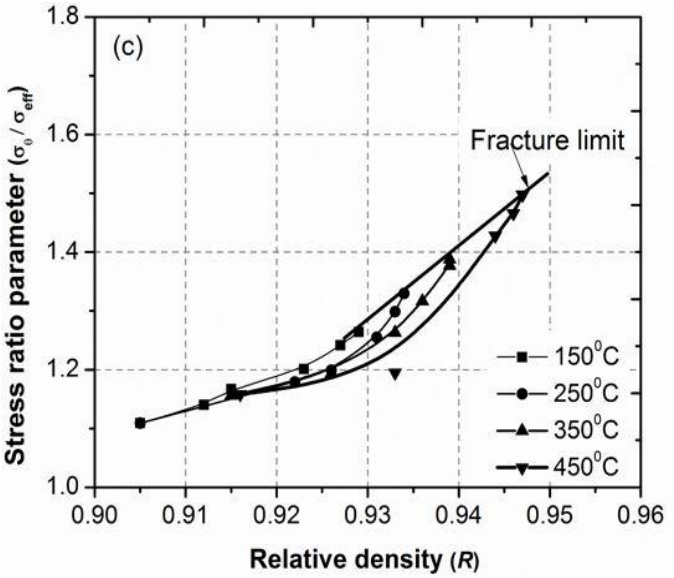

Fig. 6.12 Effect of relative density *(R)* on stress ratio parameter ($\sigma_\theta/\sigma_{eff}$) of (c) Al-15%Cu/Al composite for various temperatures under the tri-axial stress state condition.

Figs. 6.13 – 6.15 show the effect of different deformation temperatures and various Cu content 5wt. %, 10wt. %, and 15wt. % on relative density (*R*) against stress ratio parameter (σ_m/σ_{eff}) under triaxial stress state condition. With increasing deformation temperature and

relative density (*R*), the stress ratio parameter (σ_e/σ_{eff}) increases at any Cu percentage in the Al-Cu layer. With increasing Cu content, the stress ratio parameter (σ_m/σ_{eff}) also increases along with relative density at any deformation temperature. Higher stress ratio parameter (σ_m/σ_{eff}) and relative density (*R*) were observed in 10wt. % Cu preform at 450 ^{0}C deformation temperature.

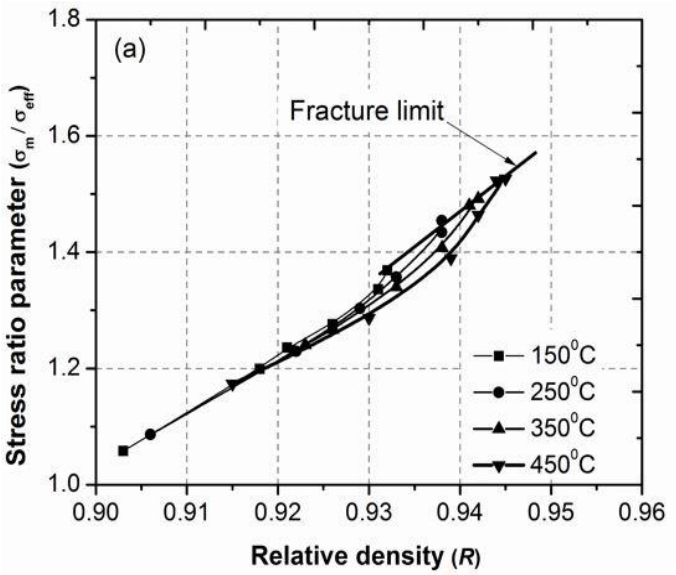

Fig. 6.13 Effect of relative density *(R)* on stress ratio parameter (σ_e/σ_{eff}) of (a) Al-5%Cu/Al composite for various temperatures under the tri-axial stress state condition.

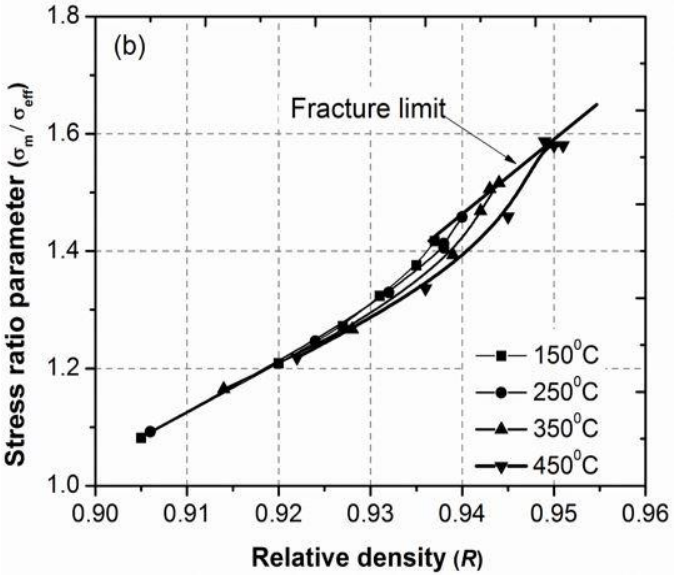

Fig. 6.14 Effect of relative density *(R)* on stress ratio parameter (σ_e/σ_{eff}) of (b) Al-10%Cu/Al composite for various temperatures under the tri-axial stress state condition.

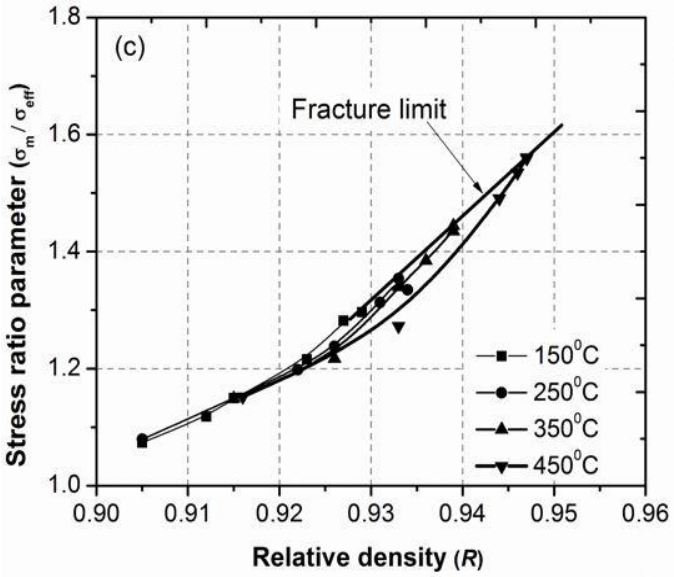

Fig. 6.15 Effect of relative density *(R)* on stress ratio parameter (σ_e/σ_{eff}) of (c) Al-15%Cu/Al composite for various temperatures under the tri-axial stress state condition.

6.4. Chapter Summary

The hot-pressed Al-Cu/Al (Cu: 5wt. %, 10wt. % and 15wt. %) two-layered preforms were successfully produced by P/M method to improve the workability and densification behavior. The formability and densification of such preforms were studied during the hot upsetting process with IRD of 0.9 and strain rate of $0.1s^{-1}$, under triaxial stress state condition at different deformation temperatures from 150-450 ^{0}C and various percentages of Cu content in Al-Cu layer. The following conclusions are obtained for aforesaid performs with respective conditions:

- The densification of preforms increased rapidly and attained peak stress at lower axial strain (approximately 0.02) in the starting phase of deformation due to pores decreases.
- The densification gradually decreased with increasing axial-strain from 0.02 to fracture, causing an increase of axial deformation, decrease in pore size and finally fracture.
- The highest relative density (*R*) of 0.95 was attained by 10wt. %Cu performs at 450 ^{0}C deformation-temperature.
- With the increase of axial-strain, the formability stress index (β) increased at any deformation- temperature with the addition of Cu content in Al-Cu layer. The higher

formability stress index was attained for 10wt. %Cu preform at 450 ^{0}C deformation-temperature.

- Both β and R increase with increase in deformation temperature and the addition of Cu content in Al-Cu layer. The maximum workability and relative density were obtained for 10wt. %Cu preform at 450 ^{0}C deformation-temperature.
- Both stress ratio parameters ($\sigma_\theta/\sigma_{eff}$,$\sigma_m/\sigma_{eff}$) versus relative density curves show that workability increases with increasing deformation-temperature and the addition of 10wt. % Cu content to Al-Cu layer.
- The cooperative deformation on the interface was obtained between Al-Cu layer and Al layer at a low deformation temperature of 150 ^{0}C for 10wt. %Cu preform.

Chapter 7

Modelling the microstructure of the dynamically recrystallized grain size of a Al–10 wt % Cu/Al two-layered sintered composite under hot upsetting

7. 1. Introduction

In the forming process, the important technological feature is the metal and alloy both of which are controlled by the grain size, because grain size plays an important role and is closely related to the mechanical performance and properties of the last product. Through hot deformation the Dynamic Recrystallization (DRX) plays a key role for the microstructure or grain size control that decreases the resistance of material. Under interface constraint effect, soft Al layer and hard Cu layer coordinate with each other during the hot compression process of Cu/Al composites materials. And the cooperative deformation capability increases with increasing stain rate and decreasing deformation temperature.

The regulation of grain size in any technical metal is extremely critical during the hot upsetting process. In most cases, the grain size of a material has a direct impact on the mechanical qualities and performance of the material. Al–Cu/Al two-layered structure composite has a wide range of uses in a variety of industries, including nuclear power, defence, and electronic manufacturing. As a result, the purpose of the present work is to investigate the dynamic recrystallization (DRX) behaviour of an Al–10 wt% Cu/Al two-layered structure composite at the interface region during a hot upsetting test. Experiments were carried out on sintered Al–10 wt % Cu/Al sintered samples by a number of initial relative density values of 80%, 85%, and 90% over a temperature limit of 150–350 ^{0}C and a strain rate range of 0.1–0.3 s^{-1}. The results were compared with theoretical predictions. An optical microscope was used to examine the DRX grain size of Al–10 wt % Cu/Al preforms for IRDes, as well as temperatures and strain rates experienced during the process. The activation energy and Zener–Hollomon constraint of Al–10 wt percent Cu/Al sintered samples were computed under a variety of deformation circumstances and IRDes, and the results are presented in this paper. In order to estimate the DRXed grain size, mathematical representations of DRX are situated to create a role for Zener–Hollomon parameter at various IRDs and apply it to various IRDs. It has been discovered that DRX grain size reduces as the Zener–

Hollomon parameter is increased. A series of verification experiments were carried out between the calculated and predicted values of DRX grain size with a variety of IRDs. The results revealed that the absolute and mean absolute errors were 8.91 and 3.75 percent, respectively.

7.2. Results and Discussion

7.2.1. Study of Hot Flow plots

The peak flow stresses from true strain (ε) - true stress (σ) experimental values of Al-10 wt %Cu/Al two layered sintered preforms hot deformed at different temperatures 150^0C, 250^0C and 350^0C with different strain rates such as 0.1 s^{-1}, 0.2 s^{-1} and 0.3 s^{-1} for different IRD's (Initial relative density) such as 80%, 85% and 90% are as shown in Table 7.1. It is observed from [144, 145, 146, 147], that flow stress is remarkably sensitive to strain rates and deformation temperatures. With increase in hot upsetting temperature and decrease in strain rate, the flow stress decreases irrespective of initial relative densities (IRD's). There is an increase in movement of grain boundaries, when hot upsetting temperature increases, thereby accelerating the growth of DRX grains [148]. In contrast, with increase in hot upsetting temperature, the vacancy due to diffusion (diffusion rate) and dislocation due to motion (motion of dislocation rate) increases [149], it is also observed that there is increase in the amount of DRX grains because there is adequate time to hot upsetting a two layered preforms while lowering strain rate.

Therefore, an increase in dynamic softening enables the flow stress decrease [150]. For every tested condition the influence of IRD is important on flow stress. Irrespective of strain rate temperature, an increase in flow stress was observed with increase in IRD. By increasing IRD, difficulties occur while deforming a two layered preform such as the dislocation slip because for deforming a sample, it requires enormous amount of load, the hardness and strength of the two layered preform also increase. When compared to low IRD, at higher IRDs, the dislocation slip movement was lower with respect to hot upsetting load. Thus, to avoid complications through deformation it needs an amount of high load to increase the movement of dislocation slip of the two layered preforms. The plots of flow stress highly increase up to strain value of 0.2 and from 0.2 it is constant till the highest strain values are attained. This occurs for maintaining the dynamic balancing between work hardening and dynamic softening stages. On low strain rate, work hardening plans an important role to increase the dislocation slip movement density [151], and leads to fast growth of flow stress up to 0.2. From 0.2 to high strain value the plots of flow stress showed a steady state, where the DRX process starts through hot upsetting. After 0.2 strain value,

increasing the strain rate leads to work hardening neutralization after when dynamic recovery takes places which causes DRX phenomenon. From the result it is clearly observed that at high strain values σ - ε plots turn out to be flat to almost zero slope.

Table 7.1 Experimental peak flow stress of Al-10%Cu/Al composite with various IRDs

		IRD-80%	IRD-85%	IRD-90%
Def. Tem. (K)	$\acute{\varepsilon}$ (s^{-1})	PFS stress (σ) (MPa)	PFS stress (σ) (MPa)	PFS stress (σ) (MPa)
423.15	0.1	108.13	111.13	113.13
423.15	0.2	111.16	114.12	116.61
423.15	0.3	113.15	116.28	118.15
523.15	0.1	86.84	89.84	91.84
523.15	0.2	89.81	92.81	94.81
523.15	0.3	91.46	94.46	96.46
623.15	0.1	61.84	64.84	66.84
623.15	0.2	64.71	67.81	69.81
623.15	0.3	66.36	68.29	71.19

7.2.2. Computation of Activation Energy (Q) and Zener–Hollomon Parameter (Z).

The change in DRX grain size is only determined by some deformation conditions [152].

The purpose of Zener–Hollomon parameter is to show the effect of both strain rate and temperature [153].

$$Z = \acute{\varepsilon} \exp\left(\frac{Q}{RT}\right) \quad (7.1)$$

The strain rate (s-1), activation energy (kJ mol-1) of hot deformation, universal gas constant (8.314 J mol-1 K-1), and the absolute temperature (T) are all denoted by the symbol (K).

For finding the results of parameters of Zener–Holloman, it is good to measure the activation energy of hot deformation. During hot deformation, Arrhenius [153, 154] -type equation is considered to measure the activation energy. The Arrhenius equation is defined as follows:

$$\acute{\varepsilon} = A\,[\sinh(\alpha\sigma)]^n \, exp\left(\frac{-Q}{RT}\right) \quad (7.2)$$

Aimed at low stress stages ($\alpha\sigma$ <0.8), $\sinh(\alpha\sigma)^n \approx \alpha\sigma$, and equation (7.2) can be reduced to:

$$\acute{\varepsilon} = A_1\, \sigma^n\, exp\left(\frac{-Q}{RT}\right) \quad [\alpha\sigma < 0.8] \tag{7.3}$$

Where $A_1 = A\alpha^n$, (fabrication material constant)

However when aimed at high stress stages ($\alpha\sigma$>1.2), $\sinh(\alpha\sigma) \approx 0.5 \exp(\alpha\sigma)$ and equation (7.2) can be reduced to:

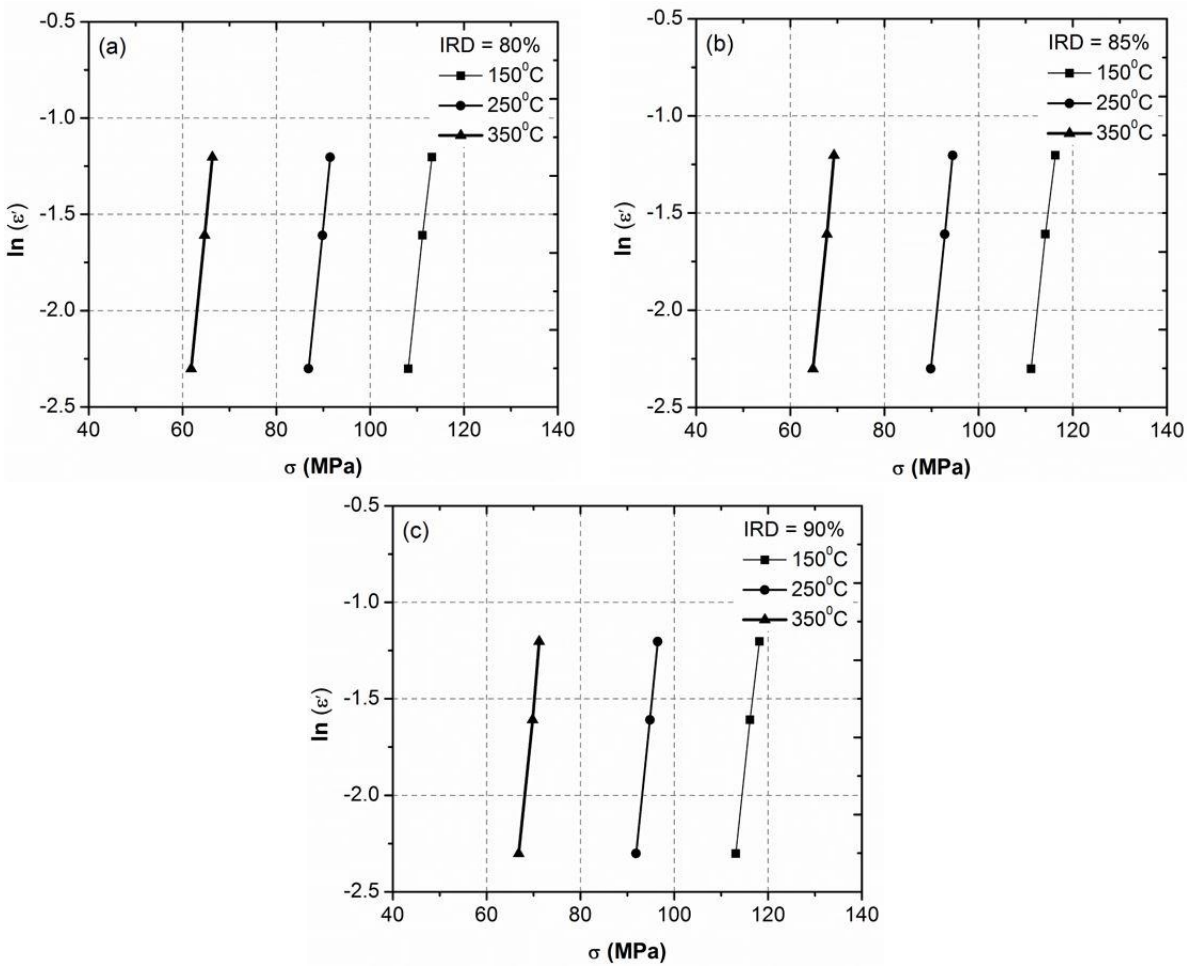

Fig. 7.1 Relationship between ln $\acute{\varepsilon}$ – $\boldsymbol{\sigma}$ of composite with various IRDs

Figs. 7.1 and 7.2 shows the associated diagrams of ln $\acute{\varepsilon}$ – ln σ & ln $\acute{\varepsilon}$ – σ. By measuring the slant average of ln $\acute{\varepsilon}$ – σ & ln $\acute{\varepsilon}$ – ln σ shapes at dissimilar temperatures, the values of β and n can be attained. Thus, the value of $\alpha = \beta/n$ is measured. Table 7.2 shows the average measures of β, α & n intended for hot deformation of Al–10wt. % Cu/Al sintered two layered composites for various IRDs.

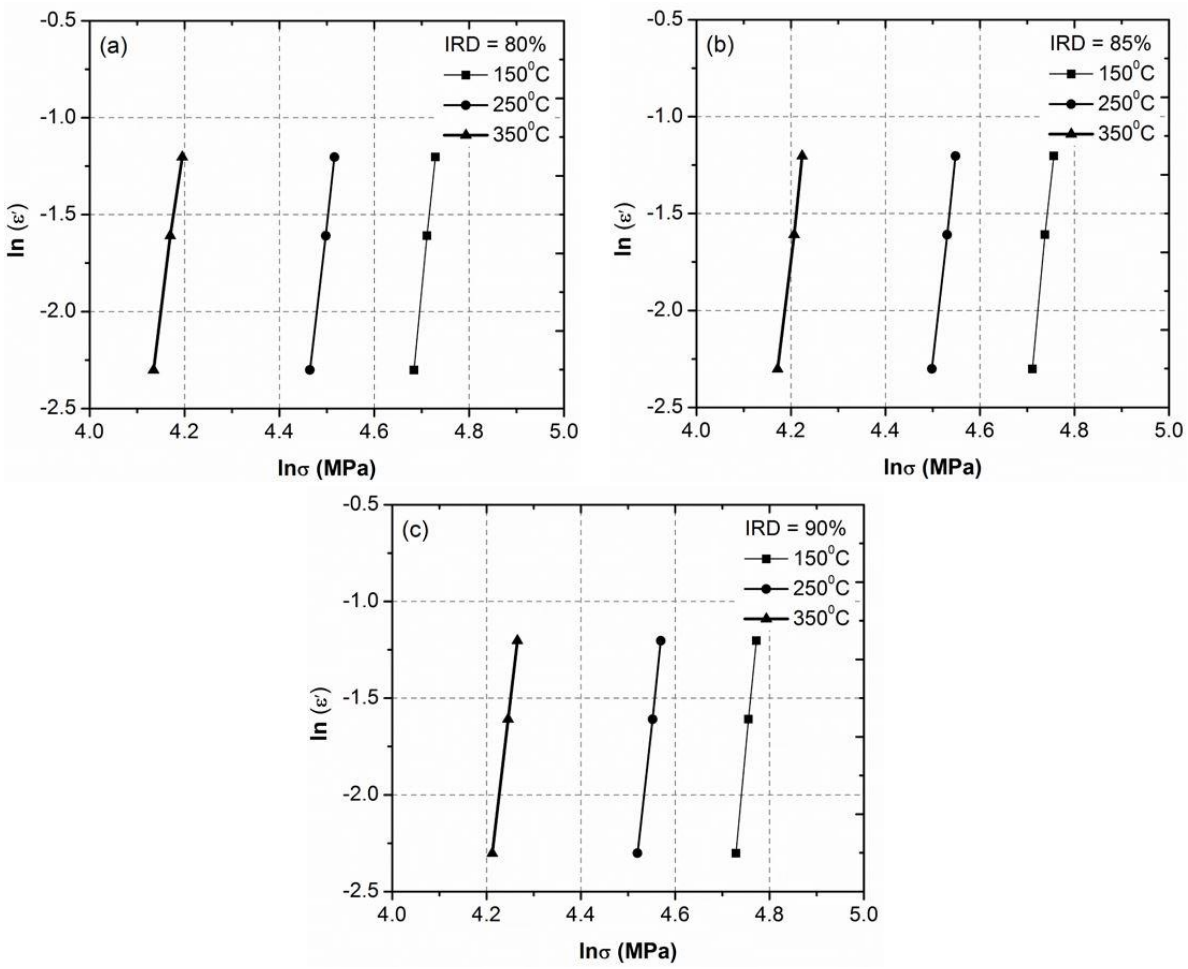

Fig. 7.2 Relationship between ln $\acute{\varepsilon}$ – ln $\boldsymbol{\sigma}$ of composite with different IRDs

$$\acute{\varepsilon} = A_2\, exp(\beta\sigma)\, exp\left(\frac{-Q}{RT}\right) \quad [\alpha\sigma > 1.2] \tag{7.4}$$

$$\acute{\varepsilon} = A\, [\sinh\,(\alpha\sigma)^n]\, exp\left(\frac{-Q}{RT}\right) [\alpha\sigma \text{ taking any values}] \tag{7.5}$$

Where A, $A_2 = A/2^n$, and $\alpha = \beta/n$, in this case, the values of n and β are estimated from the constants, based on the findings of the experiments.

Taken together, Eqs. (7.3) and (7.4) can be stated as Eqs. (7.6) and (7.7), which are the natural logarithms of the original equations.

$$\ln\acute{\varepsilon} = \ln A_1 + n\ln\sigma - \frac{Q}{RT} \tag{7.6}$$

$$\ln\dot{\varepsilon} = \ln A_2 + \beta\sigma - \frac{Q}{RT} \quad (7.7)$$

The partial differentiation of Equations (7.6) and (7.7) can be reduced as given below because the hot upsetting process led at persistent temperature.

$$n = \left[\frac{\partial \ln\dot{\varepsilon}}{\partial \ln\sigma}\right]_{T=const} \quad (7.8)$$

$$\beta = \left[\frac{\partial \ln\dot{\varepsilon}}{\partial \sigma}\right]_{T=const} \quad (7.9)$$

Table 7.2 Different IRDes of composite were used to calculate the values of β and n

IRD (%)	β	n	α
80	0.233	21.21	0.0111
85	0.232	21.78	0.0108
90	0.235	20.80	0.0104

The values of flow stress and their equivalent strain rate are substituted in equations (7.8) & (7.9) for different IRDs and temperatures and during the hot deformation of Al–10wt. % Cu/Al two layered sintered composites activation energy (Q) at dissimilar temperatures, the strain rates and IRDs can be attained through applying expected natural logarithm on both sides of Equation (7.5).

$$\ln\dot{\varepsilon} = A\, n\ln\left[\sinh(\alpha\sigma)\right] - \frac{Q}{RT} \quad (7.10)$$

When the constant strain rate requirement is stated, partial differentiation of equation (7.10) yields the result

$$Q = R\left\{\frac{\partial \ln\dot{\varepsilon}}{\partial \ln\left[\sinh(\alpha\sigma)\right]}\right\}_{T=const}\left\{\frac{\partial \ln\left[\sinh(\alpha\sigma)\right]}{\partial\left(\frac{1}{T}\right)}\right\}_{\dot{\varepsilon}=const} \quad (7.11)$$

Therefore, the relationship of $\ln\dot{\varepsilon} - \ln[\sinh(\alpha\sigma)]$ and $\ln[\sinh(\alpha\sigma)] - 1/T$ can be attained by applying the values of temperature and flow stress at a given strain rate for different IRDs into Equation (7.11), as shown in Figs. 7.3 and 7.4 the activation energy is measured form the slop of $\ln\dot{\varepsilon} - \ln[\sinh(\alpha\sigma)$ and $\ln[\sinh(\alpha\sigma)]$. Table. 7.3 denotes Al–10wt % Cu/Al two layered composites activation energy at various deformation conditions. Mostly, the values of β, n, activation energy has great effect by IRD. The Al–10wt % Cu/Al two layered composite's activation energy (Q) is more than Pure Aluminium's self-diffusion energy is (144.3 kJ/mol) [155], during hot deformation for various IRDs, strain rates and temperatures, because of the

reinforcement of Copper added to Aluminium matrix (Al-Cu layer), as clearly observed form Table. 7.3.

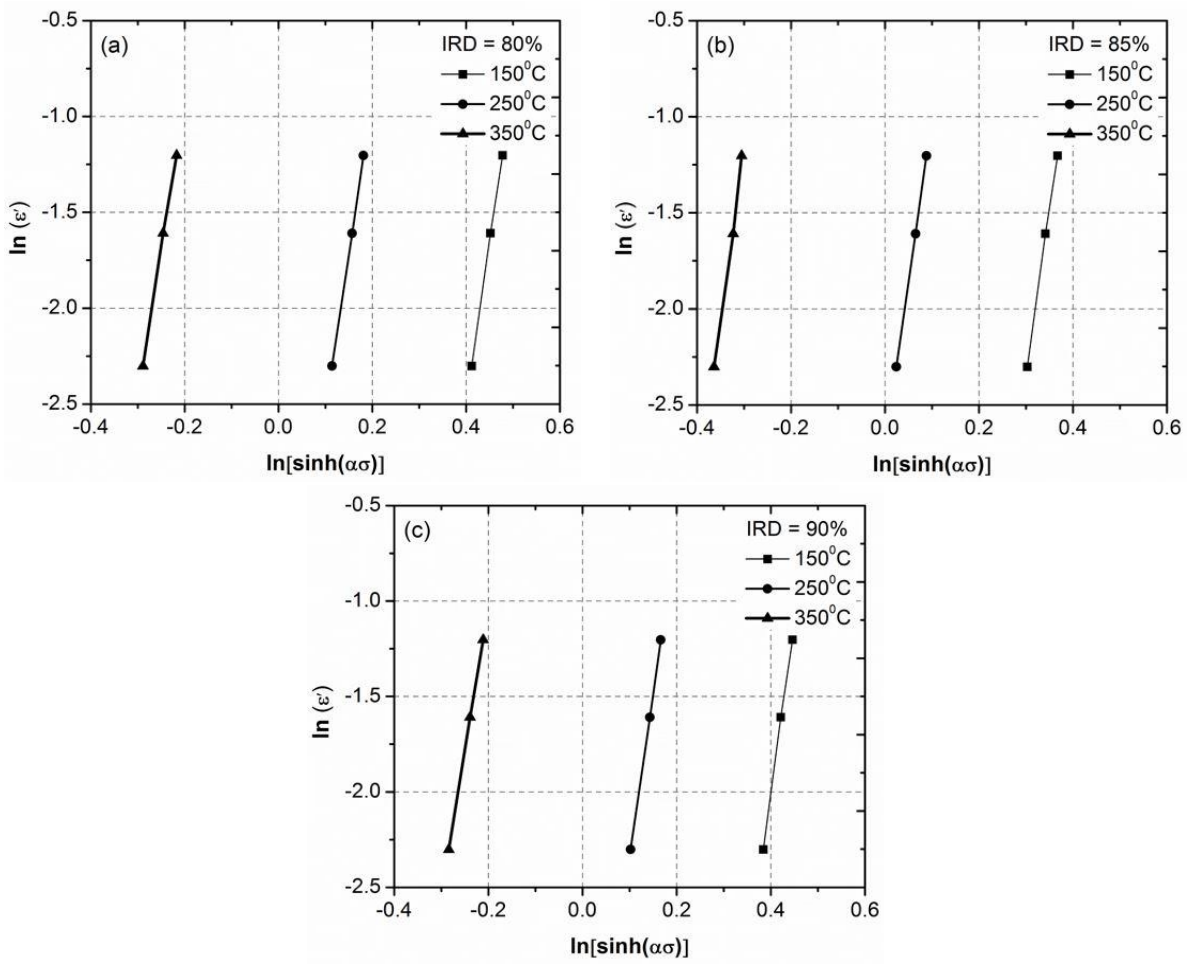

Fig. 7.3 Relationship between $\boldsymbol{ln\dot{\varepsilon} - ln[sinh(\alpha\sigma)]}$ of Al–10wt % Cu/Al sample with various IRDs

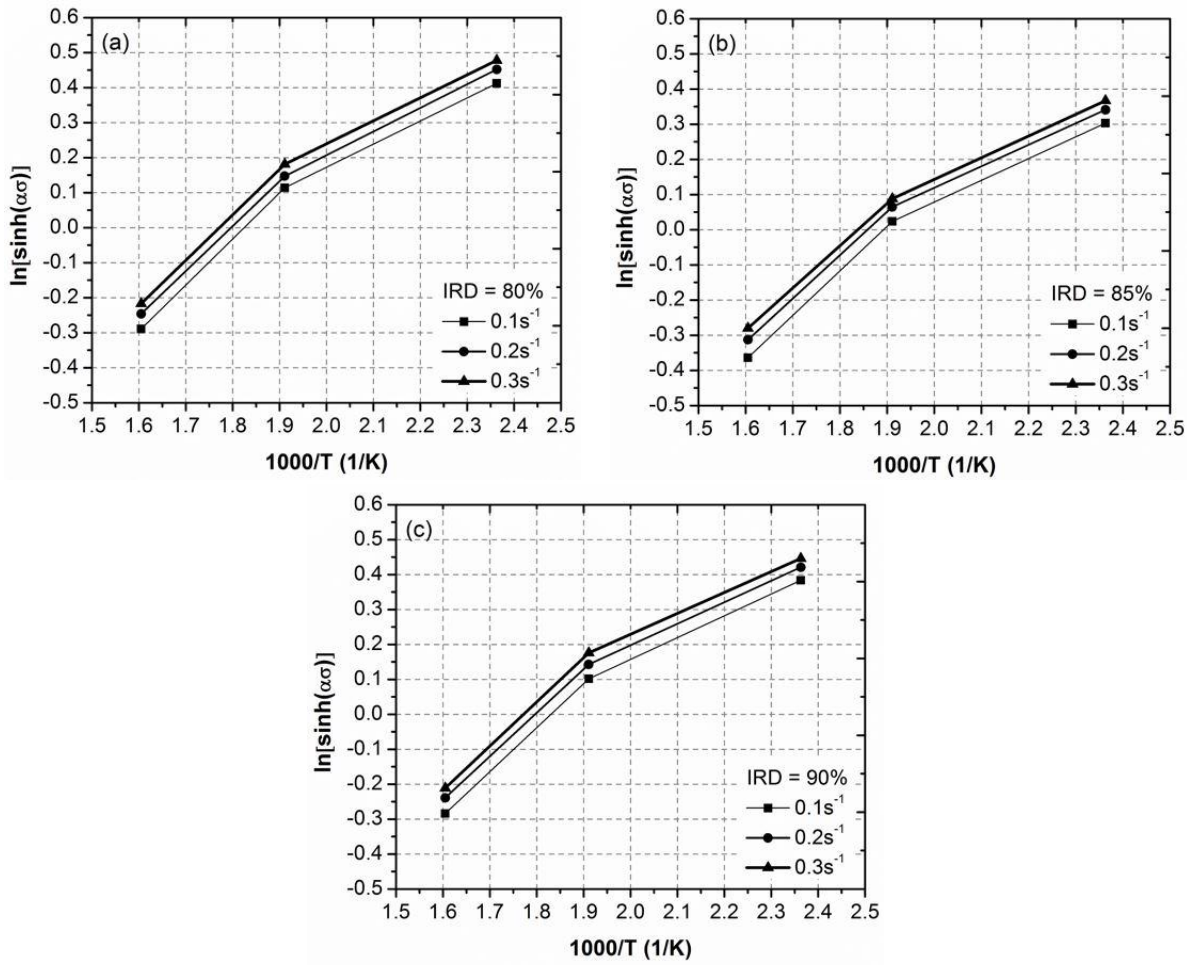

Fig.7.4 Relationship between $\boldsymbol{ln}[\boldsymbol{sinh}(\boldsymbol{\alpha\sigma})]$ – 1/T of sample with different IRDs

Table 7.3 Values of Q and Z parameter with various IRDs of Al–10wt % Cu/Al composite

		IRD-80%		IRD-85%		IRD-90%	
Def. Tem. (K)	έ (s^{-1})	Q (kJ/mol)	Z (s^{-1})	Q (kJ/mol)	Z (s^{-1})	Q (kJ/mol)	Z (s^{-1})
423.15	0.1	165.85	2.9×10^{19}	168.10	5.6×10^{19}	179.51	1.4×10^{21}
523.15	0.1	162.79	1.8×10^{15}	165.23	3.1×10^{15}	177.61	5.4×10^{16}
623.15	0.1	155.67	1.1×10^{12}	163.87	5.4×10^{12}	174.77	4.4×10^{13}
423.15	0.2	164.23	3.7×10^{19}	166.35	6.8×10^{19}	177.67	1.7×10^{21}
523.15	0.2	161.20	2.4×10^{15}	163.51	4.2×10^{15}	175.79	7.1×10^{16}
623.15	0.2	154.14	1.6×10^{12}	162.16	7.8×10^{12}	172.98	6.3×10^{13}
423.15	0.3	162.43	3.3×10^{19}	164.40	5.9×10^{19}	175.62	1.4×10^{21}
523.15	0.3	159.43	2.4×10^{15}	161.60	4.1×10^{15}	173.76	6.7×10^{16}
623.15	0.3	152.45	1.8×10^{12}	160.26	8.1×10^{12}	170.98	6.4×10^{13}

To estimate the Z constraint for equivalent strain rate range and different deformation temperatures the activation energy (Q) values are substituted in equation (7.1). At different deformation

conditions the Zener-Hollomon constraint values of Al–10wt % Cu/Al sintered two layered composite are shown in Table. 7.3.

7.2.3. Expansion of Microstructure Manner of Al–10wt % Cu/Al Composite

The association of Zener–Hollomon parameter and DRX grain size average can be defined as follows [156]:

$$d_{\mathrm{dny}} = A_{\mathrm{dny}} Z^{n\,\mathrm{dny}} \qquad (7.12)$$

Where d_{dyn} - dynamically recrystallized grain size (measured at interface of the Al–10wt % Cu/Al two layered composite) , $A_{dyn,}$ $n_{dyn\,-}$ fabrication material constants.

To conclude to DRX (d_{dyn}) grain size, a mathematical model was developed using Eq. (7.12). It is shown in Fig. 7.5. The association of d_{dyn} – Z of Al–10wt % Cu/Al two layered sample for various IRDs was developed by appropriate form of power law in Eq. (7.12). Therefore, for various IRDs (80%, 85%, and 90%) different mathematical models were established between d_{dyn} – Z.

These models figure below:

for 80% IRD $d_{\mathrm{dny}} = 10.71\, Z^{-0.009}$ ($R^2 = 0.907$) (7.13)

for 85% IRD $d_{\mathrm{dny}} = 14.67\, Z^{-0.011}$ ($R^2 = 0.915$) (7.14)

for 90% IRD $d_{\mathrm{dny}} = 21.04\, Z^{-0.01}$ ($R^2 = 0.934$) (7.15)

d_{dyn} as a function Z parameter shown in Fig. 7.5.

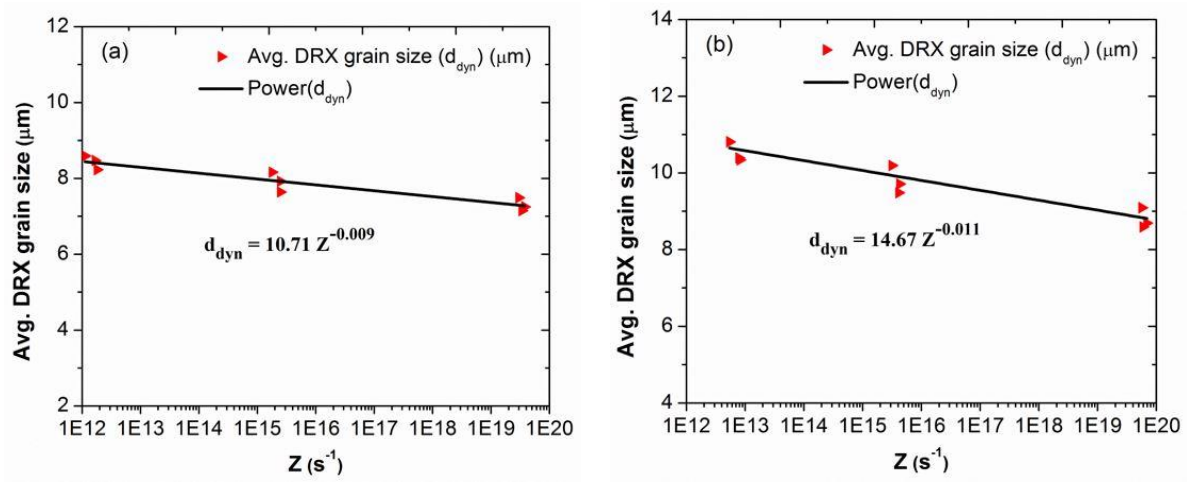

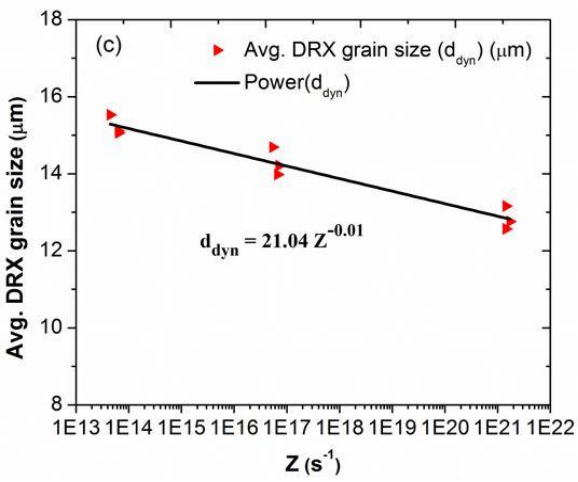

Fig. 7.5 Relationship between Z parameters and d_{dyn} of Al–10wt % Cu/Al composite with various IRDs

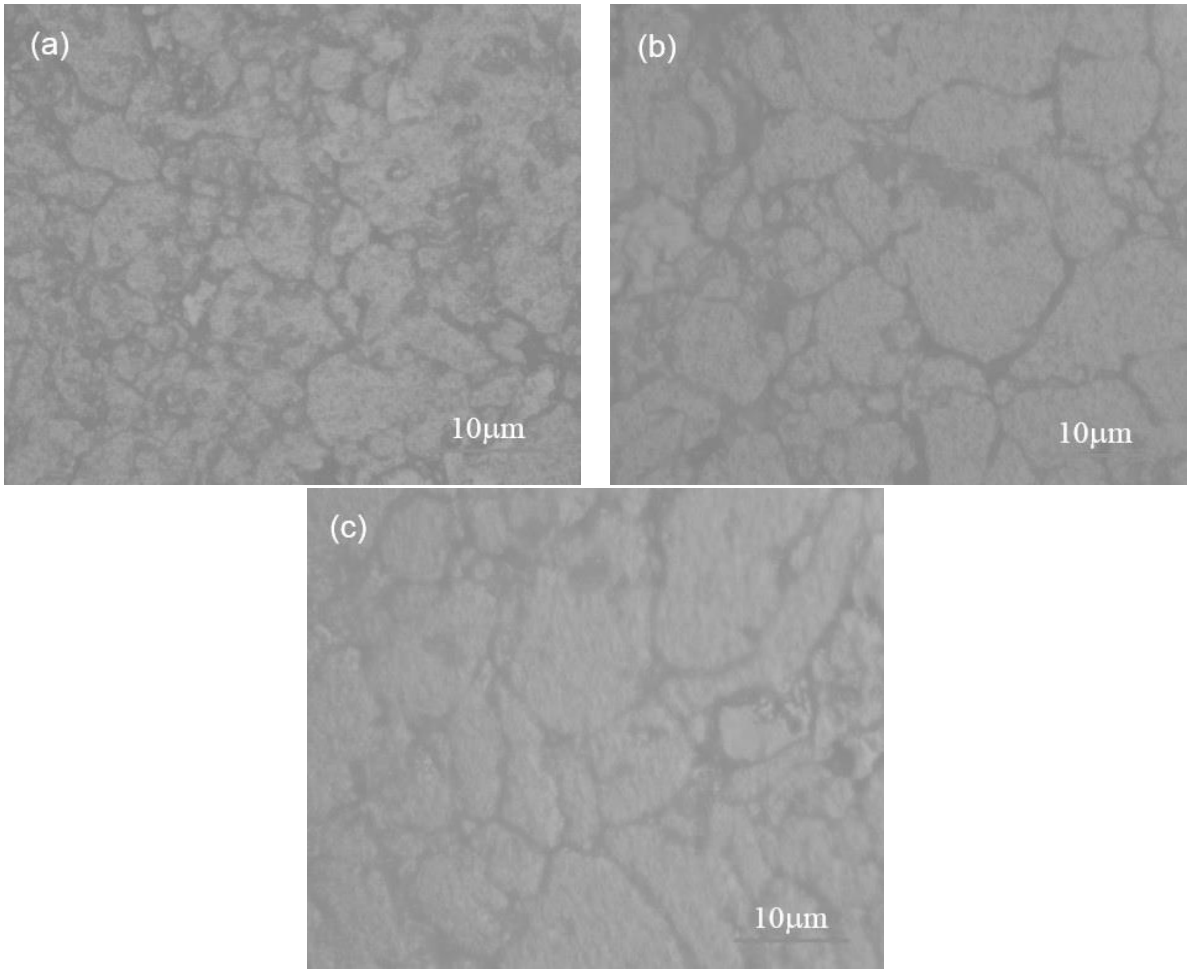

Fig. 7.6 Microstructure of Hot deformed Al–10wt. %Cu/Al samples with a strain rate of 0.1 s^{-1} and a 90% IRD at various temperatures: (a) 150 °C, (b) 250 °C, and (c) 350 °C

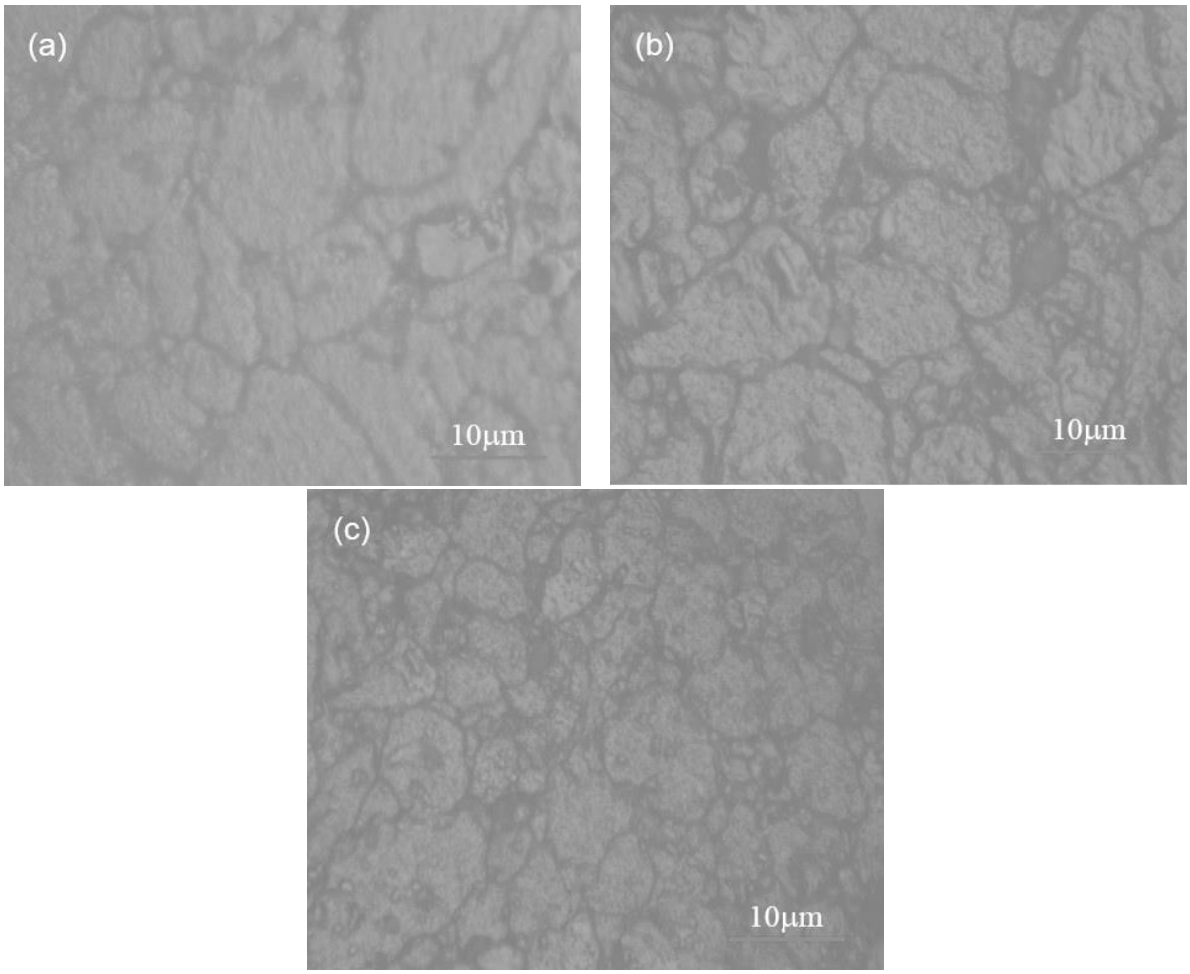

Fig. 7.7 Temperature and strain rate effects on the microstructure of Al–10wt. %Cu hot deformed samples at 90% IRD at 150 ^{0}C

The d_{dyn} is in reverse proportion to Zener-Hollomon parameter (Z), as clearly observed from the mathematical model expressed above. As shown in Figs. 7.6 and 7.7 the d_{dyn} reduced with growth in strain rate and decreased at hot deformation temperature. At low temperature, the DRX grain boundaries show slow movement. Similarly, with strain rate increase, nucleation rate also increases, therefore d_{dyn} decreases. Under other conditions, with growth in temperature and reduction in strain rate, d_{dyn} increases. At low strain rates an increase in grain size was observed because there was enough time available for grain growth, and the movement of DRX grain boundaries was high when the deformation temperature was high. As per Eq. (1), with increase in

strain rate and decrease in temperature there was an increases in Zener-Hollomon parameter. Therefore, there was an increase of Z parameter with grain size decrease shown in Fig. 7.5. As per the Eq^{n} (7.1) there was a decrease in Zener-Hollomon parameter with strain rate decrease and temperature increase. Accordingly, with decrease in Zener-Hollomon parameter grain increased. Thus, it is clearly noticed from Figs. 7.6 and 7.7 that the DRX grain size is totally dependent the Z parameters such as strain rate and temperature. From Table 7.4. It can be noticed that for different initial relative densities, from the established mathematical model Equations (7.13) – (7.15), the material constants A_{dyn} & n_{dyn} values were measured.

Table 7.4 Al–10wt% Cu/Al composites yielded different values for Adyn and ndyn

IRD (%)	A_{dyn}	n_{dyn}
80	10.71	-0.009
85	14.67	-0.011
90	21.04	-0.01

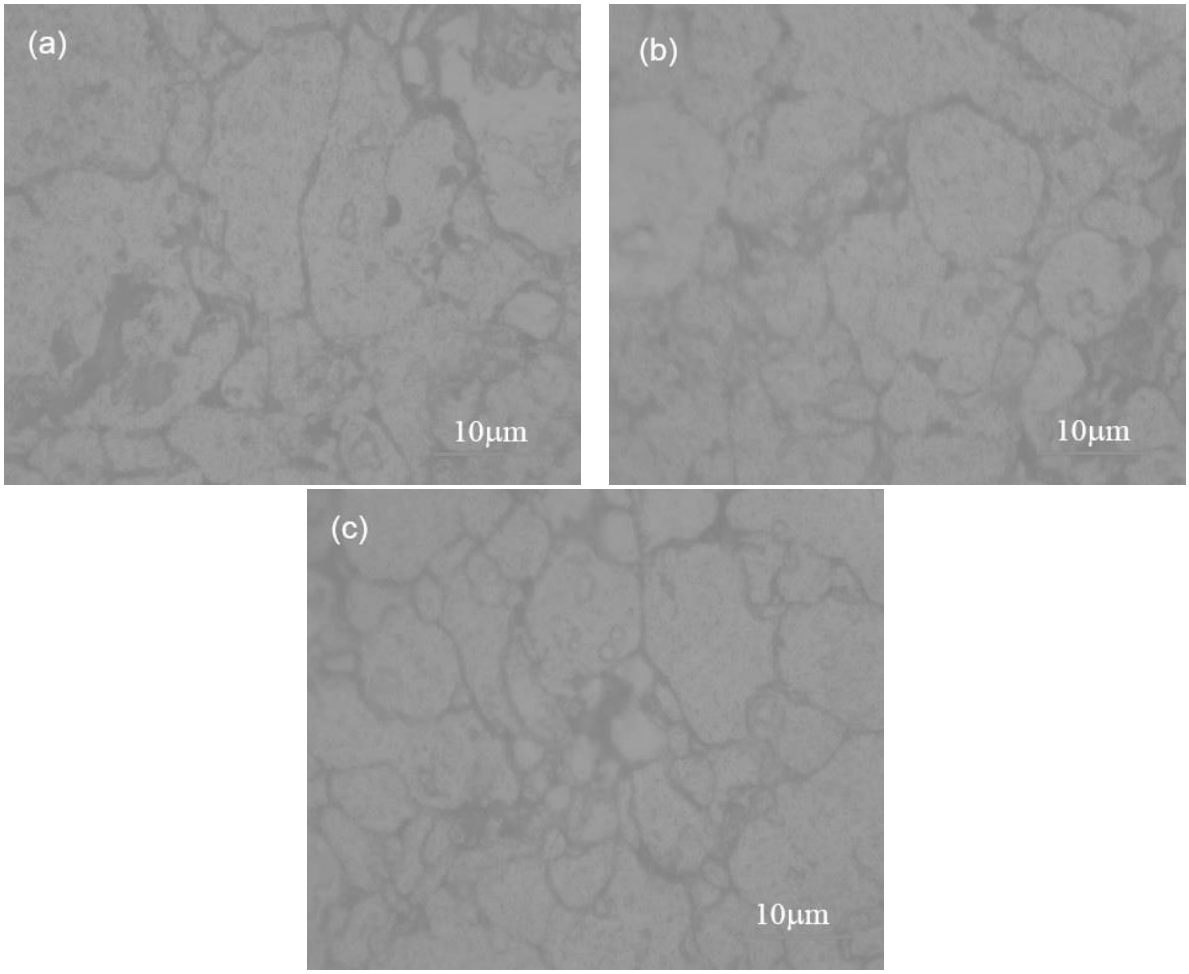

Fig. 7.8 Microstructures of Al–10wt. %Cu hot deformed samples for 90% IRD temperature of 350 ^{0}C at dissimilar strain rates

Table 7.5 Comparison between measured and calculated grain size of Al-10%Cu/Al composite with various IRDs

	Initial relative density = 80%					Initial relative density = 85%				Initial relative density = 90%			
Def. Temp (K)	Strain rate (s^{-1})	d_m (μm)	d_c (μm)	δ (%)	δ_m (%)	d_m (μm)	d_c (μm)	δ (%)	δ_m (%)	d_m (μm)	d_c (μm)	δ (%)	δ_m (%)
423	0.1	7.29	7.16	1.82	2.53	9.09	8.90	2.14	3.74	13.16	12.93	1.76	1.78
523	0.1	8.01	7.81	2.48		10.19	9.91	2.78		14.69	14.31	2.56	
623	0.1	8.69	8.98	3.31		10.95	11.64	6.31		15.53	15.37	1.04	
423	0.2	7.25	7.14	1.48	1.64	8.69	8.82	1.55	1.59	12.76	12.91	1.14	0.98
523	0.2	7.92	7.79	1.66		9.71	9.58	1.39		14.21	14.28	0.46	
623	0.2	8.47	8.32	1.79		10.39	10.58	1.85		15.11	15.31	1.36	
423	0.3	7.15	7.30	2.07	1.44	8.59	7.82	8.91	3.75	12.57	12.93	2.85	2.23
523	0.3	7.64	7.79	1.95		8.48	8.47	0.15		13.98	14.28	2.17	
623	0.3	8.13	8.11	0.30		9.14	8.94	2.16		15.06	15.31	1.67	

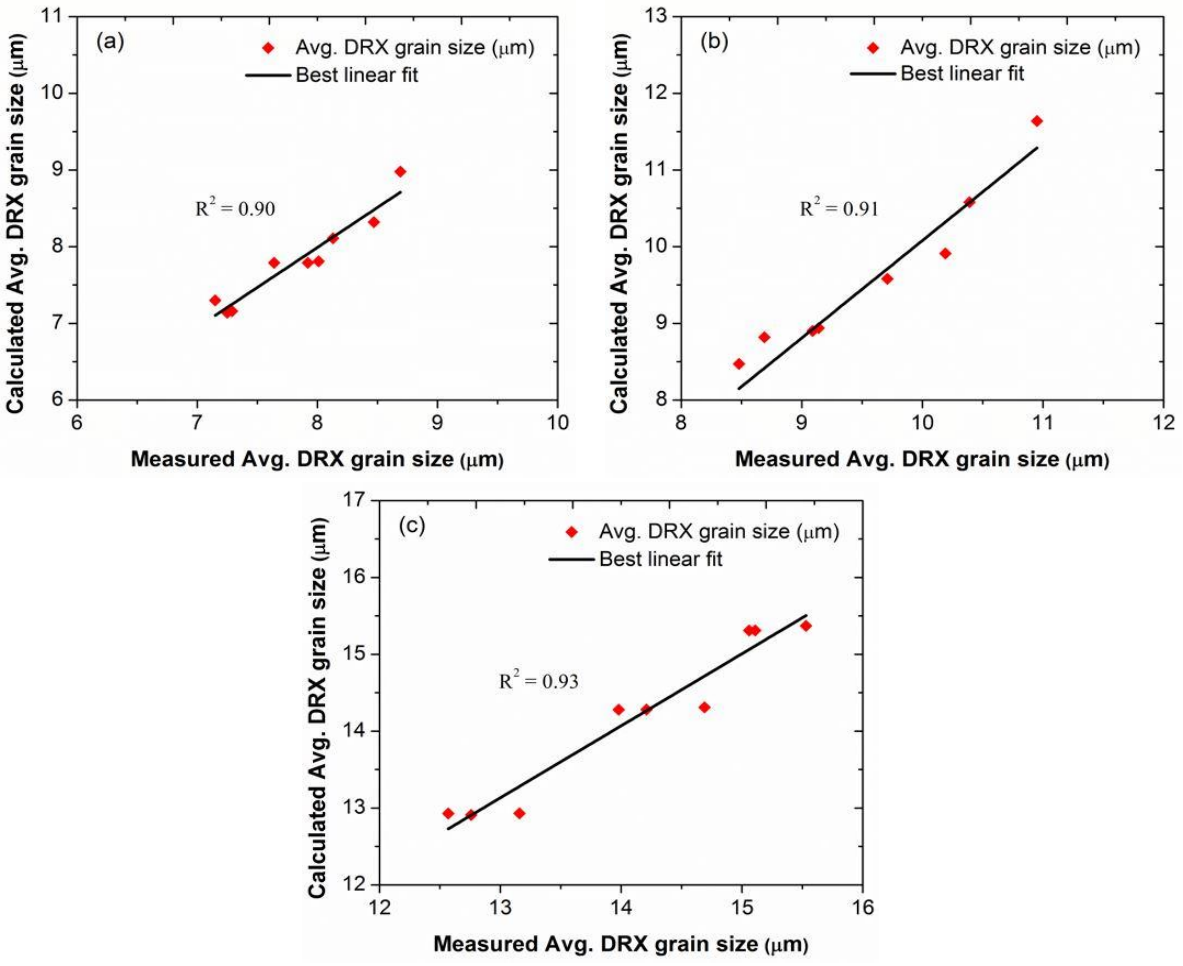

Fig. 7.9 Correlation between calculated and measured average DRX grain size of Al–10wt % Cu/Al sample with different IRDs

It was observed that with an increase in IRD, the value of n_{dyn} also increases. A reduction in the value of Z constraint tends to growth in $d_{dyn.}$ Therefore, form Fig. 7.8 it is noticed that d_{dyn} increases with increasing IRD. An increase in IRD of the sample before deformation, decreases the porosity, which enables earlier diffusion of grains throughout the deformation. From Table 7.5 it is noticed that with IRD increase, d_{dyn} also increases. Under other conditions, when IRD decreases, d_{dyn} also decreases. Hence, d_{dyn} is dependent on Initial Relative Density (IRD). The established mathematical models of DRX mentioned above can be used to measure the DRXd grain size of Al–10wt % Cu/Al sintered two layered structured composite for various IRDs

7.2.4. Confirmation of Established Mathematical Standard of Al–10wt % Cu/Al Sintered two layered structured composite.

From Table 7.5, the measured DRXd grain sizes can be observed at different deformation condition and IRDs for the established model. To estimate the accuracy of the established model of Sintered Al–10wt % Cu/Al two layered structured composite, a comparison was made between measured and calculated DRXd grains for each IRD. From Fig. 7.9 the curves between calculated and measured d_{dyn} at different IRDs are available. The maximum d_{dyn} of d_c and d_m are almost near the line of best fit. The R^2 values between d_c and d_m of d_{dyn} are said to be 0.90, 0.91 and 0.93 at each IRD of 80%, 85%, and 90%, at which d_c perfectly agreed with the d_m under all deformation conditions. Therefore, at higher IRD, the estimation capability of the established model is better. Furthermore, the accuracy of the established mathematical model of Al–10wt % Cu/Al two layered structured composite through hot upsetting was proven by applying absolute error-d and mean absolute error-dm which are called standard statistical parameters. The absolute error is calculated from the values of d_{dyn} of d_c and d_m using the below equation:

$$\delta = \left|\frac{d_c - d_m}{d_m}\right| \times 100\% \qquad (7.16)$$

From Table 7.5, at various IRDs and deformation conditions, a complete comparison was made between d_c and d_m of d_{dyn} of sintered Al–10wt % Cu/Al two layered structured composite. At different IRDs and at each deformation conditions, the average percentage error did not exceed 8.91% and the mean absolute error did not overdo 3.75%. Therefore, it was evident that the mathematical representations showed improved predictive ability at high IRDs and low strain rates

through hot deformation. Consequently, the findings show that d_c (calculated result) shows better agreement with d_m results of DRX grain size. This is the evidence for the reliability and precision of established mathematical model of Al–10wt % Cu/Al two layered structured composite at different IRDs.

7.3. Chapter Summary

The DRX behaviour of sintered Al–10 wt percent Cu/Al two-layered structure preforms was investigated by carrying out hot upsetting examinations for dissimilar IRDes of 80%, 85% and 90% at temperatures ranging from 150 to 350 ^{0}C and strain rates ranging from 0.1 to 0.3 s^{-1}. The following conclusions can be drawn:

- The intercept line approach was used to determine DRXed grain size, which ranges from 2 to 36m and is reliant on the deformation circumstances and IRDs.
- For sintered Al–10 wt % Cu/Al preforms, the activation energy and Zener–Hollomon parameter were lower than the self-diffusion of pure aluminium at varied temperatures, strain rates, and IRDes. Aluminium's kinetic energy is 144.3 kJ/mol, which is lower than the activation energies studied.
- The DRXed grain size was calculated by constructing mathematical relationships between dynamic recrystallization grain size and Zener–Hollomon parameter for various IRDes, temperatures, and strain rates.
- When comparing DRXed grain size to measured grain size, the average percentage error for various IRDes and deformation scenarios was 8.91 percent, while the mean absolute error was 3.75 percent for all conditions.
- The findings of this study can be applied to the development of hot deformation regimes for Al–10 wt percent Cu/Al preforms, which will result in the production of the needed DRXed grain size.

Chapter 8

Conclusions and Scope of Future work

8. 1. Conclusions

An experimental investigation was performed on microstructure modelling, corrosion and wear resistance of Al-Cu/Al two-layered structured composite. The two-layered structured composites having various Cu percentages in the Al-Cu layer (Cu: 5wt. %, 10wt. %, and 15wt. %) were fabricated using the powder metallurgy (P/M) method. Two-layered samples were hot-pressed layer by layer in a steel cylindrical die at 500 ^{0}C, 550 ^{0}C and 600 ^{0}C sintering temperature for 3 h. with a constant pressure of 400 MPa. As part of the investigations on hot formability and densification characteristics, the composites were hot-pressed at 550 ^{0}C temperature with 0.9 initial relative density (IRD) and 0.1 s^{-1} strain rate at different deformation temperatures such as 150 ^{0}C, 250 ^{0}C, 350 ^{0}C and 450 ^{0}C, under triaxial stress state condition. The hot deformation behaviour and DRX grain behaviour of hot-pressed Al-10wt%Cu/Al samples were investigated by conducting hot upsetting tests for various IRDes of 80%, 85% and 90%, and at different temperature range of 150 ^{0}C-350 ^{0}C and strain ranges of 0.1 s^{-1} - 0.3 s^{-1}. And also, mathematical models were developed for predicting the flow stress and grain size of the material for different deformation conditions. The following major observations are made from the study:

- The XRD and EDAX tests were analyzed and the results confirmed that Al_2Cu (intermetallic compound) was present in Al-rich phase and this Al_2Cu particle increased proportionally with an increase in Cu content.
- In the interface region of 15wt. % Cu, the greatest value of micro-hardness (100.6HV) was attained at a temperature of 550 ^{0}C.
- The corrosion behaviour of the two layered Al-Cu/Al sample developed was determined using potentiodynamic polarization test at interface region and noticed that the negative potential of 10wt. % Cu sample (990mV) was lower lesser than 5wt. % Cu sample

(1002mV) and 15wt. % Cu sample (1084mV). The experiments suggested that the corrosion susceptibility of the 15wt. % Cu sample is higher.

- The susceptibility of corrosion increases with increase of Cu content in Al-Cu layer. The 10wt. % Cu sample circuit provides minimum chi-square value. From the SEM-EDAX analysis of the samples, it was clearly observed that the intergranular and pitting corrosion occurs at various areas of θ phase.
- The coefficient of friction increases with an increase in sliding distance and sliding velocity, and after that it becomes steady for all pure Al layer, interface region and Al-10%Cu layer. It is found that during friction process, the disc takes little time to stabilize as the sliding distance and sliding velocity increase.
- Friction coefficient decreases with an increase in normal load while it increases with increase in sliding velocity for all pure Al layer, interface region and Al-10%Cu layer.
- The weight loss continuously increases with increase in sliding distance for pure Al layer, interface region and Al-10%Cu layer.
- The less amount of wear debris was noticed on the worn surface of Al-10Cu layer compared to interface region, hence, it is likely that the fluctuations in COF were lower than fluctuations at the interface region and Al layer.
- The highest relative density 0.95 was attained by 10wt. % Cu preforms at 450 ^{0}C deformation-temperature.
- With the increase of axial-strain, the formability stress index (β) increased at any deformation- temperature with the addition of Cu content in Al-Cu layer. The higher formability stress index was attained for 10wt. % Cu preform at 450 ^{0}C deformation-temperature.
- Both stress ratio parameters ($\sigma_\theta/\sigma_{eff}$,$\sigma_m/\sigma_{eff}$) versus relative density curves showed that, the workability increases with increasing deformation-temperature and the addition of 10wt. % Cu content to Al-Cu layer.
- The cooperative deformation on the interface was obtained between Al-Cu layer and Al layer at a low deformation temperature of 150 ^{0}C for 10wt. % Cu preform.
- The activation energy and Zener–Hollomon parameter of sintered Al–10 wt % Cu/Al preforms were calculated at different temperatures, strain rates, and IRDes, and it was

found that activation energies were less than self-diffusion of pure aluminium (144.3 kJ/mol).

- Validation tests performed between the measured and calculated DRXed grain size revealed that the average percentage error for various IRDes and deformation conditions were did not exceed 8.91% and the mean absolute error did not exceed 3.75%.

8. 2. Scope of Future work

The intensive work on experimental investigation on the hot formability and densification characteristics, microstructure modelling, corrosion and wear resistance of Al-Cu/Al two-layered composite can be extended to various dimensions of future research work, and is given below:

- The grain size evolution and design of a model to predict grain size can be performed for different powder materials through different forming processes for better mechanical properties.
- The microstructure evaluation and developing a model to predicting grain size of hot-pressed Al-Cu/Al preforms work can be performed by different forming processes (extrusion and rolling) at high temperature.
- The plastic deformation behavior and densification of hot-pressed Al-Cu/Al preforms can be study during extrusion processes and developing the flow stress model for the extruded samples at elevated temperature.
- It can be the development of new functionally graded materials (FGM) from Al and Cu powders through extrusion and P/M process.
- Investigation on damage characterization: Statistical analysis of porosity in hot-pressed Al-Cu/Al preforms during plastic deformation can be carried out.
- The friction behavior between tool-work piece interfaces of hot-pressed Al-Cu/Al during deformation can be studied extensively.

REFERENCES

[1] Klocke, Fritz, Christoph Broeckmann, Christoph Löpenhaus, Alexander Bezold, Tim Frech, Marko Hajeck, Philipp Scholzen, and Christian Gebhardt. "High-strength gears produced by powder metallurgical processes–KL500/93-2." Industrial Lubrication and Tribology (2019).

[2] Manohar, Guttikonda, Abhijit Dey, K. M. Pandey, and S. R. Maity. "Fabrication of metal matrix composites by powder metallurgy: a review." In AIP Conference Proceedings, vol. 1952, no. 1, p. 020041. AIP Publishing LLC, 2018.

[3] Sweet, Gregory. "IMPROVING THE MECHANICAL AND PHYSICAL PROPERTIES OF AN ALUMINUM POWDER METALLURGY METAL MATRIX COMPOSITE VIA HOT UPSET FORGING." (2019).

[4] Sweet, G. A. W., B. W. Williams, A. Taylor, R. L. Hexemer, I. W. Donaldson, and D. P. Bishop. "A microstructural and mechanical property investigation of a hot upset forged 2xxx series aluminum powder metallurgy alloy reinforced with AlN." Journal of Materials Processing Technology 284 (2020): 116742.

[5] Rajasekhar, Kotikala, V. Suresh Babu, M. J. Davidson, and G. Raghavendra. "Formability and densification behavior of two-layered structure powder metallurgical hot-pressed Al-Cu/Al composites during hot-upsetting." Proceedings of the Institution of Mechanical Engineers, Part E: Journal of Process Mechanical Engineering 235, no. 2 (2021): 582-593.

[6] Tharmaraj, R., and M. Joseph Davidson. "Workability, densification and failure characteristics of selective heated sintered powder metallurgy preforms during upsetting." Journal of Materials Engineering and Performance 29, no. 2 (2020): 933-948.

[7] Arulmani, L., H. N. Shridharmurthy, M. Chithirai Pon Selvan, and Sahith Reddy Madara. "Hot powder forging behavior analysis of sintered AISI 8740 PM steels for automotive application." Materials Today: Proceedings 28 (2020): 1068-1072.

[8] Saikrupa, Ch, G. Chandra Mohan Reddy, and Sriram Venkatesh. "Aluminium metal matrix composites and effect of reinforcements–A Review." In IOP Conference Series: Materials Science and Engineering, vol. 1057, no. 1, p. 012098. IOP Publishing, 2021.

[9] Oladijo, Oluseyi P., Samuel A. Awe, Esther T. Akinlabi, Resego R. Phiri, Lebudi L. Collieus, and Rebaone E. Phuti. "00096 High-Temperature Properties of Metal Matrix Composites." (2021).

[10] Rajasekhar, Kotikala, V. Suresh Babu, M. J. Davidson, and G. Raghavendra. "Formability and densification behavior of two-layered structure powder metallurgical hot-pressed Al-Cu/Al composites during hot-upsetting." Proceedings of the Institution of Mechanical Engineers, Part E: Journal of Process Mechanical Engineering 235, no. 2 (2021): 582-593.

[11] Rajkumar, P. R., C. Kailasanathan, A. Senthilkumar, N. Selvakumar, and A. JohnRajan. "Study on formability and strain hardening index: influence of particle size of boron carbide (B4C) in magnesium matrix composites fabricated by powder metallurgy technique." Materials Research Express 7, no. 1 (2020): 016597.

[12] Narayanasamy, R., T. Ramesh, and K. S. Pandey. "Some aspects on workability of aluminium–iron powder metallurgy composite during cold upsetting." Materials Science and Engineering: A 391, no. 1-2 (2005): 418-426.

[13] Narayan, Sumesh, and A. Rajeshkannan. "Densification behaviour in forming of sintered iron–0.35% carbon powder metallurgy preform during cold upsetting." Materials & Design 32, no. 2 (2011): 1006-1013.

[14] Kim, K. T., H. C. Yang, and S. T. Hong. "Densification behaviour of titanium alloy powder compacts at high temperature." Powder metallurgy 44, no. 1 (2001): 34-40.

[15] Wang, Haoran, Wei Wang, Ruixue Zhai, Rui Ma, Jun Zhao, and Zhenkai Mu. "Constitutive Equations for Describing the Warm and Hot Deformation Behavior of 20Cr2Ni4A Alloy Steel." Metals 10, no. 9 (2020): 1169.

[16] Patnamsetty, Madan, Ari Saastamoinen, Mahesh C. Somani, and Pasi Peura. "Constitutive modelling of hot deformation behaviour of a CoCrFeMnNi high-entropy alloy." Science and technology of advanced materials 21, no. 1 (2020): 43-55.

[17] Long, Jinchuan, Qinxiang Xia, Gangfeng Xiao, Yi Qin, and Shuai Yuan. "Flow characterization of magnesium alloy ZK61 during hot deformation with improved constitutive equations and using activation energy maps." International Journal of Mechanical Sciences 191 (2021): 106069.

[18] Zheng, Lei, Zhang Maicang, and Dong Jianxin. "Hot corrosion behavior of powder metallurgy Rene95 nickel-based superalloy in molten NaCl–Na2SO4 salts." Materials & Design 32, no. 4 (2011): 1981-1989.

[19] Dehestani, Mahdi, Kevin Trumble, Han Wang, Haiyan Wang, and Lia A. Stanciu. "Effects of microstructure and heat treatment on mechanical properties and corrosion behavior of

powder metallurgy derived Fe–30Mn alloy." Materials Science and Engineering: A 703 (2017): 214-226.

[20] Meignanamoorthy, M., Manickam Ravichandran, Vinayagam Mohanavel, Asif Afzal, T. Sathish, Sagr Alamri, Sher Afghan Khan, and C. Ahamed Saleel. "Microstructure, mechanical properties, and corrosion behavior of Boron Carbide Reinforced Aluminum Alloy (Al-Fe-Si-Zn-Cu) matrix composites produced via powder metallurgy route." Materials 14, no. 15 (2021): 4315.

[21] Dawood, Nawal Mohammed, Kadhim F. Al-Sultani, and Hussein Hatem Jasim. "Zhe role of zirconia additions on the microstructure and corrosion behavior of Ni-Cr dental alloys." Materials Research Express 8, no. 4 (2021): 045404.

[22] Zhou, Yang, Fang Yang, Yanru Shao, Boxin Lu, Tianxing Lu, and Zhimeng Guo. "Electrochemical Corrosion Behavior of Powder Metallurgy Ti6Al4V Alloy." Journal of Materials Engineering and Performance 30, no. 1 (2021): 556-564.

[23] Osório, W. R., J. E. Spinelli, I. L. Ferreira, and A. Garcia. "The roles of macrosegregation and of dendritic array spacings on the electrochemical behavior of an Al–4.5 wt.% Cu alloy." Electrochimica Acta 52, no. 9 (2007): 3265-3273.

[24] Rahmani, K., G. H. Majzoobi, G. Ebrahim-Zadeh, and M. Kashfi. "Comprehensive study on quasi-static and dynamic mechanical properties and wear behavior of Mg—B4C composite compacted at several loading rates through powder metallurgy." Transactions of Nonferrous Metals Society of China 31, no. 2 (2021): 371-381.

[25] Sadoun, A. M., A. F. Meselhy, and A. W. Abdallah. "Microstructural, mechanical and wear behavior of electroless assisted silver coated Al2O3–Cu nanocomposites." Materials Chemistry and Physics 266 (2021): 124562.

[26] Dincel, Öznur, İjlal Şimşek, and Dursun Özyürek. "Investigation of the wear behavior in simulated body fluid of 316L stainless steels produced by mechanical alloying method." Engineering Science and Technology, an International Journal 24, no. 1 (2021): 35-40.

[27] Martin, Seçkin, Sinan Kandemir, and Maksim Antonov. "Investigation of the high temperature dry sliding wear behavior of graphene nanoplatelets reinforced aluminum matrix composites." Journal of Composite Materials 55, no. 13 (2021): 1769-1782.

[28] Bharath, Katti, Arka Mandal, Anish Karmakar, Asit Kumar Khanra, and M. J. Davidson.

"Understanding the effect of hot extrusion on the evolution of microstructure and associated mechanical properties in sintered Al-Cu-Mg alloys." Materials Characterization 170 (2020): 110715.

[29] Liu, Yanhui, Zhaozhao Liu, and Miao Wang. "Gradient microstructure evolution under thermo-mechanical coupling effects for a nickel-based powder metallurgy superalloy-Dynamic recrystallization coexist with static recrystallization." Journal of Materials Processing Technology 294 (2021): 117142.

[30] Ma, K., Z. Y. Liu, X. X. Zhang, B. L. Xiao, and Z. Y. Ma. "Hot deformation behavior and microstructure evolution of carbon nanotube/7055Al composite." Journal of Alloys and Compounds 854 (2021): 157275.

[31] Ma, Kai, ZhenYu Liu, XingXing Zhang, BoLü Xiao, and ZongYi Ma. "Fabrication of high strength carbon nanotube/7055Al composite by powder metallurgy combined with subsequent hot extrusion." Science China Technological Sciences (2021).

[32] Wang, X., Y. J. Hu, J. Y. Wang, W. Zhai, and B. Wei. "Microstructure evolution and mechanical property of quaternary Cu-7% Al-4% Ni-2.5% Mn alloy solidified within ultrasonic field." Journal of Alloys and Compounds (2021): 160604.

[33] Sun, Zeyu, Xiangjun Tian, Bei He, Zhuo Li, and Haibo Tang. "Microstructure evolution and microhardness of the novel Al–Cu–Li-xSc alloys fabricated by laser rapid melting." Vacuum 189 (2021): 110235.

[34] Ramachandra, Samarth. "INVESTIGATION ON MICROSTRUCTURE AND MECHANICAL PROPERTIES OF POROUS STRUCTURES PROCESSED BY LASER POWDER BED FUSION." PhD diss., 2021.

[35] Sanaei, Niloofar, and Ali Fatemi. "Defects in additive manufactured metals and their effect on fatigue performance: A state-of-the-art review." Progress in Materials Science 117 (2021): 100724.

[36] Sakai, Taku. "Dynamic recrystallization microstructures under hot working conditions." Journal of Materials Processing Technology 53, no. 1-2 (1995): 349-361.

[37] Shimizu, I. "Theories and applicability of grain size piezometers: The role of dynamic recrystallization mechanisms." Journal of Structural Geology 30, no. 7 (2008): 899-917.

[38] Zhang, Cunsheng, Cuixue Wang, Ran Guo, Guoqun Zhao, Liang Chen, Wenchao Sun, and Xiebin Wang. "Investigation of dynamic recrystallization and modeling of microstructure

evolution of an Al-Mg-Si aluminum alloy during high-temperature deformation." Journal of Alloys and Compounds 773 (2019): 59-70.

[39] Zhang, Chi, Liwen Zhang, Wenfei Shen, Cuiru Liu, Yingnan Xia, and Ruiqin Li. "Study on constitutive modeling and processing maps for hot deformation of medium carbon Cr–Ni–Mo alloyed steel." Materials & Design 90 (2016): 804-814.

[40] Froes, F. H., and Joseph R. Pickens. "Powder metallurgy of light metal alloys for demanding applications." JOM 36, no. 1 (1984): 14-28.

[41] Szanto, M., W. Bier, N. Frage, S. Hartmann, and Z. Yosibash. "Experimental based finite element simulation of cold isostatic pressing of metal powders." International Journal of Mechanical Sciences 50, no. 3 (2008): 405-421.

[42] Elwakil, Sherif, and R. Davies. "High-Speed Compaction of Metal Powders." In Proceedings of the Thirteenth International Machine Tool Design and Research Conference, pp. 435-440. Palgrave, London, 1973.

[43] Nishida, Yoshinori, Hiroaki Arima, Jin-Chun Kim, and Teiichi Ando. "Rotary-die equal-channel angular pressing of an Al–7 mass% Si–0.35 mass% Mg alloy." Scripta materialia 45, no. 3 (2001): 261-266.

[44] Liu, Yong, L. F. Chen, H. P. Tang, Chain T. Liu, Bin Liu, and B. Y. Huang. "Design of powder metallurgy titanium alloys and composites." Materials Science and Engineering: A 418, no. 1-2 (2006): 25-35.

[45] Karaguiozova, Zdravka, Adelina Miteva, Aleksander Ciski, and Grzegorz Cieślak. "Some aerospace applications of aluminium alloys." SES 2017 (2017): 327.

[46] Osório, W. R., J. E. Spinelli, I. L. Ferreira, and A. Garcia. "The roles of macrosegregation and of dendritic array spacings on the electrochemical behavior of an Al–4.5 wt.% Cu alloy." Electrochimica Acta 52, no. 9 (2007): 3265-3273.

[47] Osório, Wislei R., Leandro C. Peixoto, Leonardo R. Garcia, and Amauri Garcia. "Corrosion behavior of hypoeutectic Al-Cu alloys in H2SO4 and NaCl solutions." Acta Metallurgica Sinica (English Letters) 22, no. 4 (2009): 241-246.

[48] Osório, Wislei R., Celia M. Freire, Rubens Caram, and Amauri Garcia. "The role of Cu-based intermetallics on the pitting corrosion behavior of Sn–Cu, Ti–Cu and Al–Cu alloys." Electrochimica Acta 77 (2012): 189-197.

[49] Morquecho, CP Castillo, C. López Meléndez, M. I. Flores-Zamora, R. G. Bautista-

Margulis, HE Esparza Ponce, F. Almeraya Calderón, C. Gaona Tiburcio, and A. Martínez-Villafañe. "Electrochemical impedance spectroscopy behavior of nanometric Al-Cr and Cr-Al coatings by magnetron sputtering." Int. J. Electrochem. Sci 7 (2012): 1125-1133.

[50] Ares, Alicia Esther, Liliana Mabel Gassa, Sergio Fabian Gueijman, and Carlos Enrique Schvezov. "Correlation between thermal parameters, structures, dendritic spacing and corrosion behavior of Zn–Al alloys with columnar to equiaxed transition." Journal of Crystal Growth 310, no. 7-9 (2008): 1355-1361.

[51] Ares, Alicia E., and Liliana M. Gassa. "Corrosion susceptibility of Zn–Al alloys with different grains and dendritic microstructures in NaCl solutions." Corrosion Science 59 (2012): 290-306.

[52] Ares, Alicia Esther, Liliana Mabel Gassa, Carlos Enrique Schvezov, and Mario Roberto Rosenberger. "Corrosion and wear resistance of hypoeutectic Zn–Al alloys as a function of structural features." Materials Chemistry and Physics 136, no. 2-3 (2012): 394-414.

[53] Acarer, Mustafa. "Electrical, corrosion, and mechanical properties of aluminum-copper joints produced by explosive welding." Journal of Materials Engineering and Performance 21, no. 11 (2012): 2375-2379.

[54] Toptan, Fatih, A. C. Alves, Işıl Kerti, E. Ariza, and L. A. Rocha. "Corrosion and tribocorrosion behaviour of Al–Si–Cu–Mg alloy and its composites reinforced with B4C particles in 0.05 M NaCl solution." Wear 306, no. 1-2 (2013): 27-35.

[55] LIANG, Wenjie, P. A. N. Qinglin, H. E. Yunbin, L. I. Yunchun, Z. H. O. U. Yingchun, and L. U. Congge. "Effect of aging on the mechanical properties and corrosion susceptibility of an Al-Cu-Li-Zr alloy containing Sc." Rare Metals 27, no. 2 (2008): 146-152.

[56] Kairy, S. K., B. Rouxel, J. Dumbre, J. Lamb, T. J. Langan, T. Dorin, and N. Birbilis. "Simultaneous improvement in corrosion resistance and hardness of a model 2xxx series Al-Cu alloy with the microstructural variation caused by Sc and Zr additions." Corrosion Science 158 (2019): 108095.

[57] Tabor, David. "Friction and wear-developments over the last fifty years." IMechE 245 (1987): 157-172.

[58] Oktay, S. Tu¨ rker, and Nam P. Suh. "Wear debris formation and agglomeration." (1992): 379-393.

[59] Saka, Nannaji, Ming J. Liou, and Nam P. Suh. "The role of tribology in electrical contact

phenomena." Wear 100, no. 1-3 (1984): 77-105.

[60] Suh, N. P., and H. C. Sin. "On the genesis of friction and its effect on wear." Solid Contact and Lubrication, AMD 39 (1980): 167-183.

[61] Aronov, V., A. F. D'souza, S. Kalpakjian, and I. Shareef. "Experimental investigation of the effect of system rigidity on wear and friction-induced vibrations." (1983): 206-211.

[62] Aronov, V., A. F. D'souza, S. Kalpakjian, and I. Shareef. "Interactions among friction, wear, and system stiffness—Part 1: effect of normal load and system stiffness." (1984): 54-58.

[63] Aronov, V., A. F. D'souza, S. Kalpakjian, and I. Shareef. "Interactions among friction, wear, and system stiffness—part 3: wear model." (1984): 65-69.

[64] Lin, Jau-Wen, and M. D. Bryant. "Reductions in wear rate of carbon samples sliding against wavy copper surfaces." (1996): 116-124.

[65] Ludema, Kenneth C., and Oyelayo O. Ajayi. Friction, wear, lubrication: a textbook in tribology. CRC press, 2018.

[66] Berger, Edward J., Charles M. Krousgrill, and Farshid Sadeghi. "Stability of sliding in a system excited by a rough moving surface." In International Design Engineering Technical Conferences and Computers and Information in Engineering Conference, vol. 17186, pp. 553-563. American Society of Mechanical Engineers, 1995.

[67] Bhushan, Bharat. Principles and applications of tribology. John Wiley & Sons, 1999.

[68] Lepper, K., M. James, J. Chashechkina, and D. A. Rigney. "Sliding behavior of selected aluminum alloys." Wear 203 (1997): 46-56.

[69] Prasad, B. K. "Dry sliding wear response of some bearing alloys as influenced by the nature of microconstituents and sliding conditions." Metallurgical and Materials Transactions A 28, no. 13 (1997): 809-815.

[70] Upadhyaya, Anish, N. S. Mishra, and S. N. Ojha. "Microstructural control by spray forming and wear characteristics of a Babbit alloy." Journal of materials science 32, no. 12 (1997): 3227-3235.

[71] Dowson, D. "History of tribology. Number." (1998).

[72] Enomoto, Yuji, and Takashi Yamamoto. "New materials in automotive tribology." Tribology Letters 5, no. 1 (1998): 13-24.

[73] Bhushan, Bharat. "Friction." In Tribology and Mechanics of Magnetic Storage Devices, pp.

231-365. Springer, New York, NY, 1996.

[74] Blau, Peter J. "Scale effects in sliding friction: an experimental study." In Fundamentals of friction: macroscopic and microscopic processes, pp. 523-534. Springer, Dordrecht, 1992.

[75] Bhushan, Bharat. Principles and applications of tribology. John Wiley & Sons, 1999.

[76] Kang, Yung-Chang, and Sammy Lap-Ip Chan. "Tensile properties of nanometric Al2O3 particulate-reinforced aluminum matrix composites." Materials chemistry and physics 85, no. 2-3 (2004): 438-443.

[77] Chaudhury, S. K., A. K. Singh, C. S. S. Sivaramakrishnan, and S. C. Panigrahi. "Preparation and thermomechanical properties of stir cast Al-2Mg-11TiO 2 (rutile) composite." Bulletin of Materials Science 27, no. 6 (2004): 517-521.

[78] Sawla, S., and S. Das. "Combined effect of reinforcement and heat treatment on the two body abrasive wear of aluminum alloy and aluminum particle composites." Wear 257, no. 5-6 (2004): 555-561.

[79] Hassan, Adel Mahmood, Ghassan Mousa Tashtoush, and Jafar Ahmed Al-Khalil. "Effect of graphite and/or silicon carbide particles addition on the hardness and surface roughness of Al-4 wt% Mg alloy." Journal of composite materials 41, no. 4 (2007): 453-465.

[80] Costa, E. M., M. Compani, A. R. Floriani, and B. A. Dedavid. "AA380 aluminum alloy-based metal matrix composites reinforced with alumina produced by compocasting process." Acta Microscopia 12 (2003): 253-254.

[81] Candan, S., and E. Bilgic. "Corrosion behavior of Al–60 vol.% SiCp composites in NaCl solution." Materials letters 58, no. 22-23 (2004): 2787-2790.

[82] Das, Sanjeev, Siddhartha Das, and Karabi Das. "RETRACTED: Abrasive wear of zircon sand and alumina reinforced Al–4.5 wt% Cu alloy matrix composites–A comparative study." (2007): 746-751.

[83] Akhlaghi, F., A. Lajevardi, and H. M. Maghanaki. "Effects of casting temperature on the microstructure and wear resistance of compocast A356/SiCp composites: a comparison between SS and SL routes." Journal of Materials Processing Technology 155 (2004): 1874-1880.

[84] Nuruzzaman, Dewan Muhammad, and Mohammad Asaduzzaman Chowdhury. "Friction coefficient and wear rate of copper and aluminum sliding against mild steel." Int. Trans. J. Eng. Manag. Appl. Sci. Technol 4, no. 1 (2013): 29-40.

[85] Hassan, Adel Mahamood, Abdalla Alrashdan, Mohammed T. Hayajneh, and Ahmad Turki Mayyas. "Wear behavior of Al–Mg–Cu–based composites containing SiC particles." Tribology International 42, no. 8 (2009): 1230-1238.

[86] Mondi, Rama Karthik, and Brahma Raju Golla. "Processing and characterization of super strong and wear resistant Al–5Cu-(0-20 vol%) ZrB2 composites." Journal of Alloys and Compounds 814 (2020): 152323.

[87] Perrin, C., and W. M. Rainforth. "The effect of alumina fibre reinforcement on the wear of an Al-4.3% Cu alloy." Wear 181 (1995): 312-324.

[88] Wang, Yu, W. Mark Rainforth, H. Jones, and Marcela Lieblich. "Sliding wear behaviour of novel AA2124 aluminium alloy/Ni3Al composites." In Materials Science Forum, vol. 396, pp. 1473-1478. Trans Tech Publications Ltd., Zurich-Uetikon, Switzerland, 2002.

[89] Narayan, Sumesh, and Ananthanarayanan Rajeshkannan. "Workability studies of sintered aluminium composites during hot deformation." Proceedings of the Institution of Mechanical Engineers, Part B: Journal of Engineering Manufacture 230, no. 3 (2016): 494-504.

[90] Narayan, Sumesh, and Rajeshkannan Ananthanarayanan. "Densification behaviour of sintered aluminum composites during hot deformation." AIMS Materials Science 5, no. 5 (2018): 902-915.

[91] Khan, Mohammed Nizam, Sumesh Narayan, and Ananthanarayanan Rajeshkannan. "Influence of process parameters on the workability characteristics of sintered Al and Al–Cu composites during cold deformation." AIMS Materials Science 6, no. 3 (2019): 441-453.

[92] Wolla, Desalegn Wogaso, M. J. Davidson, and A. K. Khanra. "Studies on the formability of powder metallurgical aluminum–copper composite." Materials & Design 59 (2014): 151-159.

[93] Liu, Shuaiyang, and Aiqin Wang. "Hot deformation behaviors of Cu/Al laminated composites." In IOP Conference Series: Materials Science and Engineering, vol. 381, no. 1, p. 012162. IOP Publishing, 2018.

[94] Ahasan, Md, M. J. Davidson, and N. Selvakumar. "Experimental investigations on the densification and deformation behaviour of Al-TiB 2 composite preforms." Transactions of the Indian Institute of Metals 69, no. 5 (2016): 1059-1068.

[95] Canakci, Aykut, Temel Varol, Serdar Özkaya, and Fatih Erdemir. "Microstructure and properties of Al-B4C functionally graded materials produced by powder metallurgy method." Universal Journal of Materials Science 2, no. 5 (2014): 90-95.

[96] Li, Defu, Qingmiao Guo, Shengli Guo, Haijian Peng, and Zhigang Wu. "The microstructure evolution and nucleation mechanisms of dynamic recrystallization in hot-deformed Inconel 625 superalloy." Materials & design 32, no. 2 (2011): 696-705.

[97] Shaban, M., and B. Eghbali. "Characterization of austenite dynamic recrystallization under different z parameters in a microalloyed steel." Journal of Materials Science & Technology 27, no. 4 (2011): 359-363.

[98] Ashtiani, HR Rezaei, and P. Shahsavari. "Strain-dependent constitutive equations to predict high temperature flow behavior of AA2030 aluminum alloy." Mechanics of Materials 100 (2016): 209-218.

[99] Mann, R. E. D., R. L. Hexemer Jr, I. W. Donaldson, and D. P. Bishop. "Hot deformation of an Al–Cu–Mg powder metallurgy alloy." Materials Science and Engineering: A 528, no. 16-17 (2011): 5476-5483.

[100] Li, Jun-peng, S. H. E. N. Jian, Xiao-dong Yan, Bai-ping Mao, and Liang-ming Yan. "Microstructure evolution of 7050 aluminum alloy during hot deformation." Transactions of Nonferrous Metals Society of China 20, no. 2 (2010): 189-194.

[101] Taleghani, MA Jabbari, EM Ruiz Navas, M. Salehi, and J. M. Torralba. "Hot deformation behaviour and flow stress prediction of 7075 aluminium alloy powder compacts during compression at elevated temperatures." Materials Science and Engineering: A 534 (2012): 624-631.

[102] Guo, Junhang, Shengdun Zhao, Ri-ichi Murakami, Rixian Ding, and Shuqin Fan. "Modeling the hot deformation behavior of Al alloy 3003." Journal of Alloys and Compounds 566 (2013): 62-67.

[103] McQueen, H. J., and W. Blum. "Dynamic recovery: sufficient mechanism in the hot deformation of Al (< 99.99)." Materials Science and Engineering: A 290, no. 1-2 (2000): 95-107.

[104] Huang, Xudong, Hui Zhang, Yi Han, Wenxiang Wu, and Jianghua Chen. "Hot deformation behavior of 2026 aluminum alloy during compression at elevated temperature." Materials Science and Engineering: A 527, no. 3 (2010): 485-490.

[105] Taleghani, MA Jabbari, EM Ruiz Navas, M. Salehi, and J. M. Torralba. "Hot deformation behaviour and flow stress prediction of 7075 aluminium alloy powder compacts during compression at elevated temperatures." Materials Science and Engineering: A 534 (2012): 624-631.

[106] Lin, Y. C., Qi-Fei Li, Yu-Chi Xia, and Lei-Ting Li. "A phenomenological constitutive model for high temperature flow stress prediction of Al–Cu–Mg alloy." Materials Science and Engineering: A 534 (2012): 654-662.

[107] Li, Xue-Song, Lai-zhi Wu, C. H. E. N. Jun, and Hong-Bing Zhang. "New approach for modeling flow stress of aluminum alloy 6A10 considering temperature variation." Transactions of Nonferrous Metals Society of China 20, no. 8 (2010): 1482-1487.

[108] Wolla, Desalegn Wogaso, M. J. Davidson, and A. K. Khanra. "Constitutive modeling of powder metallurgy processed Al–4% Cu preforms during compression at elevated temperature." Materials & Design (1980-2015) 65 (2015): 83-93.

[109] Lin, Y. C., and Xiao-Min Chen. "A critical review of experimental results and constitutive descriptions for metals and alloys in hot working." Materials & Design 32, no. 4 (2011): 1733-1759.

[110] He, Shuai, Chang-sheng Li, Zhen-yi Huang, and Jian-jun Zheng. "A modified constitutive model based on Arrhenius-type equation to predict the flow behavior of Fe–36% Ni Invar alloy." Journal of Materials Research 32, no. 20 (2017): 3831-3841.

[111] Li, Defu, Qingmiao Guo, Shengli Guo, Haijian Peng, and Zhigang Wu. "The microstructure evolution and nucleation mechanisms of dynamic recrystallization in hot-deformed Inconel 625 superalloy." Materials & design 32, no. 2 (2011): 696-705.

[112] Shaban, M., and B. Eghbali. "Characterization of austenite dynamic recrystallization under different z parameters in a microalloyed steel." Journal of Materials Science & Technology 27, no. 4 (2011): 359-363.

[113] Kodzhaspirov, G. E., and M. I. Terentyev. "Modeling the dynamically recrystallized grain size evolution of a superalloy." Mater. Phys. Mech 13, no. 1 (2012): 70-76.

[114] Chakravarthi, K. V. A., N. T. B. N. Koundinya, SVS Narayana Murty, and B. Nageswara Rao. "Microstructural evolution and constitutive relationship of M350 grade maraging steel during hot deformation." Journal of Materials Engineering and Performance 26, no. 3

(2017): 1174-1185.

[115] Guo, Qingmiao, Defu Li, Shengli Guo, Haijian Peng, and Jie Hu. "The effect of deformation temperature on the microstructure evolution of Inconel 625 superalloy." Journal of Nuclear Materials 414, no. 3 (2011): 440-450.

[116] Chen, Xiao-Min, Y. C. Lin, Dong-Xu Wen, Jin-Long Zhang, and Min He. "Dynamic recrystallization behavior of a typical nickel-based superalloy during hot deformation." Materials & Design 57 (2014): 568-577.

[117] Xu, S. W., N. Matsumoto, S. Kamado, T. Honma, and Y. Kojima. "Dynamic microstructural changes in Mg–9Al–1Zn alloy during hot compression." Scripta Materialia 61, no. 3 (2009): 249-252.

[118] Narayan, Sumesh, and A. Rajeshkannan. "Densification behaviour in forming of sintered iron–0.35% carbon powder metallurgy preform during cold upsetting." Materials & Design 32, no. 2 (2011): 1006-1013.

[119] Narayanasamy, R., V. Anandakrishnan, and K. S. Pandey. "Effect of geometric work-hardening and matrix work-hardening on workability and densification of aluminium–3.5% alumina composite during cold upsetting." Materials & Design 29, no. 8 (2008): 1582-1599.

[120] Venugopal, P., S. Venkatraman, R. Vasudevan, and K. A. Padmanabhan. "Ring-compression tests on sintered iron preforms." Journal of mechanical working technology 16, no. 1 (1988): 51-64.

[121] Taleghani, MA Jabbari, EM Ruiz Navas, M. Salehi, and J. M. Torralba. "Hot deformation behaviour and flow stress prediction of 7075 aluminium alloy powder compacts during compression at elevated temperatures." Materials Science and Engineering: A 534 (2012): 624-631.

[122] Liu, Wenyi, Huan Zhao, Dan Li, Zhiqing Zhang, Guangjie Huang, and Qing Liu. "Hot deformation behavior of AA7085 aluminum alloy during isothermal compression at elevated temperature." *Materials Science and Engineering: A* 596 (2014): 176-182.

[123] Ares, Alicia Esther, Liliana Mabel Gassa, Sergio Fabian Gueijman, and Carlos Enrique Schvezov. "Correlation between thermal parameters, structures, dendritic spacing and corrosion behavior of Zn–Al alloys with columnar to equiaxed transition." Journal of Crystal Growth 310, no. 7-9 (2008): 1355-1361.

[124] Ares, Alicia E., and Liliana M. Gassa. "Corrosion susceptibility of Zn–Al alloys with

different grains and dendritic microstructures in NaCl solutions." Corrosion Science 59 (2012): 290-306.

[125] Ares, Alicia Esther, Liliana Mabel Gassa, Carlos Enrique Schvezov, and Mario Roberto Rosenberger. "Corrosion and wear resistance of hypoeutectic Zn–Al alloys as a function of structural features." Materials Chemistry and Physics 136, no. 2-3 (2012): 394-414.

[126] Zhou, Y. T., Y. N. Zan, X. X. Wei, B. Yang, B. Zhang, S. J. Zheng, X. H. Shao et al. "Corrosion onset associated with the reinforcement and secondary phases in B4C-6061Al neutron absorber material in H3BO3 solution." Corrosion Science 153 (2019): 74-84.

[127] Heard, D. W., I. W. Donaldson, and D. P. Bishop. "Metallurgical assessment of a hypereutectic aluminum–silicon P/M alloy." Journal of Materials Processing Technology 209, no. 18-19 (2009): 5902-5911.

[128] Savaşkan, Temel, Ali Paşa Hekimoğlu, and Gençağa Pürçek. "Effect of copper content on the mechanical and sliding wear properties of monotectoid-based zinc-aluminium-copper alloys." Tribology International 37, no. 1 (2004): 45-50.

[129] Morquecho, CP Castillo, C. López Meléndez, M. I. Flores-Zamora, R. G. Bautista-Margulis, HE Esparza Ponce, F. Almeraya Calderón, C. Gaona Tiburcio, and A. Martínez-Villafañe. "Electrochemical impedance spectroscopy behavior of nanometric Al-Cr and Cr-Al coatings by magnetron sputtering." Int. J. Electrochem. Sci 7 (2012): 1125-1133.

[130] Acarer, Mustafa. "Electrical, corrosion, and mechanical properties of aluminum-copper joints produced by explosive welding." Journal of Materials Engineering and Performance 21, no. 11 (2012): 2375-2379.

[131] Kear, G., B. D. Barker, K. Stokes, and F. C. Walsh. "Flow influenced electrochemical corrosion of nickel aluminium bronze–Part I. Cathodic polarisation." Journal of applied electrochemistry 34, no. 12 (2004): 1235-1240.

[132] Blundy, R. G., and M. J. Pryor. "The potential dependence of reaction product composition on copper-nickel alloys." Corrosion Science 12, no. 1 (1972): 65-75.

[133] Kear, G., B. D. Barker, K. Stokes, and F. C. Walsh. "Flow influenced electrochemical corrosion of nickel aluminium bronze–Part II. Anodic polarisation and derivation of the mixed potential." Journal of applied electrochemistry 34, no. 12 (2004): 1241-1248.

[134] Nemati, N., R. Khosroshahi, M. Emamy, and A. Zolriasatein. "Investigation of microstructure, hardness and wear properties of Al–4.5 wt. % Cu–TiC nanocomposites

produced by mechanical milling." *Materials & Design* 32, no. 7 (2011): 3718-3729.

[135] Hassan, Adel Mahamood, Abdalla Alrashdan, Mohammed T. Hayajneh, and Ahmad Turki Mayyas. "Wear behavior of Al–Mg–Cu–based composites containing SiC particles." *Tribology International* 42, no. 8 (2009): 1230-1238.

[136] Bhushan, Bharat. Principles and applications of tribology. John Wiley & Sons, 1999.

[137] Raj, AP Mohan, N. Selvakumar, R. Narayanasamy, and C. Kailasanathan. "Experimental investigation on workability and strain hardening behaviour of Fe–C–Mn sintered composites with different percentage of carbon and manganese content." Materials & Design 49 (2013): 791-801.

[138] Kumar, D. R., R. Narayanasamy, and C. Loganathan. "Effect of glass and SiC in aluminum matrix on workability and strain hardening behavior of powder metallurgy hybrid composites." Materials & Design 34 (2012): 120-136.

[139] Narayanasamy, R., T. Ramesh, and K. S. Pandey. "Some aspects on workability of aluminium–iron powder metallurgy composite during cold upsetting." Materials Science and Engineering: A 391, no. 1-2 (2005): 418-426.

[140] Vujovic, V., and A. H. Shabaik. "A new workability criterion for ductile metals." (1986): 245-249.

[141] Gökçe, Azim, Fehim Fındık, and Ali Osman Kurt. "Microstructural examination and properties of premixed Al–Cu–Mg powder metallurgy alloy." Materials Characterization 62, no. 7 (2011): 730-735.

[142] Liu, Shuaiyang, and Aiqin Wang. "Hot deformation behaviors of Cu/Al laminated composites." In IOP Conference Series: Materials Science and Engineering, vol. 381, no. 1, p. 012162. IOP Publishing, 2018.

[143] Chen, Wenchao, Pengqi Chen, Jianfeng Li, Jianhua Zhang, Laima Luo, and Jigui Cheng. "Functionally graded W-Cu materials prepared from Cu-Coated W Powders by microwave sintering." Journal of Materials Engineering and Performance 28, no. 10 (2019): 6135-6144.

[144] Chen, Xiao-Min, Y. C. Lin, Dong-Xu Wen, Jin-Long Zhang, and Min He. "Dynamic recrystallization behavior of a typical nickel-based superalloy during hot deformation." Materials & Design 57 (2014): 568-577.

[145] Chakravarthi, K. V. A., N. T. B. N. Koundinya, SVS Narayana Murty, and B. Nageswara Rao. "Microstructural evolution and constitutive relationship of M350 grade maraging steel

during hot deformation." Journal of Materials Engineering and Performance 26, no. 3 (2017): 1174-1185.

[146] Chen, Xiao-Min, Y. C. Lin, Ming-Song Chen, Hong-Bin Li, Dong-Xu Wen, Jin-Long Zhang, and Min He. "Microstructural evolution of a nickel-based superalloy during hot deformation." Materials & Design 77 (2015): 41-49.

[147] Seetharam, R., S. Kanmani Subbu, and M. J. Davidson. "Microstructure modeling of dynamically recrystallized grain size of sintered Al–4 wt% B4C composite during hot upsetting." Journal of Engineering Materials and Technology 140, no. 2 (2018).

[148] Bedir, Fevzi. "Modeling approach and plastic deformation analysis of 6063 aluminum alloy during compression at elevated temperatures." Materials & Design 49 (2013): 953-956.

[145] Chen, Fei, Zhenshan Cui, and Shijia Chen. "Recrystallization of 30Cr2Ni4MoV ultra-super-critical rotor steel during hot deformation. Part I: Dynamic recrystallization." Materials Science and Engineering: A 528, no. 15 (2011): 5073-5080.

[150] Zhou, Mi, Y. C. Lin, Jiao Deng, and Yu-Qiang Jiang. "Hot tensile deformation behaviors and constitutive model of an Al–Zn–Mg–Cu alloy." Materials & Design 59 (2014): 141-150.

[151] Zhang, Hongbin, Kaifeng Zhang, Haiping Zhou, Zhen Lu, Changhong Zhao, and Xiaoli Yang. "Effect of strain rate on microstructure evolution of a nickel-based superalloy during hot deformation." Materials & Design 80 (2015): 51-62.

[152] Shaban, M., and B. Eghbali. "Characterization of austenite dynamic recrystallization under different z parameters in a microalloyed steel." Journal of Materials Science & Technology 27, no. 4 (2011): 359-363.

[153] Zener, Clarence, and John Herbert Hollomon. "Effect of strain rate upon plastic flow of steel." Journal of Applied physics 15, no. 1 (1944): 22-32.

[154] Rokni, M. R., A. Zarei-Hanzaki, Ali A. Roostaei, and A. Abolhasani. "Constitutive base analysis of a 7075 aluminum alloy during hot compression testing." Materials & Design 32, no. 10 (2011): 4955-4960.

[155] Gale, W. F., and Totemeier, T. C., eds., 2003, Smithells Metals Reference Book, Butterworth–Heinemann, Burlington, VT.

[156] Matsui, T., H. Takizawa, H. Kikuchi, and S. Wakita. "The microstructure prediction of alloy 720LI for turbine disk applications." In 9th International Symposium on Superalloys, pp.

127-133. 2000.

RESEARCH PUBLICATIONS

1. Rajasekhar Kotikala, V. Suresh Babu, and M. J. Davidson. "Influence of copper addition on corrosion properties and hardness of Al–Cu/Al two-layered-structure composites." Proceedings of the Institution of Mechanical Engineers, Part C: Journal of Mechanical Engineering Science (2021): 09544062211034209.

2. Rajasekhar Kotikala, V. Suresh Babu, and M. J. Davidson. "Formability and densification behavior of two-layered structure powder metallurgical hot-pressed Al-Cu/Al composites during hot-upsetting." Proceedings of the Institution of Mechanical Engineers, Part E: Journal of Process Mechanical Engineering 235.2 (2021): 582-593.

3. Rajasekhar Kotikala, V. Suresh Babu, and M. J. Davidson. "Interfacial microstructure and properties of Al-Cu functionally graded materials fabricated by powder metallurgy method." Materials Today: Proceedings 46 (2021): 9212-9216.

4. Rajasekhar Kotikala, V. Suresh Babu, and M. J. Davidson. "Microstructural and mechanical properties of Al-Cu functionally graded materials fabricated by powder metallurgy method." Materials Today: Proceedings 41 (2021): 1156-1159.

CURRICULUM VITAE

KOTIKALA RAJASEKHAR was born on 24th July, 1983, to Mr. K. Rosaiah and Mrs. Vimalamma parents at Ongole, Andhra Pradesh, India. He completed his B.Tech. Degree in Mechanical Engineering at V. R. Siddhartha Engineering College, Acharya Nagarjuna University, Vijayawada, in the year 2008. He completed his M.Tech. (Mechanical Engineering) degree specialization in Product design and development at National Institute of Technology, Warangal, in the year 2010. Presently he is pursuing Ph.D in Mechanical Engineering at National Institute of Technology, Warangal.